Differential anti-cancer signaling exerted by an *in silico*-designed compound in tumorigenic and non-tumorigenic breast cells

by
Michelle Helen Visagie
04412168

Submitted in fulfilment of the requirements for the degree

PhD: Human Physiology

in the Department of Physiology
School of Medicine
Faculty of Health Sciences
University of Pretoria
Pretoria

Promoter: Professor AM Joubert
Department of Physiology
University of Pretoria

Co-promoter: Professor L-M Birkholtz
Department of Biochemistry
University of Pretoria

June 2014

Declaration

I declare that the thesis, which I hereby submit for the degree PhD: Human Physiology at the University of Pretoria, is my own work and has not previously been submitted by me for a degree at this, or any other tertiary institution.

Signature — 15 April 2014

MH Visagie — Date

Table of contents

Summary

Microtubule-disrupting agents have been studied for decades for their potential anticancer activity and resulted in discovery of an endogenous 17β-estradiol derivative, 2-methoxyestradiol (2ME2). Since 2ME2 possesses low bioavailability, several analogues with improved efficacy was *in silico*-designed to target tumorigenic cells. This study investigated the influence of an 17β-estradiol analogue, (8R, 13S, 14S, 17S)-2-ethyl-13-methyl-7, 8, 9, 11, 12,13, 14, 15, 16, 17-decahydro-6H-cyclopenta[a]phenanthrane-3, 17-diyl bis(sulphamate) (EMBS) on cell growth, cytotoxicity, metabolism, morphology, cell cycle progression, reactive oxygen species generation and induction of cell death via apoptosis in two adenocarcinoma cell lines (MCF-7 and MDA-MB-231) and the non-tumorigenic epithelial breast cell line (MCF-12A).

Crystal violet staining and the real-time xCELLigence approach indicated statistically significant antiproliferative activity in an estrogen-independent manner (0.4 μM; 24 h) in all three cell lines. Influence on morphological demonstrated several apoptotic hallmarks including compromised cell density, apoptotic bodies, shrunken cells, hypercondensed chromatin and several cells trapped in metaphase culminating in apoptosis. Cell cycle progression studies revealed apoptosis induction and cells blocked in the G_2M phase. Apoptosis induction was verified by means of Annexin V-FITC.EMBS-treated cells demonstrated a reduced mitochondrial membrane potential. Furthermore, autophagy characteristics were observed including vacuoles and autophagosomes. Mitotic indices demonstrated an increase in cells possessing abnormal morphology associated with apoptosis and the number of cells trapped in metaphase culminating in apoptosis. This was confirmed by cell cycle progression studies that revealed apoptosis induction and a G_2M block. Apoptosis induction was verified by means of Annexin V-FITC and additional flow cytometry studies indicated EMBS-treated cells demonstrated a reduced mitochondrial membrane potential.

Fluorescent microscopy exhibited increased lysosomal staining suggesting autophagy induction which was verified by conducting flow cytometry employing LC3B conjugated to DyLight 488. Flow cytometry studies also demonstrated that EMBS exposure resulted in statistically significant increased hydrogen peroxide and superoxide

production. EMBS exposure resulted in a statistically significant increase in p53 protein expression, decreased Bcl-2 expression and a decrease in pBcl-2(s70) phosphorylation supporting the notion that EMBS utilises crosstalk pathways to induce both autophagy and apoptosis. These results were observed in all three cell lines with caspase 6 and 8 activation being more prominent in the tumorigenic cell lines and cell growth recovering after 24 h exposure in the non-tumorigenic MCF-12A cell line.

Further research will focus on the molecular signal transduction utilized by EMBS and an in-depth analysis of specific anticancer targets identified *in vitro* and subsequent *in vivo* investigation. Thus this study contributes to the discovery of targets for cancer therapies that will aid in the design of microtubule disrupting agents.

Keywords

Apoptosis, autophagy, antimitotic, EMBS, crosstalk, antiproliferative, reactive oxygen species

Acknowledgements

- Professor AM Joubert (professor of Department of Physiology) as my promoter for this project. Her assistance, insight, motivation, support and positive attitude made this project possible.
- Professor D van Papendorp (Head of the Department of Physiology) for allowing me the opportunity to further my postgraduate studies in the Department and allowing me to use the facilities and apparatus at the department.
- Cancer Association of South Africa, the Struwig Germeshuysen Trust, Research Council of the University of Pretoria (RESCOM), National Research Foundation and The Medical Research Council for providing financial support.
- The Electron Microscopy Unit (University of Pretoria' Hatfield Campus, Pretoria, South Africa) for the use of the transmission electron microscopy and scanning electron microscope.
- The Flow Cytometry Unit (Department of Pharmacology, University of Pretoria, Pretoria, South Africa) for the availability of the flow cytometer for use during the research project.
- A very special thank you to my parents who always supported and motivated me throughout my studies.
- Colleagues, friends and relatives for motivation, support and insight.
- Francina and Ezekiel for maintenance of the lab and sterilization of glassware.
- God Almighty, for without Him, none of this would have been possible.

List of Figures

List of Tables

Abbreviations

4EBP	Eukaryotic Translational Initiation Factor 4E Binding Protein 1
2ME2	2-Methoxyestradiol
2MEBM	2-Methoxyestradiol-bis-sulphamate
APAF-1	Apoptosis Activating Factor 1
Adiol	Androstenediol
AIF	Apoptosis Inducing Factor
AMP	Adenosine Monophosphate
AMPK	AMP-Activated Protein Kinase
APC	Anaphase Promoting Complex
APC/C	Promoting Complex/Cyclosome
APO-2L	Apo-2 Ligand
ADP	Adenosine Diphosphate
ANG-1	Angiopoietin 1
ANG-2	Angiopoietin 2
APO1	NF Receptor Superfamily, Member 6
ARGs	Autophagy-Related Genes
ASK1	Apoptosis Signal-Regulated Kinase 1
ATG	Autophagy-Related Proteins
ATG6	Autophagy-Related Protein 6
ATG8p	Autophagy-Related Protein 8 Precursor
ATM	Ataxia Telangiectasia Mutated
ATP	Adenosine Triphosphate
ATR	Rad3-Related Kinase
BAD	Bcl-2 Antagonist Of Cell Death
BAK	Bcl-2 Homologous Antagonist/Killer
BAX	Bcl-2-Associated X Protein
BCL-2	B-Cell Lymphoma-2 Family Members
BFP	Back Focal Plane
BH3	Bcl-2 Homology Region 3
BID	BH3-Interacting Domain Death Agonist
BIK	Bcl-2-Interacting Killer
BIM	Bcl-2-Interacting Mediator Of Cell Death

BRCA 1	Breast Cancer Gene 1
BRCA 2	Breast Cancer Gene 2
BSA	Bovine Serum Albumin
BUB1	Budding Inhibited Benzimidazole 1
BUB2	Budding Inhibited Benzimidazole 2
BUB3	Budding Inhibited Benzimidazole 3
CA	Carbonic Anhydrase
Ca^{2+}	Calcium
CARD	Caspase-Recruiting Domain
CAK	Cyclin Activated Kinase
CBP	CREB-Binding Protein
CD95	Clonal Deletion 95
CD95L	CD95 Ligand
CDC	Cell Division Cycle
CDC14	Cell Division Cycle 14
CDC20	Cell Division Cycle 20
CDC25A	Cell Division Cycle 25A
CDC25B	Cell Division Cycle 25B
CDC25C	Cell Division Cycle 25C
CDC6	Cell Division Cycle 6
cdh1	Cadherin 1
CDK	Cyclin Dependent Kinases
CDK1	Cyclin Dependent Kinases 1
CDK2	Cyclin Dependent Kinases 2
CDK4	Cyclin Dependent Kinases 4
CDK6	Cyclin Dependent Kinases 6
CDK7	Cyclin Dependent Kinases 7
cDNA	Complementary Deoxyribonucleic Acid
CHK1	Checkpoint Kinase 1
CHK2	Checkpoint Kinase 2
CI	Cell Index
CK	Cytokeratin
CMA	Chaperone-Mediated Autophagy

CRDs	Cysteine Rich Domains
DAPK-1	Death-Associated Protein Kinase 1
D-BOX	Destruction Box
DCFDA	2,7-Dichlorofluorescein Diacetate
DD	Death Domain
DED	Death Effector Domain
DHEA	Dehydroepiandrostene
DIC	Differential Interference Contrast
DISC	Death Inducing Signaling Complex
DMEM	Dulbecco's Minimum Essential Medium Eagle
DMSO	Dimethyl Sulfoxide
DNA	Deoxyribonucleic Acid
DRAM	Damage-Regulated Autophagy Modulator
DR4	Death Receptor 4
DR5	Death Receptor 5
E2F	Elongation Factor 2
EMBS	(8*R*,13*S*,14*S*,17*S*)-2-Ethyl-13-Methyl-7,8,9,11,12,13,14,15,16,17-Decahydro-6H-Cyclopenta[*A*]Phenanthrane-3,17-Diyl Bis(Sulphamate)
EGFR	Epidermal Growth Factor Receptor
EndoG	Endonuclease G
EOR	ER-Overload Response
ER	Endoplasmic Reticulum
ERAD	ER-associated Degradation
ERK	Extracellular Signal-Regulated Kinase
FACS	Fluorescence Activated Cell Sorting
FADD	Fas Associated Death Domain
FCS	Fetal Calf Serum
FFP	Front Focal Plane
FITC	Fluorescein Isothiocyanate
FLD	Flexible Loop Domain
FSC	Forward Scatter
G_0 phase	Quiescent Phase
G_1 phase	Gap 1 Phase

G_2 phase	Gap 2 Phase
GATA-6	GATA binding protein 6
GMNN	Geminin
H	Hours
HC	Immunohistochemical
HE	Hydroethidine
HER2	Human Epidermal Growth Factor Receptor 2
HIF	Hypoxia Inducible Factor
HIF-1	Hypoxia Inducible Factor 1
HIF-1α	Hypoxia Inducible Factor 1α
HIFU	High Intensity Frequency Ultrasound
JNK	C-Jun N-Terminal Kinase
LAMPA-2A	Lysosomal-Associated Membrane Protein-2A
LDH	Lactate Dehydrogenase
M Phase	Mitotic Phase
MAD1	Mitotic Arrest-Deficient 1
MAD2	Mitotic Arrest-Deficient 2
MAD3	Mitotic Arrest-Deficient 3
MAPK	The p38 Mitogen Activated Protein Kinase
Mdm2	Murine Double Minute 2
MMP	Mitochondrial Membrane Potential
MMP-2	Matrix Metaloproteinases 2
MMP-9	Matrix Metaloproteinases 9
MOMP	Mitochondrial Outer Membrane Permeabilization
MPS1	Meiotic Recombination 11 Homolog
mRNA	Messenger RNA
mTOR	Mammalian Target Of Rapamycin
mTORC1	mTOR Complex 1
mTORC2	mTOR Complex 2
MTT	3-(4,5-Dimethylthiazol-2-Yl)-2,5-Diphenyltetrazolium Bromide
NADH	Reduced Nicotinamide Adenine Dinucleotide
NAMN	Nicotinic Acid Mononucleotide
NMN	Nicotinamide Mononucleotide

NOS	Nitric Oxide Synthase
ORC	Origin Recognition Complex
PAI-1	Plasminogen Activator Inhibitor-1
PDGF	Platelet-Derived Growth Factor B
PBS	Phosphate Buffer Solution
PCD	Programmed Cell Death
PCNA	Proliferating Cell Nuclear Antigen
PCR	Polymerase Chain Reaction
PE	Phosphatidylethanolamine
PLASDIC	Polarization-Optical Transmitted Light Differential Interference Contrast
PgR	Progesterone Receptor Gene
P13K	Phosphatidyllinositol 3-OH Kinase
P13K/AKT	Phosphatidyl-3-Kinase
PPAR	Peroxisome Proliferators-Activator Receptors
pRB	Retinoblastoma Protein
PS	Phospholipid Phosphatidylserine
RAPTOR	Regulatory-Associated Protein mTOR Complex 1
RICTOR	Rapamycin-Insensitive Companion Of mTOR Complex 2
RMC1	Ruthenium(II) Methylimidazole Compound 1
ROS	Reactive Oxygen Species
RPM	Revolutions Per Min
RTCA	The Real Time Cell Analyzer
S Phase	Synthesis Phase
SCF	Skp1/CUL1/F Box Protein
SEM	Scanning Electron Microscopy
siRNA	Small Interfering Ribonucleic Acid
SSC	Side Scatter
SKK1	Ribosomal protein S6 kinase polypeptide
STS	Steroid Sulfatase
TEM	Transmission Electron Microscopy
TIGAR	TP53-Induced Glycolysis And Apoptosis Regulator
TNF	Tumor Necrosis Factor
TNFR	Tumor Necrosis Factor Receptor

TNFR1	Tumor Necrosis Factor Receptor 1
Tao kinases	Thousand And One Kinases
TRAIL	Tumor Necrosis Factor Related Apoptosis-Inducing Ligand
TRADD	Receptor Associated Death Domain
TRPM2	Melastin-Related Transient Receptor Potential
TSC2	Tuberous Sclerosis Protein 2
TUNEL	Terminal Deoxynucleotidyl Transferase Nick End Labelling
Ubl	Ubiquitin-Like Protein
UCP-1	Uncoupling Protein 1
UCP-2	Uncoupling Protein 2
UPR	Unfolded Protein Response
VEGF	Vascular Endothelial Growth Factor
Vps	Vacuolar Protein Sorting
WAF-1	Wild-Type p53-Activated Fragment 1
WEE-1	Wee1-Like Protein Kinase

Graphic demonstration of signaling pathways

All graphical diagrams of signaling- and transduction pathways were created using Microsoft® Office Publisher (Microsoft office enterprise 2007, 2006 Microsoft Corporation, United States of America). Structures were created by MH Visagie using ACD/ ChemSketch version 1101 released on 2007/10/19 (Advanced Chemistry Development, Inc., ACD/ Labs, Toronto, Canada). All figures of the results section were done using CorelDraw X3 version 13.0.0.0576 (2005 Corel Corporation, Canada) and exported in the TIFF format.

Chapter 1

1. Introduction

1.1 Cancer

1.1.1 Cancer incidence and risk factors

Cancer is the principal mode of death in developed countries and the second leading cause of death in developing countries (1). Breast cancer is the most frequently diagnosed cancer amongst women worldwide and an estimated 1.7 million new diagnoses will be made annually by the year 2020 (2, 3). Breast cancer patients (40%) often suffer a recurrence with 60-70% that experience distal metastases resulting in death (3, 4).

Complementary deoxyribonucleic acid (cDNA) microarray studies and immunohistochemical markers demonstrated different categories into which breast cancer can be classified including luminal A (estrogen receptor positive), progesterone receptor positive, human epidermal growth factor receptor 2 (HER2) negative, luminal B (estrogen receptor positive and/or progesterone receptor negative), HER2 overexpression (estrogen receptor negative, progesterone receptor positive, HER2 positive), basal-like (estrogen receptor negative, progesterone receptor negative, HER2 negative, cytokeratin 5/6 positive and/or epidermal growth factor receptor (EGFR) positive) and normal breast-like tumors (5, 6).

Risk factors for breast cancer include high socioeconomic status, being of Caucasian descent, obesity, increasing age, late onset of menopause, advanced age of first pregnancy carried to term, and having a first relative diagnosed with breast cancer (6). Elevated genetic susceptibility to breast cancer is due to a mutation in breast cancer gene 1 (BRCA 1) or breast cancer gene 2 (BRCA 2) (7). Furthermore, p53 mutations also increase breast cancer risk (8).

Northern America and Northern Europe reported amplified cancer incidence in women who postpone childbearing and who exert a lifestyle with a Western diet accompanied with little exercise (9). Supplementing steroid hormones including oral contraceptives, hormone replacement therapy and endogenous hormones also results in increased breast cancer risk. Environmental causes leading to increased breast cancer risk

include cigarette smoke, high alcohol consumption, disrupted sleeping routine and night shift occupations, use of anti-hypertensive agents for five years or more, exposure to diethylstilbestrol and ionisation radiation (10).

1.1.2 Current available breast cancer treatments

Primary breast cancer is confined to a small area; however, subclinical metastasis may still occur. Secondary breast cancer arises once tumorigenic cells separate from the primary breast cancer location, and are redistributed to different parts of the body for example in the brain, lungs and liver (4).

Local treatment affects the tumor and immediate surrounding cells and includes lumpectomy, mastectomy and radiotherapy; however metastasis is still possible (11). Surgery risks include infection, pulmonary complications, cardiac arrhythmias, heart attack and stroke. Radiotherapy is a significant part of conserving breast tissue in local therapy (11). Side effects of radiotherapy include hyperpigmentation, dry or moist desquamation, fatigue, meylosuppression, contralateral breast cancer, myocardial infarction, pneumonitis, lymph oedema, brachial plexopathy and skin shrinkage (8, 11). High intensity frequency ultrasound (HIFU) employs high intensity auditory waves and heat directing it at the tumor and surrounding tissues and destroys the target tissue. Since tissues are largely composed of fluids, HIFU potentially results in cavitation and significant cellular thermal damage (12).

Systemic treatment entails hormone- and chemical-infusions that lead to cell cycle arrest. Specific treatment is dependent on several factors including the tumor characteristics, cancer stage at time of diagnosis, age, weight and the physical condition of the individual (13).

Hormonal-dependent breast cancer treatment options typically utilize estrogen deprivation by means of ovarian ablation, estrogen receptor-specific interactions and aromatase inhibitors. Treatment options demonstrate aromatase inhibition and they include aminoglutethimide, formesatane, rogletimide, fadrozole, anastrozole, letrozole and exemestane. These compounds exert their anti-tumorigenic activity by inhibiting estrogen production through blocking the conversion of androstenedione to oestrone

(14, 15). Aromatse inhibition takes place by competing for the substrate of androgens. This is demonstrated by anastrozole and letrozole which contain triazole groups that interact with the heme group of aromatase (14). Aminoglutethimide, a non-selective aromatase inhibitor, is frequently accompanied with lethargy and rashes, while anastrozole is associated with headaches, hot flushes, gastrointestinal disturbances, weight gain, oedema, thrombo-embolic disturbances (16).

Analysis of estrogen receptor positive tumors treated with tamoxifen after primary surgery demonstrated differentially expressed genes of responders when compared to non-responders (17). Qualitative polymerase chain reaction (PCR) data revealed that HOXB14 and IL17BR messenger RNA (mRNA) levels are sufficient to predict the outcome of the therapy (17). *In vitro* research showed that these genes confer motile and invasive properties of the MCF-10A mammary cell line (17, 18). The progesterone receptor expression has been linked to benefits of tamoxifen treatment and letrozole (14). Tamoxifen treatment exerts several side-effects including increased risk of deep vein thrombosis, pulmonary embolus, hot flashes, vaginal discharge, irregular menstruation, weight gain, depression, cataracts and an increased possible risk of stroke in postmenopausal women (11, 18). However, tamoxifen in combination with lapatinib, results in rapid synergistic antipropliferative activity when compared to the drugs on its own (19). Lapatinib is also able to restore cells' sensitivity to tamoxifen. This is supported by studies involving lapatinib and trastuzumab in various different ErbB-2-overexpressing cell lines (19). Side effects of lapatinib include diarrhoea, rash, nausea, vomiting, headache and anorexia (18, 19).

1.1.3 Estrogen and estrogen receptors in breast carcinogenesis

A correlation between breast cancer risk and persistently elevated estrogen levels have been found consistently in various studies. Biologically strong estrogens such as 16α-hydroxylated estrogen metabolites are associated with breast cancer risk (20). In addition, woman diagnosed with breast cancer possessed an overall 15% higher concentration of estradiol present in their blood when compared to women that remained cancer-free (21). Animal studies have demonstrated that estrogens and estrogen-metabolites exert carcinogenic effects on several tissues including kidneys, liver, uterus and mammary glands (22).

The exact mechanisms responsible for estrogen-mediated carcinogenesis remains poorly understood. The conventional theory states that estradiol stimulates cell proliferation via the estrogen receptor α, and initiates mutations developing from replicative errors during pre-mitotic deoxyribonucleic acid (DNA) synthesis. Subsequently, estradiol enhances proliferation of cells harbouring mutations. Over a period of time, an adequate quantity (10-15%) of mutations occurs inducing tumorigenic transformation (23). More than 70% of breast cancers express high levels of estrogen receptors and many of these tumors require estrogen for sustained growth and progression (24). Increased estrogen receptor activity is mainly regulated by HER2 gene upregulation and results in poor response to endocrine therapy. The latter is treated with HER2-targeted therapy and endocrine therapy (25, 26). This combination leads to antiproliferative activity accompanied with inhibition of survival signaling originating from the estrogen receptor pathway (27).

1.2 Overview of the cell cycle

The cell cycle is a sequence of coordinated events resulting in cellular proliferation, senescence and cell death. The eukaryotic cell cycle consists of five stages: quiescent phase (G_0), the synthesis (S) phase, the mitotic phase (M) and two gap phases (G_1 and G_2). The S phase entails DNA replication, the M phase involves the segregation of two complete sets of chromosomes resulting in two daughter cells. The G_1 phase separates the M phase and the S phase, the G_2 phase separates the S phase and M phase (28).

The cell cycle is regulated and controlled by several protein heterodimer complexes that involve cyclins and cyclin-dependent kinases (CDKs). Kinase activity requires the presence of cyclins (28). There are 11 CDK family members recognised presently. CDK1, 2, 3, 4 and 6 play essential roles in the cell cycle and CDK7 activates the CDKs involved in the cell cycle (28, 29). Cyclins are of importance in the control of cells moving from the S phase to the M phase. B cyclins are essential in G_2M transition and the regulation of cells in the M phase. H cyclins are plays a role in CDK-activating kinase process (30).

Phosphorylation and dephosphorylation of CDK and cyclins are essential in the cell cycle since they regulate kinase activity (31). Phosphorylation is accomplished utilizing cyclin-activating kinase and the cell division cycle 25 (CDC25) family of dual-specificity protein phosphatases is responsible for mediating dephosphorylation (32). An example of the latter includes $p34^{cdc2}$ phosphorylation at threonine 14 and tyrosine 15 resulting in the subsequent inactivation of CDC2/cyclin B complexes regulating cells entering the M phase. Once cells are prepared for the G_2M transition, CDC25 removes the phosphates from the kinase (31). CDK-activating kinase (CAK) is an enzyme accountable for activation by CDK1, CDK2, CDK4 and CDK6 phosphorylation (33). The subunit of CAK is CDK7. Active human CAK contains additional polypeptides of approximately 36 and 32-kDa. The 32kDa polypeptide is also known as cyclin H (31).

1.2.1 Cell cycle phases

1.2.1.1 The G_1 phase

The G_1 phase determines whether all conditions based on nutrients and growth factor availability are acceptable for the cell to enter the S phase (28). This is accomplished by utilizing the retinoblastoma (RB)/E2F/DP pathway (30). In the G_1 phase, D cyclins are produced and bind to CDK4 and CDK6. The RB gene is phosphorylated by CDK4-cyclin D and CDK6-cyclin D and subsequently transcription factor E2F release. This results in transcription of genes necessary for the G_1/S transition and S phase. CDK2-Cyclin E also phosphorylates Rb and E2F to ensure its own transcription. These two actions create a positive feedback loop promoting the S phase (28). The E2F family can be divided into 2 categories based on the function namely, activating E2F (E2F1, E2F2 and E2F3) and repressing E2F's (E2F4 and E2F5). Activated E2Fs upregulates target gene transcription during the G_1/S transition. Repressed E2F's mediates gene silencing during G_0/G_1. pRB, p107 and p130/Rbl2 confer cell cycle dependent-regulation to the E2F activities by means of phosphorylation and dephosphorylation. During the G_1/S transition, the above-mentioned genes are hyperphosphorylated by CDK-complexes liberating E2F1, E2F2 and E2F3 that activate gene transcription necessary for DNA synthesis and cell cycle progression (34).

1.2.1.2 The S phase

During the S phase, chromosomes are replicated by means of DNA replication. It is essential that this step occurs correctly since the eukaryote cell's fate depends on it (35). Initiation of DNA replication during the S phase involves six-subunit complexes called origin recognition complex (ORC) binding to chromosomal regions called origins of replication (36). There are 6 ORC's currently known, ORC1 to ORC6, named in descending molecular mass; which is located among six chromosomes (37). Cdt1 and CDC6 bind and recruit the MCM2-7 complex to the origin. The MCM2-7 refers to the putatative replication origin that unwinds DNA and allows downstream factors to access DNA replication initiating. The pre-replicative complex (pre-RC) active in M and G_1 phases consists of ORC, Cdt1, CDC6 and MCM2-7 complex (38). Geminin, a DNA replication inhibitor, (also known as GMNN) avoids chromosomal polyploidy, while contributing to cell cycle progression and proliferation (38).

1.2.1.3 G_2M phase

The G_2 phase and the S phase are compelled to continue through activated CDK1-cyclin A and CDK1-cyclin B complexes. Cyclin B expression is upregulated in the G_2 phase and when cyclin B reaches the threshold, depending on this kinase and the cell will enter mitosis. Mitosis consists of several phases including prophase, metaphase, telophase and anaphase. Cyclin B activity continuous during mitosis and is degraded in anaphase. CDK1 activity loss results in activation of the mitotic exit and subsequent cell cycle completion (39). Mitotic exit consists of an orchestrated sequence of events leading to the segregation of sister chromatids to mitosis completion. Anaphase is initiated by the anaphase promoting complex (APC) ubiquitination and its activator CDC20 (APC^{CDC20}). Securin is degraded, allowing for the release of separase that cleaves cohesions and instigates chromatid separation (40). APC^{CDC20} targets mitotic cyclins for degradation accompanied with CDK downregulation (41). The APC consists of multi-subunit E3 ubiquination ligase that is responsible for the transitions in the cell cycle. A subunit *emb-30* is required for the metaphase-anaphase transition and encodes APC4 (41).

1.2.2 Protein degradation in the cell cycle

Protein degradation is essential for several cellular processes including cell cycle transitions. Cell cycle regulators are degraded by two ubiquitin E3-ligase complexes

namely, Skp1/CUL1/F box protein (SCF) and anaphase promoting complex/cyclosome (APC/C) (42, 43). Proteins contain domains and sequence motifs that serve as degradation signals for proteolysis by proteases. These regions are rich in proline, glutamic acid, serine and threonine indicating that the protein possesses a short lifetime (44). The majority of proteins in eukaryotic cells are degraded by 26S proteases that contain 20S core and 19S regulatory complexes. The 20S core unit included two chymotrypsin-like sites responsible for severing peptide bonds, two trypsin-like sites that cleave basic residues and two caspase-like proteolytic sites that separate acidotic residues (44, 45).

A short sequence near their N terminus called the destruction box (D-box) is essential for ubiquitin/proteasome-dependent proteolysis of cyclin A and cyclin B. The ubiquitin ligase E3 for cyclin B1 in mitosis is the anaphase-promoting complex/cyclosome complex with CDC20. Cyclin A is degraded by anaphase-promoting complex/cyclosome-CDC20, although the difference in the timing of degradation between cyclin A and cyclin B1 argues for the involvement of distinctive mechanisms (45).

Thus, eukaryotic cells react to cellular stress by utilizing several cell cycle checkpoints that is accountable for the cell cycle arrest. Two major cell cycle checkpoints have been classified namely, G_1/S and the G_2M checkpoint. The p38 mitogen activated protein kinase (MAPK) pathway is involved in both these checkpoints (46).

1.2.3 Cell cycle checkpoints

1.2.3.1 G_1/S checkpoint

Prior and following DNA replication the G_1/S checkpoint is responsible and active (46). Cellular damage leading to slower DNA replication resulted in the detection of *Ataxia Telangiectasia Mutated (ATM*) that phosphorylates several proteins active in checkpoint signaling. DNA replication is possibly slowed down by the checkpoint or ORC resulting in inhibition of the replication fork (47). Stress activates ATM and Rad3-related kinase (ATR) or only ATM that activates checkpoint kinase 2(CHK2). CHK2 phosphorylates CDC25A resulting in its degradation. ATR activates checkpoint kinase 1 (CHK1) and subsequent CDC25A degradation in reaction to UV radiation. CDC25A phosphatase

degradation prevents dephosphorylation and activation of CDK2-cyclin E (47). Double strand DNA breaks activates p38 MAPK pathway that is dependent on Ser/Thr protein kinases activation. ATM activates thousand and one (TAO) kinases that induce the p38 MAPK pathway. Furthermore, the p38 MAPK pathway is also activated in the presence of caffeine which is an ATM inhibitor. Thus, p38 MAPK pathway activation can be induced by additional signaling pathways where ATM/ATR is not involved. Nonetheless, these alternative signaling pathways that induce the p38 MAPK pathway still remains elusive and several questions remain (46).

1.2.3.2 Restriction point

The transition from the serum-dependent (cells entering G_1 from mitosis needs serum mitogens) to the serum-independent state is known as the restriction (R) point (48, 49). Cyclin D (D1, D2 and D3) and their associated partners, CDK4/CDK6 are implicated in the initial pRB phosphorylation (49, 50). Phosphorylation of pRB at the entry and exit of the S phase are regulated by CyclinE/CDK2. When pRB is hypophosphorylated, the cell is unable to enter S phase due to the association of pRB with a group of E2F transcription factor members (E2F1-5). E2F1-3 binds to pRB, E2F4 and E2F5 binds to pRB-related proteins p107 and p130 (50). Following cell transition past the restriction point, the cell is committed to DNA replication even in the absence of proliferative signals (33).

1.2.3.3 G_2M checkpoint

Double strand DNA breakage activates the p38 MAPK pathway resulting in the activation of the G_2M checkpoint (46). The pathway by which p38 MAPK induces G_2M arrest remains inadequately understood. One possibility involves the p53 phosphorylation and activation leading to the G_2M checkpoint. Dissociation of p53 and Murine double minute 2 (Mdm2) results in p53 accumulation. Mdm2 is a protein that inhibits p53 and induces degradation using ubiquitination. Activation of p53 results in the activation of genes involved in the G_2M checkpoint including DNA damage inducible factor α, p21 and 14-3-3 (46). Furthermore, p38 MAPK activates the G_2M checkpoint through CDC25B phosphorylation. CDC25B dephosphorylates CDC2, activating cyclin B/CDC2 responsible for cell cycle progression. CDC25B phosphorylation inhibits its own activity by enhancing association with 14-3-3 proteins sequestered in the

cytoplasm. MAPK promotes CDC25B phosphorylation by activating MK2, a substrate of p38 MAPK. Activation of MK2 has been suggested as an essential component for G_2M checkpoint induction (46).

The CDK1/cyclin B1 complex regulates mitosis entry, cyclin B degradation permits mitosis entry for the cell (51). Unsuitable CDK1/cyclin B1 complexes activation result in cell cycle succession, bypassing the G_2M checkpoint and subsequent improper mitosis entry and formation of tetraploidy cells containing damaged DNA (52). Cyclin B is degraded by p21 however. Studies demonstrate that cyclin B associates with p21 after DNA damage has occurred. Cyclin B1 then is directed to the APC/C that targets it obliteration (51).

1.2.3.4 Mitotic checkpoint

During mitosis, replicated chromosomes segregate to both daughter cells. Sister chromatids attach to the bipolar mitotic spindle in prometaphase and then advances through mitosis. Erroneous attachment of chromatids to mitotic spindle results in asymmetrical separation of chromosomes (53). The spindle checkpoint regulates the transition of metaphase to anaphase until the chromosomes are attached in the correct bipolar way to the mitotic spindle (53). The mitotic checkpoint postpones anaphase by employing inhibitory signals produced by the kinetochore to prevent APC/C activation. This leads to high levels of cyclin B and securin that delay anaphase onset. The kinetochore coordinates the assembly of centromeres. With the occurrence of chromosomal attachment at the sister kinetochores, the inhibitory signals discontinue to be generated, resulting in the transition of the cell into anaphase (54).

The APC is inactive in cells arrested via the mitotic checkpoint. APC is thus believed to be targeted by the mitotic checkpoint. Previous reports indicate that several genes are involved in the mitotic checkpoint machinery, including MAD1, MAD2, MAD3, BUB1, BUB2, BUB3 and MPS1 (55). Bub1 and Mad1 serve as scaffolds for recruitment of Mad2 and BubR1/Mad3 that are capable of generating inhibitory signals. Mad2 interacts with CDC20 which is required for inhibition of APC by the mitotic checkpoint (53).

1.3 Mechanisms of cell death

Several modes of cell death including apoptosis, oncosis, autophagy, mitotic catastrophe, metabolic catastrophe and necrosis are acknowledged and will be discussed below. Cell death may be classified according to its morphological appearance (which may be apoptotic, necrotic, autophagic or associated with mitosis), enzymological criteria (the possible involvement of nucleases of proteases, such as caspases, cathepsins and transglutaminases), functional aspects (programmed or accidental) and immunological characteristics (immunogenic or non-immunogenic) (56, 57, 58). Programmed cell death (PCD) is critical for development, regulation and maintenance of multicellular organisms. Although PCD is used several times as a synonym for apoptosis, other forms of PCD also exist including autophagy. Necrosis and metabolic catastrophe are types of uncontrolled cell death (56, 57).

1.3.1 Apoptosis

The term ‘apoptosis’ originates from Greek referring to the falling off of leaves (58, 89). Apoptosis is an energy-dependent irreversible systematic eradication of redundant, aged, injured and abnormal cells by a series of controlled molecular steps regulated by an intracellular program (60). Apoptosis is a well-known vital component of several processes including controlled cell turnover, appropriate development and functioning of the immune system, hormone-dependent degeneration, embryonic development and chemically-induced cell death. Improper apoptosis regulation results in serious consequences including neurodegenerative diseases, ischemic damage, autoimmune disorders and cancer (60). Apoptosis is generally categorized as one of three modes namely, intrinsic (also known as the mitochondrial pathway), extrinsic (also known as death receptor pathway) and the endoplasmic pathway.

The extrinsic pathway entails death receptors and the intrinsic pathway entails the mitochondria and the BCL-2 family (Figure 1.1) (58). Intrinsic and extrinsic apoptosis are triggered by cell death stimuli from intracellular- and extracellular environments, respectively. This results in caspase activation which is the core component of the apoptotic machinery (60, 61). In addition, caspase-independent apoptotic pathways have also been described.

Apoptosis encompasses specific morphological hallmarks including rounding of the cell, retraction of pseudopodes, cytoplasmic- and nuclear condensation, chromatin condensation, nuclear fragmentation, plasma membrane blebbing and engulfment by surrounding phagocytes (58, 59). An additional characteristic of apoptosis is the externalization of the lipid phosphatidylserine bilayer regulated by activation of calcium-dependent phospholipid scramblase activity accompanied with aminophospholipid translocase inactivation at the cellular surface (56, 59, 61, 62). This results in expression of cell surface indicators that generates early phagocytic recognition by surrounding cells of apoptotic cells, allowing for phagocytosis with minimal damage to the neighbouring tissue (56).

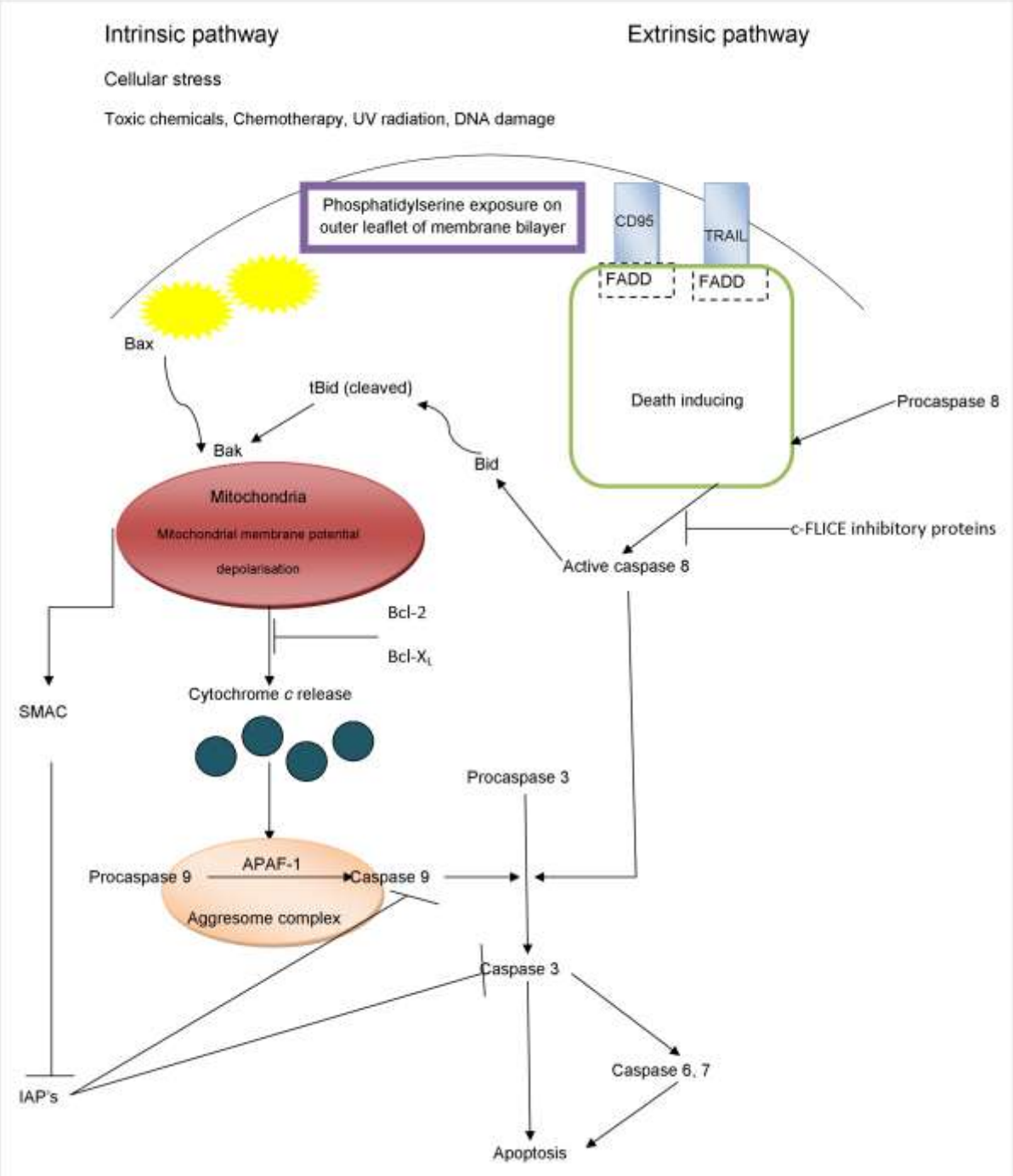

Figure 1.1: The intrinsic (mitochondrial) and extrinsic (death receptor) apoptotic pathway. During the intrinsic pathway the cell experiences an injury (toxic stress and DNA damage) resulting in a mitochondrial membrane potential depolarisation and subsequent cytochrome *c* release. Apoptosis activating factor 1 (APAF-1) activates caspase 9 leading to caspase 3 activation. Furthermore, SMAC/Diablo inhibits the inhibitor of factors (IAPs). In the extrinsic pathway the ligand binds the receptors (CD95 and Tumor Necrosis Factor Related Apoptosis-Inducing Ligand (TRAIL)) resulting in the formation of death inducing signaling complex (DISC) which assists in caspase 8 activation. Caspase 8 can cleave BH3-Interacting Domain Death Agonist (Bid) resulting in activation of the intrinsic pathway or caspase 8 also cleave caspase 3. Caspase 3 activation will result in apoptosis or can induce apoptosis by activating caspase 6 or caspase 7 (56, 58, 60, 61).

1.3.1.1 Caspase-dependent apoptosis

Caspases is a family of cysteinyl aspartate proteinases (cysteine proteases that cleave substrates at specific aspartyl residues) and are required for apoptosis induction (63, 64). Apoptotic caspases belong to one of two categories; initiator (upstream) caspases or effector/executioner (downstream) caspase (65). Initiator caspases include caspases 2, 8, 9, and 10 (66). Effector caspases include caspases 3, 6, and 7 (65). An example of the latter is caspase 9 that is involved in muscle differentiation (67). There are three caspase-dependent cell death pathways including the mitochondrial pathway (intrinsic), death receptor pathway (extrinsic) and endoplasmic-specific pathway (56). Although the intrinsic and extrinsic cell death pathways operate independently to initiate cell death in particular signaling pathways, in most tumorigenic cells, there is a delicate crosstalk between these pathways which results in the activation of executioner caspases (68).

1.3.1.2 Death receptor (extrinsic) pathway

The extrinsic pathway eliminates abnormal or unnecessary cells and is initiated by the ligand-bound death receptors at the plasma membrane, including tumor necrosis factor/tumor necrosis factor receptor 1 (TNF-TNFR1), FasL-Fas and TRAIL-death receptor (DR) 4 or -DR5 (Figure 1.1) (69, 70). Death receptors are a component of the tumor necrosis factor receptor (TNFR) gene superfamily and have numerous responsibilities including triggering apoptosis. The TNFR superfamily is characterised by presence of cysteine-rich domains (CRDs) that regulate binding between ligands and type I transmembrane domain receptors including TNF receptor-1 (TNFR1), CD95 (also known as Apo-1 or Fas) and TRAIL receptors DR4 and DR5. A soluble Fas decoy receptor, DcR3, and additional decoys for TRAIL including DcR1, DcR2 and OPG were also identified (68, 70). Following extrinsic pathway initiation, death receptors accumulate at the cell surface after ligand binding to the extracellular domains. Subsequently, adaptor molecules are recruited to the receptors at the aggregated intracellular domains of (70). One of the adaptor molecules, Fas-associated death domain (FADD) consists of two domains where the death domain (DD) interacts with ligand directly or by using another adaptor molecule namely, TNF-receptor associated death domain (TRADD) (56, 68). The second FADD protein interaction domain, death effector domain (DED) interacts with the DED of the zymogen, pro-caspase 8

producing DISC (68). DISC facilitates the cleavage of caspase 8 resulting in activation of effector caspases 3- and 7 (Figure 1.1) (8, 71). More than 280 proteins have been identified so far that are degraded by these effector caspases. These proteins are involved in various areas of cellular processes including scaffolding of the cytoplasm and nucleus, signaling transduction, regulation of cell cycle progression and DNA replication and repair (72, 73).

Several chemotherapeutic compounds trigger apoptosis by altering death receptors on the cell surface. For example, doxorubin elevates FAS expression on tumor cell surfaces (74). Apo-2 ligand (Apo-2L) is a member of the TNF-superfamily with structural and functional similarities to Fas/Apo-1L (75). Apo-2L induces apoptosis in tumors. Combination treatment of Apo-2L and 5-fluorouracil (CPT-11) demonstrated considerable tumor regression (74). Studies indicate that TRAIL alone is inadequate in cancer treatment since resistance frequently occurs. Receptor regulation and cytosolic factors modulating apoptosis are induced by TRAIL and regularly results in TRAIL resistance. Infant neuroblastoma cells possessing a silent caspase 8 gene is resistant to TRAIL (76). However, chemotherapy agents including doxorubicin, epirubicin and cisplatin associated with TRAIL successfully treated TRAIL-resistant renal, prostate and bladder carcinomas as the chemotherapeutic agents, sensitize the tumorigenic cells to TRAIL (77, 78).

1.3.1.3 Mitochondrial (intrinsic) pathway

The intrinsic pathway initiates apoptosis by means of mitochondria involvement and is triggered by DNA damage due to irradiation, chemicals, lack of growth factors or oxidative stress (Figure 1.1) (70). Mitochondrial apoptotic pathway is characterised by mitochondrial outer membrane permeabilization (MOMP) that is considered the ‘point of no return’ (79). MOMP occurs as the electrochemical gradient across the mitochondrial membrane collapses through the formation of pores in the mitochondria by B-cell lymphoma-2 (BCL-2) proapoptotic family members proteins (79, 80, 81, 82, 83).

The BCL-2 family consists of anti-apoptotic and pro-apoptotic proteins and these proteins share regions of sequence homology within conserved regions known as BCL-2 (BH) domains. Anti-apoptotic protein members (Bcl-2 and Bcl-X_L) and the pro-

apoptotic protein subset (Bax and Bak) are multidomain proteins sharing sequence homology within three or four BH domains (84). The BCL-2 Homology Region 3-subset (BH3) of pro-apoptotic proteins include Bad, Bid, Bim, Noxa, Bik, Hrk, and Puma that all demonstrate sequence homology located within a single a helical segment, the BH3 domain. These domains are also identified as the minimal death domain necessary for binding to multidomain BCL-2 family members (84, 85).

MOMP involvement in apoptosis takes place by releasing molecules necessary for apoptosis induction and loss of mitochondrial functions crucial for cell survival. Permeabilization of the outer membrane results in release of cell death activating factors into the cytosol including cytochrome *c*, second mitochondria-derived activator caspase/direct IAP protein with low PI (Smac/DIABLO), apoptosis-inducing factor (AIF) and endonuclease G. These cell death activating factors activate caspases that cleave cellular substrates resulting in the demise of the cell (86). Once cytochrome *c* is released into the cytosol, the apoptosome forms and functions as a molecular platform for caspase 9 activation (87). The apoptosome contains three components namely, cytochrome *c*, apoptosis activating factor 1 (APAF-1) and ATP/dATP. APAF-1 contains three domains including a N-terminal caspase-recruiting domain (CARD), an expanded nucleotide domain and a 12-13 WD40 repeats domain (negative regulatory element which binds to CARD) at the carboxy terminal (88, 89). CARD interacts with the prodomain of caspase-9, and in combination with the nucleotide binding domains are responsible for oligomerization of APAF-1 in the presence of cytochrome *c*. The WD repeats interact with cytochrome *c* for the removal of this domain. The aforementioned activities result in caspase 9 activation. Furthermore, the binding of cytochrome *c* and APAF-1 result in hydrolysis of ATP to dATP, releasing energy and heat (90). Active caspase 9 cleaves executioner caspases to induce apoptosis mainly through the activation of caspase 3 and caspase 7 (91, 92).

The mitochondrial pathway is targeted in several cancer treatments. Reports indicate that a compound, MPT0B214 derived from the backbone of 5-amino-2-aroylquinolines activates the intrinsic mitochondrial-dependent pathway by a reduction in the mitochondrial membrane and caspase 9 activation in cervical adenocarcinoma cells contaminated papilloma virus (KB cells) (93). Exposure to a ruthenium(II)

methylimidazole compound, RMC1, resulted in a reduction in the mitochondrial membrane potential, upregulated Bax and Bad expression, downregulated Bcl-2 and Bcl-xl expression and cytochrome *c* release in the human lung adenocarcinoma A549 cell line cells (94). Another study demonstrated allyl isiothiocyanate induced the mitochondrial pathway in human breast adenocarcinoma (MDA-MB-468) cell line by loss of mitochondrial membrane potential and release of cytochrome c and APAF-1 (95). Mitochondrial dynamics and their regulation are potential crucial targets for cancer cells resulting in improved and increased proliferation, as well as a manner to efficiently escape the programmed cell death machinery, the major protective mechanism against tumorigenesis. Thus, treatment targeting the mitochondria may be hugely beneficial in eradicating cancer (96).

1.3.1.4 Endoplasmic reticulum pathway

The endoplasmic reticulum (ER) is highly sensitive to modifications in the surrounding environment including calcium (Ca^{2+}) homeostasis (97). The ER also possesses an imperative role serving as the major supplier of Ca^{2+} within the cell. This Ca^{2+} source is essential for several signaling pathways including fertilization, differentiation, proliferation and transcription factor activation thereby influencing gene transcription and expression, protein and steroid synthesis and apoptosis (98).

Chemical agents, inhibitors of glycosylation, oxidative stress and accumulation of misfolded proteins can potentially disrupt ER function known as ER stress. This results in unfolded protein response (UPR), ER-overload response (EOR) and ER-associated degradation (ERAD) (97). Prolonged ER stress might be due to apoptosis activation via both the mitochondrial dependent and independent pathway.

The mitochondrial-independent pathway takes place using initiator caspase 12. Activation of caspase 12 appears to be triggered only by various stimuli that activate ER stress. Caspase 12, localised in the ER membrane is produced as an inactive proenzyme consisting of a regulatory prodomain and two catalytic subunits and is cleaved and activated by the Ca^{2+}-dependent protease m-calpain. Active caspase 12 activates caspase 9 which activates effector caspase 3 (97, 98, 99). Caspase 4 is the human homolog of murine caspase 12 and is localized to the ER membrane and is

specifically activated by and required for ER stress-induced apoptosis (100). Overexpression of the transmembrane portion of Bap31 leads to premature Ca^{2+} release into the mitochondria, resulting in the mitochondria being sensitized to caspase 8 and cytochrome *c* (101). Recent findings demonstrated that Bcl-2 is involved in the ER pathway as well. Release of Ca^{2+} from the ER is taken up into the mitochondria resulting in reduced apoptosis in Bax and Bak knockout mice (102).

1.3.2 Caspase-independent apoptosis

Non-caspase proteases including cathepsins, calpains (cytosolic calcium activated cysteine proteases), granzymes, endonuclease G (endoG) and AIF are reportedly effectors of apoptosis (58,103). The release of EndoG and AIF occurs during the permeabilization of the outer mitochondrial membrane resulting in cell obliteration (86). Subsequently, EndoG and AIF translocate to the nucleus, where AIF induces DNA fragmentation and peripheral nuclear condensation. Furthermore, mitochondrial EndoG is a mitochondrial nuclease that aids in preservation the mitochondrial genome by participating in mitochondrial DNA duplication and repair (104, 105). Following EndoG entrance into the nucleus, endoG cleaves the nuclear chromatin (56, 86). Calpain and cathepsin activated by Ca^{2+} influx degrade cytoplasmic proteins resulting in the ultimate cell destruction (70). Granzyme B is a serine protease family member exclusively expressed by cytotoxic T-lymphocytes. Granzyme subfamilies are first expressed as zymogens containing cytolytic granules. Following receptor-mediated fusion cytotoxic lymphocyte with an infected target cell, granzyme enters the cell and triggers apoptosis. Granzyme B includes active sites similar to cysteine proteases of the caspase family. The latter permits for the cleavage of aspartate residues and activates the caspase cascade by activating several procaspases (106). Furthermore, granzymes are also able to cleave the pro-apoptotic Bcl-2 family members Bid and Bax, thereby inducing mitochondrial membrane permeabilization (107).

1.3.3 Autophagy

Another form of cell death is autophagy which literally means ‘self-eating when translated from the original Greek word (108). Autophagy is an evolutionary conserved multistep catabolic pathway where unnecessary or impaired intracellular contents are degraded while providing nutrition. Autophagy functions include remodelling during

development, amino acid production, energy creation and removal of unwanted or damaged organelles.

Autophagy is induced by a variety of stimuli including stress, starvation, changes in cell volume, oxidative stress, accumulation of misfolded proteins, irradiation, TRIAL treatment and hormonal signaling (Figure 1.2).

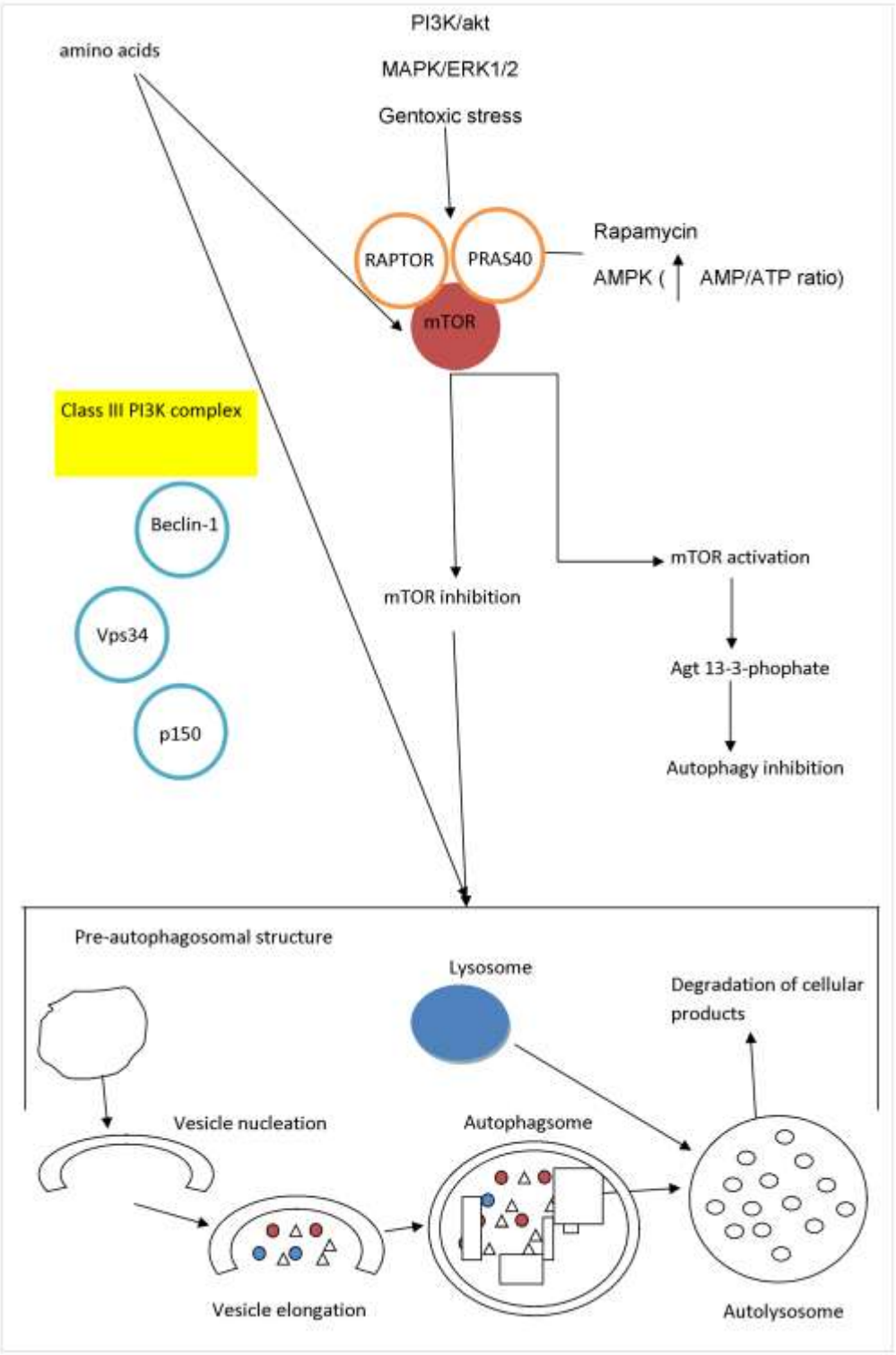

Figure 1.2: Autophagy is a result of nutrient deprivation, genotoxic stress and signaling from Phosphatidyl-3-Kinase (PI3K/akt) and P38 Mitogen Activated Protein Kinase/Extracellular Signal-Regulated Kinase 1/2 (MAPK/ERK1/2). Mammalian Target Of Rapamycin (mTOR) interacts with Regulatory-Associated Protein mTOR Complex 1 (RAPTOR) and proline-rich Akt substrate of 40 kilodaltons (*PRAS40*). If mTOR is activated, autophagy does not take place. However, if mTOR is effectively inhibited by rapamycin, autophagy is induced and cellular nutrients are sequestered and degraded (67, 102, 108).

Two major systems involved in protein degradation include the ubiquintin-proteosome pathway and autophagic system (102). Autophagy includes numerous steps namely nucleation, expansion, maturation and docking and fusion. During nucleation an unidentified membrane source transports lipid bilayers for phogophore formation (preautophagosomal structure in yeast). The expansion step (also known as isolation membrane stage) refers to the double-membrane vesicle formation by means of invagination from the preautophagosomal structure.

During maturation the autophagsosome experiences several steps including fusion events with multi-vesicular and endosomes. During docking and fusion the inner membrane compartment and its constituents are fused with the lysosome/autolysosome that is degraded by lysosomal hydrolases (108, 109). Several modes of autophagy have been described including chaperone-mediated autophagy (CMA), piecemeal microautophagy, macroautophagy and microautophagy. During CMA, unfolded proteins are the transported across the membrane at the lysosomal membrane. Piecemeal microautophagy has only been reported to occur in yeast and degrades nucleus portions by transporting them to the vacuole yeast. Macroautophagy utilizes specialised cytosolic vesicles that fuse with lysosome with the intention of cytoplasm sequestering and consequent degrading. During microautophagy the cytoplasm is internalised into the lysosome by means of invaginations in the lysosome membrane (110).

1.3.3.1 Chaperone-mediated autophagy

Starvation induces CMA resulting in protein degradation in a molecule-to-molecule fashion (111). CMA involvement has been found in autophagy induced by nutrient deficiency, stress and several diseases like Parkinson's disease (wild-type α-synuclein degradation) (111, 112, 113). The substrate of CMA consists of cytosolic proteins recognised by the heat shock protein (hsp) 70 chaperones. The chaperone-substrate complex attaches to the CMA receptor, lysosomal-associated membrane protein-2A (LAMP-2A) (112). Three different isoforms of LAMP-2 exist by alternative splicing namely, LAMP-2A, LAMP-2B and LAMP-2C. LAMP-2A alone acts as a receptor in autophagy. The role of LAMP-2B and LAMP-2C are uncertain (111, 112). Removal of all LAMP-2A isoforms results in accumulation of autophagic vacuoles in cytoplasm

(114). A pool of LAMPA-2A residues in the lysosomal lumen is capable of reinserting themselves for CMA activation. In old liver cells this process is defective indicating that LAMP-2A levels in older cells are declining, suppressed or inactive. Nevertheless, the degradation rate of LAMP-2A is accelerated in senescent fibroblasts (114). This accelerated process is due to different proteases than proteases used in younger cells for LAMP-2A degradation. An increase in LAMP-2A transcription rate may restore CMA rates (111).

1.3.3.2 Macroautophagy

Macroautophagy is a process by which cellular components and organelles are sequestered into double membrane vesicles known as autophagosomes with subsequent degradation conducted by lysosomes and endosomes (115). Following autophagy induction, autophagy-related genes (ATGs) coordinate the configuration of autophagic vesicles from the phogophore, segregation of the membrane to the phagosome and ultimately the autolysosome. The ULK-ATG13-FIP200 and the Beclin-1-hVps34-p150 complexes mediate nucleation events, whereas the ubiquitin-like conjugation systems (ATG5–ATG12 and LC3-II) direct vesicle elongation and autophagosome formation. Cellular constituents are eventually sequestered within the autophagosome and are thus removed from the cytoplasm. Intracellular content is degraded into autolysosomes, which is the product of lysosome and autophagosome fusion (108). The autolysosome refers to an acidic vesicle in which the intracellular material is destroyed by lysosomal hydrolases, for example cathepsins. Amino acids and other end products generated during the catabolic process are subsequently released from the autolysosome in order to fuel cellular processes and cell maintenance (108, 115, 116).

Studies have identified 30 ATG genes in yeast including ATG genes involved in starvation-induced autophagy and cytoplasm-to-vacuole targeting pathway. The core machinery includes ATG9, the recycling system consisting of ATG9 and the ATG1 kinase complex, ATG2 and ATG18. Other core machinery include phosphatidylinositol 3-OH kinase (PI3K) complex (vacuolar protein sorting (Vps) 34, Vsp15, ATG6, ATG14) and the ubiquitin-like protein (Ubl) system. The latter consists of two Ubl proteins (ATG8 AND AGT12), an activating enzyme namely AGT7, two analogues of ubiquintin-

conjugating enzyme (AGT10 and AGT3), Agt8 modifying protease (Agt4) and the protein target of ATG12 attachment (ATG5) and ATG 16 (Figure 1.3) (110). Vesicle nucleation development is dependent on PI3K activity, hVsp34 and the formation of the complex with Beclin 1 (Agt6) and hVps35.

Vesicle elongation and completion is dependent on two Ubl systems which is triggered through ATG7 and binds to AGT10 that is transferred to ATG5. Subsequently, ATG5 forms a multimeric complex (ATG12-ATG5-ATG16) with ATG16. Several ortholoques has been identified in mammalian cells namely MAP1LC3 (LC3), GABARAPL2 (GATE16), GABARAP and GABARAPL1 (ATG8L) (52). LC3 is the target of post-translational modifications. LC3-I (distributed in the cytoplasm) is transformed to LC3-II by a series of reactions catalyzed by Apg7 and Apg3 (117). In addition, LC3 competes with LC3-I in order to bind to phosphatidylethanolamine (PE) to form LC3-II on the autophagosome surface (Figure 1.3) (108, 117). Enhancement of LC3-I conversion to LC3-II results in the increased occurrence of autophagy. Detection of LC3-II is thus a valuable indicator for autophagy induction (118).

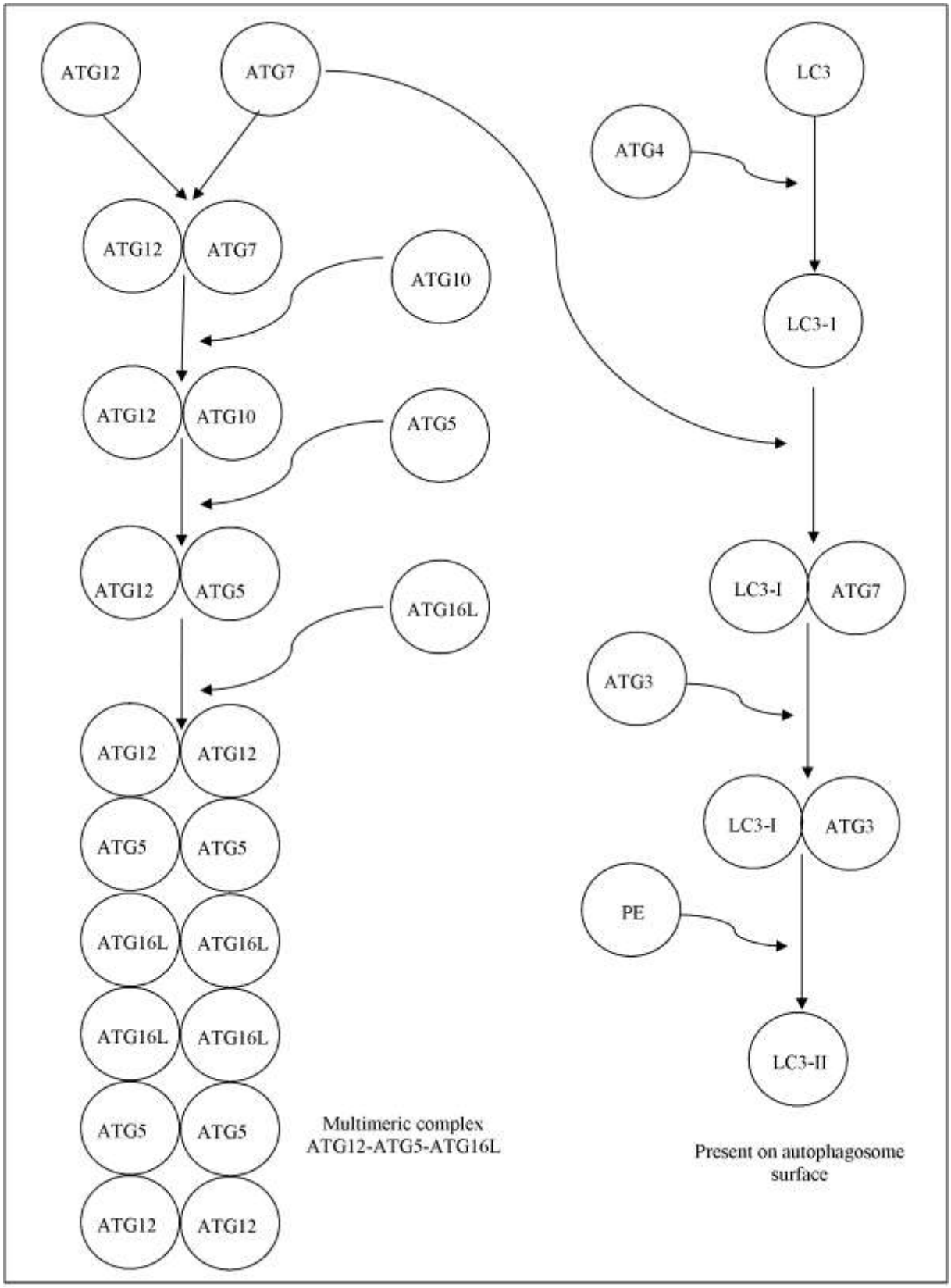

Figure 1.3: Macroautophagy elongation and completion is dependent on the interaction between various components and genes. ATG12 interacts with ATG7, ATG5 and ATG16L to produce a multimeric complex containing ATG12-ATG5-ATG16L. LC3-II is formed by a sequence of steps with LC3 interacting with ATG4, LC3-1 binds to ATG7 and ATG3 and lastly with PE and subsequently LC3-II is formed on the autophagosome surface (52, 110, 117).

Autophagy is mediated by negative feedback mechanism since the final products namely, amino acids, act as a negative feedback regulator (119). Furthermore, serine/threonine kinase mTOR inhibition containing ULK1/2 triggers autophagy, even in the presence of amino acids. mTOR is an upstream regulator of amino acid-dependent suppression of autophagy (119). Inhibition of mTOR-induced phosphorylation of ULK and ATG13 releases ULK kinase activity (120, 121). mTOR serves as the major kinase for two multiprotein complexes including mTOR complex 1 and mTOR complex 2 (mTORC1/2). Regulatory-associated protein mTOR complex 1 (RAPTOR) is a constituent of TORC1 and mTORC1. Rapamycin-insensitive companion of mTOR complex 2 (RICTOR) is a component of mTORC2. Activation of mTORC1 results in protein production using RPS6KBI, ribosomal protein S6 kinase polypeptide (SKK1) and EIF4EBP1, eukaryotic translational initiation factor 4E binding protein 1 (4EBP1). Studies suggest that mTORC2 initiates AKT activity using phosphorylation and enhances hypoxia-inducible factor 1α (HIF-1α) (108). TORC1 activity is mediated by TSC1, TSC2 and LKB1 that blocks mTOR activation by inhibiting small GTPase. AKT regulates mTOR activity through phosphorylating and TSC2 downregulation, which in turn impedes the function of the TSC1–TSC2 complex, promoting mTOR activation (115).

Beclin 1 is the mammalian homologue of the yeast protein AGT14 (53). Beclin 1 forms a complex with PI3K. Beclin 1 is a haploinsufficient tumor suppressor and inhibited by anti-apoptotic proteins such as the BCL-2 family members (120). Beclin 1 forms a heterodimer that is stabilised by BCL-2 anti-apoptotic members through the BCL-2-homology domain 3 domain (108). This complex is present in the Golgi complex indicating that it responsible for autophagy regulation through providing phosphatidyllinositol 3-phosphate to the isolation membranes (119). Beclin 1 also participates in proteolytic processing of procathepsin D from the Golgi apparatus to the lysosomes (120). MCF7 breast epithelial adenocarcinoma cells expressing low Beclin 1 levels do not exhibit starvation-induced upregulation of autophagy. Beclin 1-regulated rescue of starvation-induced autophagy in MCF-7 cells is subdued by Bcl-2 and Bcl-X_L expression (120).

1.3.3.3 Microautophagy

Microautophagy is a term first used in 1966 and is defined as the degradation process in which portions of the cytoplasm, organelles and intracellular components including the macromolecules are directly taken up and internalised into the lysosomal matrix by means of invaginations in the lysosomal membrane that provides intralysosomal vesicles (121, 122). Lysosomal membrane invaginations are then pinched off and degraded with the sequestered cytoplasm and cellular components (122). Dubouloz *et al.* (2005) reported that rapamycin-sensitive mTOR signaling pathways positively regulate proliferation in reaction to nutrient availability. mTOR depletion or treatment with rapamycin demonstrated that cells were present in the quiescent phase (123). Microautophagy is employed in fungi for selective organelle destruction for example oleate-induced cells of *Aspergillus nidulans* indicated microautophagy induction of peroxisomes during nutrient deprivation of (113, 124).

1.3.4 Mitotic catastrophe

'Mitotic catastrophe' was initially used to describe the lethal fate of cells compelled to enter mitosis prematurely attributable to upregulated CDC2 (125). Mitotic catastrophe refers to the consequence of inadequate mitotic checkpoints, tubulin-targeting agents or unsuccessful cell cycle arrest prior to mitosis followed by DNA injury, resulting in severe chromosomal abnormalities, segregation and finally cell death (125, 126, 127).

Mitotic catastrophe is a highly conserved response that occurs due to damaging agents disrupting the mitotic spindle. For example, paclixatel treatment resulting in abnormal metaphase accompanied with CDC2 activation leading to prolonged metaphase and mitotic catastrophe is induced (102). In addition, mitotic catastrophe is another entry point for apoptosis and necrosis (58, 126). Morphological hallmarks of mitotic catastrophe include fragmented nucleus, the formation of multinucleated, giant cells containing uncondensed chromosomes and micronucleation (58, 125). Multinucleated cells are the result of two or more nuclei with heterogeneous sizes derived from an incomplete division during cytokinesis and micronucleation occurs due to evenly distributed chromosomes (58).

As discussed earlier, the cell cycle comprises of various phases including the M phase which involves mitosis (prophase, metaphase, anaphase and telophase) and cytokinesis (125). The G_2 checkpoint is responsible for cell cycle arrest of abnormal or damaged cells prior to its entrance into mitosis as DNA damage results in the release of various agents leading to cell cycle arrest, apoptosis or DNA repair. However, if the G_2 checkpoint is defective the damaged cell enters mitosis prior to DNA damage can be repaired (70). Impaired mitotic checkpoints and anti-tubulin compounds potentially result in unscheduled CDC2 activation forcing the cell into mitosis (127). Mitotic cell fusion with interphase cells produce mitotic catastrophe due to premature entry in mitosis accompanied by incomplete S and G_2. In addition, the G_2 checkpoint also involves ATR, CHK1 and WAF1 resulting in DNA damaged cells and mitotic catastrophe (95). An inhibitory spindle assembly checkpoint 'wait-anaphase' signal is generated at unattached or inappropriately attached kinetochores. This signal arrives at the APC/C resulting in the stabilization of securin and cyclin B (128).

1.3.5 Metabolic catastrophe

During the 1920s, Otto Warburg demonstrated that tumorigenic cells metabolize more glucose to lactate when compared to non-tumorigenic cells (129, 130). Quantifying lactate production and oxygen expenditure rates indicated that normal tissue inhibited lactate production in the presence of oxygen. However, tumor tissue sustained lactate production despite of oxygen availability. The latter is known as the Warburg effect (129, 130).

Glycolysis is a vital cellular process where glucose is converted to pyruvate and 2 ATP molecules. In non-tumorigenic cells pyruvate is transformed to acetyl coenzyme A that enters the citric acid cycle and the product undergoes oxidative phosphorylation. However, in cancer cells pyruvate is converted to lactate with tumor hypoxia and hypoxia-inducible factor (HIF) playing a critical role in tumorigenesis, angiogenesis and higher glycolysis levels (130). Hypoxia-inducible factor 1 (HIF-1) has been implicated in angiogenesis-independent tumor proliferation by means of glucose metabolism and biosynthetic pathways (131). Hypoxia is a well-known cause of HIF activation in tumors since 50-60% of solid tumors containing hypoxic/anoxic tissues produced by an imbalance between oxygen availability and oxygen consumption. HIF activates the

expression of various pro-angiogenic genes including vascular endothelial growth factor (VEGF), plasminogen activator inhibitor-1 (PAI-1), angiopoietins (ANG-1 and -2), Platelet-derived growth factor B (PDGF-B) and matrix Metaloproteinases (MMP-2 and -9) (132).

Several genes involved in glucose uptake and glycolysis are HIF-1 target genes resulting in elevated lactate production and an increased acidotic environment due to enhanced anaerobic glycolysis (133). Genes mediating glucose metabolism is regulated by peroxisome proliferators-activator receptors (PPAR). During nutrient deprivation PPAR and AMP-dependent protein kinase collaborate to trigger metabolic catastrophe (134). Elevated glycolysis potentially produces mutations contributing to enhanced cellular proliferation accompanied by a hypoxic tumorigenic environment. Furthermore, signaling pathways enabling uncontrolled cellular proliferation also inhibit autophagy leading to genomic instability and enhanced tumor development (135). Constant PI3 kinase pathway activity and oxidative metabolism in tumorigenic cells may also result in metabolic catastrophe (134, 135).

1.3.6 Oncosis

The term oncosis is derived from the Greek word ‘onco’ and refers to swelling and was first used by von Recklinghausen in 1910 (136). Morphological characteristics of oncosis include cellular swelling, membrane blebbing, vacuolization, protein denaturing and increased membrane permeability with a non-specific DNA fragmentation pattern (136, 137). Oncosis is a passive uncontrolled process triggered due to severe tissue damage as a result of either ischemia, heat or toxic agents (136, 138). The molecular signaling transduction of oncosis remains elusive, although autophagy, apoptosis and oncosis possibly share common signaling pathways in the early cell death pathway. A common stimulus induces cell death may also follow apoptosis, autophagy or oncosis pathways depending on the energy and magnitude of the cell (139). Furthermore, oncosis develops into necrosis within 24 h (136). The most popular proposed mechanism responsible for oncosis is related to malfunctioning of ion pumps located at the plasma membrane accompanied by reduced ATP levels (136, 140).

1.3.7 Necrosis

Necrosis is defined as a passive energy-independent degradation process accompanied with cellular alterations the cell experiences after cell death (141, 142). Necrotic morphological hallmarks include cellular swelling, chromatin condensation, chromatin devastation, nuclear fragmentation, cell membrane disruption, insignificant cytoplasmic vacuoles, cytoplasmic blebs, swollen or injured mitochondria, ribosome detachment, disrupted organelle membranes and disrupted lysosomes (56). Disruption of the cell membrane results in release of cellular constituents into the surrounding environment (56, 74). The latter responds by sending chemotatic signals resulting in subsequent inflammation and cytokine release (70, 143). Several death domain receptors, Toll-like receptors, CA^{2+}, ceramide and the C-Jun N-terminal kinase (JNK)/p38 pathway and TNF-R1 are involved in necrosis (70, 144).

1.3.8 Involvement of reactive oxygen species in cell death

Reactive oxygen species (ROS) refer to molecules produced from incomplete one-electron reduction of oxygen (145). ROS are generated through the mitochondrial electron transport chain, arachidonic acid metabolizing enzymes, lipoxygenase and cyclooxygenase, cytochrome P450, xanthine oxidase, NAD(P)H oxidases, uncoupled nitiric oxide synthase (NOS), peroxidase and hemoproteins. ROS include hydrogen peroxide, superoxide, singlet oxygen, hydroxyl radicals, nitric oxide and hypocholorous acid (146). Additionally, ROS are products of cellular metabolism and signaling transduction including proliferation, senescence, apoptosis, autophagy and necrosis (147, 148).

During standard physiological circumstances, a balance between ROS generation and eradication is preserved. As ROS are hazardous, it must be eliminated by superoxide dismutase, peroxidases and redox molecules (149). Reduction of oxygen produces superoxide and may potentially be converted to several other ROS (148). Superoxide dismutase catalyses superoxide producing hydrogen peroxide that is capable of generating hydroxyl radicals in the presence of transitional metals (148).

Since the mitochondria are responsible for superoxide production that is capable of producing various other ROS, the mitochondria are regarded as the major source of ROS generation (149). Increased ROS levels result in oxidative stress leading to

damaged nucleic acid, proteins and lipids and subsequent pathological conditions. These damaged nucleic acid, proteins and lipids are responsible for chromosomal instability, mutations and membrane injury contributing to tumorigenesis (148).

ROS generation is controlled by Ras on the transcriptional level. Once GATA binding protein 6 (GATA-6) is phosphorylated at the serine residue by MEK-activated ERK, GATA-6 DNA binding is facilitated. A site-directed mutation (PYA (120) P to PYA (120)P) of GATA-6 eliminates the trans-activation activity which inhibits epithelial colorectal adenocarcinoma cells (CaCo-2). In addition, NOX1 (homolog of the catalytic subunit of the superoxide-generating NADPH oxidase of phagocytes, gp91phox) is required for tumorigenic angiogenesis and transcription is enhanced by means of Ras signaling (148).

Elevated ROS generation results in cytochrome *c* release that binds to apaf-1 in the presence of dATP and ATP. This results in caspase 9 activation that induces apoptosis (149). Myc is a transcription factor that regulates the expression of genes involved in proliferation, metabolism and apoptosis. Previous research studies have indicated that ROS generation can result in *c-Myc* activation and that *c-Myc* treatment can lead to reduced ROS quantities (147).

Studies have reported mitochondrial ROS play an essential role in survival and cell death by means of autophagy. Low ROS levels potentially promotes survival by autophagy induction in order to redistribute intracellular resources under starvation, while increased ROS production promotes controlled autophagic cell death when survival is unachievable (150). Caspase inhibition leading to autophagic cell death requires ROS accumulation, membrane lipid oxidation and impaired cell membrane integrity (57). ROS is an integral part in the induction of autophagy due to nutrient deprivation and involves Agt4 activity. Starvation results in hydrogen peroxide formation that directly targets cysteine protease Agt4 contributing to ATG8 lipidation and promoting autophagosome formation. Some studies have indicated that nerve growth factor deprived neurons demonstrated ROS accumulation in the mitochondria and subsequent autophagy induction (151). Furthermore, TP53-induced glycolysis and apoptosis regulator (TIGAR) inhibit glycolysis and reduce ROS production. TIGAR

regulates ROS generation in response to starvation and inhibits autophagy (146). Induction of ROS production is thus a potential target for anticancer therapy.

1.4 Estradiol analogues as antimitotic agents

Antimitotic agents represent a class of anticancer drugs including taxanes and vinca alkaloids which are both potent microtubule-disrupting agents (152, 153). Vinca alkaloids including either vinblastine or vincristine that binds to the vinca tubulin domain and either nocodazole or combretastatins that bind to the colchicine tubulin domain are destabilizing agents resulting in inhibition of microtubule polymerization. Stabilizing agents include taxanes, such as paclitaxel, docetaxel, and epothilones that enhance tubulin polymerization (152). These agents target microtubuli that are part of the microtubule network which are essential in cell proliferation (152, 153).

The endogenous metabolite of 17β-estradiol, 2-methoxyestradiol (2ME2) possesses antiproliferative, antiangiogenic and antitumor *in vitro* and *in vivo* activity by targeting tubulin for destruction (154). 2ME2 exerts antitumor activities; previous literature revealed that its effects are biphasic, as well as dose- and cell line-dependent (155, 156, 157, 158, 159). 2ME2 has a low affinity for estrogen receptors; thus its antiproliferating effect on cells is independent of the presence of estrogen receptors (155). 2ME2 targets several proteins including cofactors of DNA replication and repair, proliferating cell nuclear antigen (PCNA), cell division cycle kinases and regulators (p34 and cyclin B) and DR5 upregulation (154). Inhibition of cell proliferation mainly results from the induction of apoptosis, since 2ME2 targets active proliferating cells thereby not affecting quiescent cells (154, 155). Due to the above-mentioned *in vitro* effects, 2ME2 phase II clinical trials for 2ME2 (Panzem^{TM}) was completed; however lacked sufficient affectivity to continue to stage III trials (156).

Due to limited bioavailability and rapid metabolic degradation *in vivo*, several promising analogues of 2ME2 were developed. 2-Methoxyestradiol-bis-sulphamate (2MEBM) is a bis-sulphamoylated derivative of 2ME2 with antiproliferative activity that inhibits steroid sulphatase (STS) activity (160, 161, 162). STS is accountable for the conversion of estrogen sulphate to estrone. STS activity is elevated by (1000x) in breast tissues when compared to aromatase activity (163). Estrone synthesis in breast tumor tissue is ten

times higher via the sulfatase pathway (89%) when compared to the aromatase pathway (63%) (164, 165, 166). The latter suggests that steroid sulfatase may have a central role in the regulation of estrogen synthesis in breast tissues (163).

STS is one of twelve sulfatases that have been characterized in human cells. Seven of these twelve STSs are present in lysosomes and play an essential role in the lysosome function in an acidic environment where they are critical for glycoaminoglycan-and sulpholipid degradation (167). The remaining five STS's are involved with the intracellular membranes and abide by a neutral pH (167). STS also assists in the hydrolysis of oestrone sulphate to oestrone which contribute to oestradiol production in breast tumor tissues (167, 168). STS participates in the conversion of dehydroepiandrostene (DHEA) from DHEA-sulphate (162, 167). DHEA is found significantly increased in tumorigenic breast tissue (166). Studies have shown that STS mRNA expression is higher in malignant than in normal breast tissue and also suggested that high levels of STS mRNA expression in breast tumors are associated with poor prognosis (168). Androstenediol (adiol) is produced by the reduction of DHEA. Adiol can bind to the estrogen receptors and stimulate breast cancer cell growth. Adiol production is thus dependent on the sulfatase pathway (167, 168, 169).

Cancer cells are known to have a high rate of aerobic glycolysis and this in turn contributes to the production excess lactic acid and a decrease in pH in the immediate environment of the hyper proliferative neoplastic cells (170). The acidotic environment contributes to metastatic processes associated with malignant cancers through breakdown of the basement membrane and breachment into the circulation (171). Carbonic anhydrases (CAs) are ubiquitous zinc-dependent metalloenzymes present in vertebrates. Among the important physiological functions of CAs is the regulation of acid/base homeostasis by controlling the CO_2/bicarbonate ratio (169). Two membrane bound CA isozymes (IX and XII) are overexpressed in many tumors and contribute to the regulation and adaptation of cancer cells in acidotic environment (172). Both of these isoenzymes are thus targets for drug design that could be specifically targeted towards malignant cancer phenotypes with an abrogated acid/base homeostasis. In addition, the estrogen 3-*O*-sulphamates are highly reversible inhibitors of carbonic anhydrase II. The latter is most likely responsible for the high bioavailability of the

sulphamoylated analogues as reversible uptake by red blood cells and interaction with carbonic anhydrase II ensures transiting the liver without undergoing first pass metabolism (173, 174, 175).

Previous reports indicate that estrogen sulphamate analogues featuring a 2-methoxy, 2-ethyl, or 2-methyl sulphanyl group possess optimal antiproliferative activity (173, 174, 175). Compounds possessing a 2-methoxy, 2-ethyl, or 2-methyl sulphanyl group exert potent antitumor activity due to their ability to interact sulphatase, carbonic anhydrase and tubulin (174). The addition of the 3-*O*-sulphamate group to the original 2ME2 compound ensures more potent antiproliferative activity (10x) and also allows for resistance to inactivating conjugation of the C-3 hydroxyl group to which the corresponding estradiol derivatives are subject (173). Research studies conducted in our laboratory demonstrated that addition of an ethyl group to position 2' and a sulphamate group to position 3' to give 2ME2 resulted in superior antiproliferative activity in estrogen receptor negative breast metastatic cell line (MDA-MB-231), estrogen receptor positive breast adenocarcinoma cell line (MCF-7), oesophageal cell line (SNO) and cervical cell line (HeLa) in nanomolar concentration range and significant antimitotic activity and apoptosis induction in the MDA-MB-231 cell line (175).

However, 2ME2 possesses poor bioavailability when compared to its sulphamoylated derivatives. Research conducted in our laboratory involved the *in silico* identification of several sulphamoylated analogues of 2ME2. *In silico* identification of several antimitotic sulphamoylated 2ME2 compounds was conducted by means of docking studies that involved structures related to the binding to CAII, tubulin and CAIX to optimize anticancer activity. Our research group thus has *in silico*-designed new and improved estradiol analogues for tubulin-, kinesin motor protein and carbonic anhydrase (CA) (CA II, IX, XII) binding affinity and subsequent detailed elucidation of each compound's biochemical pathway of signaling needs to be investigated to verify potential anticancer activity *in vitro* to complement the improvement of analogues with therapeutic potential. (175).

The chemical modifications made by additions of the sulphamate groups, ethyl and the methyl group merits investigation of possible *in vitro* anticancer activity exerted by (8*R*, 13*S*,14*S*,17*S*)-2-ethyl-13-methyl-7,8,9,11,12,13,14,15,16,17-decahydro-6H-cyclopenta[*a*]phenanthrane-3,17-diyl bis(sulphamate) (EMBS) (Figure 1.4). This project investigated the differential *in vitro* effects on an adenocarcinoma receptor positive cell line (MCF-7), estrogen receptor negative metastatic cell line (MDA-MB-231) and a non-tumorigenic epithelial breast cell line (MCF-12A).

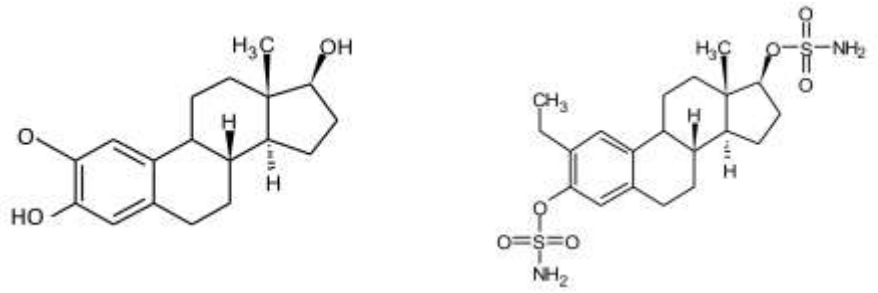

2-Methoxyestradiol

(8R, 13S, 14S, 17S)-2-Ethyl-13-methyl-7, 8, 9, 11, 12,13, 14, 15, 16, 17-decahydro-6H-cyclopenta[*a*]phenanthrane-3, 17-diyl bis(sulphamate) (EMBS)

Figure 1.4: (8*R*,13*S*,14*S*,17*S*)-2-Ethyl-13-methyl-7,8,9,11,12,13,14,15,16,17-decahydro-6H-cyclopenta[*a*]phenanthrane-3,17-diyl bis(sulphamate) (EMBS) is a sulphamoylated analogue of 2ME2. Structural differences between EMBS and 2ME2 are shown above. Structures were created by MH Visagie using ACD/ ChemSketch version 1101 released on 2007/10/19 (Advanced Chemistry Development, Inc., ACD/ Labs, Toronto, Canada).

1.5 Relevance and aim of research project

This research project is regarded as a preclinical *in vitro* study and data cannot directly be extrapolated to an *in vivo* environment. Scientific information gained from this investigation contributes to establishing the mechanism of action used by EMBS in the induction of cell death by investigating the biochemical pathways and *in vitro* effects of EMBS on various targets in estrogen receptor positive and estrogen receptor negative breast adenocarcinoma cell lines and a estrogen receptor negative non-tumorigenic breast cell lines, paving the way for *in vivo* studies.

The main aim is this research was to investigate differential cell signaling events exerted by the sulphamoylated 2ME2 analogue , EMBS, in adenocarcinoma cell lines (MCF-7 and MDA-MB-231) and the non-tumorigenic epithelial breast cell line (MCF-12A) respectively by analyzing its influence on cell growth, cytotoxicity, metabolism, redox reactions and energy transformation, morphology, cell cycle progression, mitochondrial membrane potential, caspase activation, reactive oxygen species generation and possible induction of apoptosis and autophagy.

1.6 Objectives

This knowledge involved an in silico-designed 17β-estradiol analogue with unknown antiproliferative and antimitotic activity with possible induction of apoptosis and autophagy. This study investigated the biochemical pathways of signaling events to verify potential anticancer activity *in vitro* to complement the improvement of analogues with therapeutic potential. Potential targets included in this project included lactate dehydrogenase and metabolic activity, cell cycle progression, caspase activation, reactive oxygen species production, p53 activation, bcl-2 regulation and cell death via apoptosis and autophagy and the crosstalk between these modes of cell death.

In this study the differential *in vitro* signal transduction is exerted by EMBS in an estrogen receptor positive breast adenocarcinoma cell line (MCF-7), an estrogen receptor negative metastatic cell line (MDA-MB-231) and a non-tumorigenic breast epithelial cell line (MCF-12A) were investigated by:

- to perform time- and dose dependent growth studies in order to determine the effect of EMBS on cell numbers by means of spectrophotometry and xCELLigence real-time label-independent approach
- to determine the effects of EMBS on lactate dehydrogenase production, redox reactions and energy transformation by means of spectrophotometry.
- to study morphological changes induced by EMBS in tumorigenic and non-tumorigenic cell lines with polarization-optical transmitted light differential interference contrast, light microscopy (haematoxylin and eosin staining), fluorescent staining (hoechst 33342, acridine orange and propidium iodide triple), transmission electron microscopy and scanning electron microscopy techniques.

- to determine the influence of EMBS on reactive oxygen species production.
- to investigate the effects that EMBS exerts on cell cycle progression, apoptosis and autophagy.
- to demonstrate the influence of EMBS on the crosstalk between autophagy and apoptosis

Chapter 2

2. Materials and methods

2.1 Materials

2.1.1 Cell lines

MCF-12A is an estrogen receptor negative non-tumorigenic spontaneously immortalised adherent human breast epithelial cell line (176). The MCF-12A cell line was established from tissue taken at reduction mammoplasty from a nulliparous patient with fibrocystic breast disease that contained focal areas of intraductal hyperplasia. These cells are produced by long-term cultures and demonstrate luminal epithelial morphology and forms domes in confluent cultures. The MCF-12A cells were a gift from Professor Parker (Department of Medical Biochemistry, University of Cape Town, South Africa). Cells were grown in sterile 25 cm^2 tissue culture flasks at a humidified atmosphere at 37°C and 5% CO_2. MCF-12A cells were cultured in growth medium consisting of a 1:1 mixture of Dulbecco's minimum essential medium eagle (DMEM) and Ham's-F12 medium, 20 ng/ml epidermal growth factor, 100 ng/ml cholera toxin, 10 µg/ml insulin and 500 ng/ml hydrocortisone, supplemented with 10% heat-inactivated fetal calf serum (FCS) (56°C, 30 min), 100 U/ml penicillin G, 100 µg/ml streptomycin and fungizone (250 µg/l).

MCF-7 is an estrogen receptor positive human tumorigenic adherent breast epithelial cell line that is derived from adenocarcinoma metastatic sites (176). MCF-7 cells are able to process estradiol via cytoplasmic estrogen receptors and are capable of forming domes and are positive for cytokeratin and negative for desmin, endothelin, GFAP, neurofilament and vimentin. MCF-7 cells are commercially accessible from Highveld Biological (Pty) Ltd (Sandringham, South Africa). These cells were grown and maintained in 25 cm^2 tissue culture flasks in a humidified atmosphere at 37°C and 5% CO_2, Dulbecco's Minimum DMEM supplemented with 10% heat-inactivated FCS (56°C, 30 min), 100 U/ml penicillin G, 100 µg/ml streptomycin and fungizone (250 µg/l) was used to propagate cells.

MDA-MB-231 is a triple negative tumorigenic breast cell line indicating that MDA-MB-231 cells do not express receptors for steroid hormones (estrogen and progesterone), type II receptor tyrosine kinase (RTK) Her-2, but do possess upregulation of basal

cytokeratins and epidermal growth factor response (177). The MDA-MB-231 cell line was derived for adenocarcinoma metastatic site and is commercially available from Microsep (Pty) Ltd. (Johannesburg, South Africa). Cells were grown and maintained in 25 cm^2 tissue culture flasks in a humidified atmosphere at 37°C and 5% CO_2 in DMEM supplemented with 10% heat-inactivated FCS (56°C, 30min), 100 U/ml penicillin G, 100 µg/ml streptomycin and fungizone (250 µg/l).

2.1.2 Reagents

All required reagents of cell culture analytical grade were purchased from Sigma (St. Louis, United States of America) unless otherwise specified. DMEM, Trypsin-EDTA and crystal violet were supplied by Sigma Chemical Co. (St. Louis, United States of America). Heat-inactivated FCS, sterile cell culture flasks and plates were acquired through Sterilab Services (Kempton Park, Johannesburg, South Africa). Penicillin, streptomycin and fungizone were obtained from Highveld Biological Pty (Ltd) (Sandringham, SA).

Phosphate buffered saline (PBS) was prepared by diluting a ten times concentrated solution consisting of 80 g/l NaCl, 2 g/l KCl, 2 g/l KH_2PO_4 and 11 5g/l Na_2HPO_4 (purchased from Merck (Munich, Germany)) to a 1 times concentrated solution. Diluted PBS solution was autoclaved (20 min, 120°C, 15psi) before use (Sterilizer Technologies CC, South Africa).

EMBS was synthesized by iThemba Pharmaceuticals (Pty) Ltd. (Modderfontein, Gauteng, South Africa), since this compound is not commercially available. Stock solutions of EMBS were prepared with a concentration of 10 mM and were stored at 4°C. Appropriate controls were used in each experiment and included controls where cells were propagated in growth medium and vehicle-treated controls where media of all control experiments were supplemented with an equal volume of dimethyl sulfoxide (DMSO). The DMSO content of the final dilutions never exceeded 0.05% (v/v) (178, 179). Vehicle controls containing and growth medium, as well as positive controls for apoptosis- and autophagy were included.

Aseptic techniques were applied throughout, with all work being conducted in a laminar flow cabinet from Labotec (Midrand, South Africa). Solutions were filtered-sterilized (0.22 µm pore size) and all glassware and non-sterile equipment were sterilized by autoclaving (20 min, 120°C, 15psi).

2.2 Generalised methods followed for experiments

For experiments, cells were seeded in a 96-well (5 000 cells per well) tissue culture plates, on heat-sterilized coverslips in 6-well culture plates (350 000 cells per well) or in 25 cm^2 tissue culture flasks (500 000 cells per flask). Cells were incubated for 24 h to allow for attachment after which medium was removed and cells were exposed to EMBS appropriate concentrations ranging from 0.2-1 µM including vehicle-treated controls and incubated for 24 h at 37^oC. These conditions were selected since previous studies in our laboratory have demonstrated successful antiproliferative activity in tumorigenic cell lines within this [0.2-1 µM] series. Sample controls for apoptosis- and autophagy were also included. Actinomycin D (0.1 µg/ml in the growth medium) was used as a positive control for apoptosis. Controls for autophagy consisted of cells that were starved (1:3 ratio relative to growth medium: phosphate buffered saline (PBS)).

Cells were harvested by tripsinization and counted by making use of a haemocytometer. Suspended cells (20 µl) where mixed with 80 µl PBS, 20 µl of that solution was then resuspended in 20 µl trypan blue to provide a concentration of cells with a dilution factor 10 X. Dead cells take up the dye and are consequently stained blue, which is then left uncounted.

The number of viable cells per ml was determined by:

Cells/ml = Average count of viable cells in corner squares in haemocytometer x dilution factor x 10^4

2.3 Analytical protocol for experiments

2.3.1 Antiproliferative activity

2.3.1.1 Spectrophotometry (crystal violet)

Crystal violet is a method used to determine cell number by staining DNA (180). Staining cell nuclei of fixed cells with the triphenylmethane cationic dye, crystal violet

allows for rapid, accurate and reproducible quantification of cell numbers in cultures grown in 96-well plates. Crystal violet thus allows for the quantification of the cell number in monolayer cultures as a function of the absorbance of the dye taken up by the cells (180, 181, 182). Quantification is possible by solubilising the absorbed dye into a solution of triton X-100 and determining optical density using spectrophotometry. Absorbance of the dye measured spectrophotometrically at 570 nm corresponds to cell numbers (179, 180, 181).

A time-dependent study was conducted with time intervals of 24 h, 48 h and 72 h. A dose-dependent study was conducted with a concentration range of 0.2 µM - 1 µM since previous studies conducted by our collaborators in Grenoble, France and conducted in our laboratory (Department of Physiology, South Africa) demonstrated successful anticancer activity within this concentration range (175).

A) Materials

Glutaraldehyde, crystal violet and triton X-100 were purchased from Merck (Munich, Germany).

B) Methods

Crystal violet staining was conducted according to Visagie *et al.* (2010) (178). Exponentially growing MCF-7, MDA-MB-231 and MCF-12A cells were seeded in 96-well tissue culture plates at a cell density of 5 000 cells per well. Cells were incubated at 37°C for 24 h to allow for attachment. Medium was discarded and cells were exposed to a 0.2-1 µM EMBS concentration series for 24 h, 48 h and 72 h respectively 37^{o}C. A baseline was also included, seeded in a separate 96-well plate and cells were stained before exposure to determine the starting number. Cells were fixed with 100 µl of 1% gluteraldehyde and incubated for 15 min at room temperature. Subsequently, glutaraldehyde was discarded and cells were stained using 100 µl 0.1% crystal violet (incubated at room temperature for 30 min). The crystal violet solution was discarded and the 96-well plate was submersed under running water. Crystal violet dye was solubilized using 200 µl 0.2% triton X-100 and incubated at room temperature for 30 min. The solution (100 µl) was transferred to a new microtitre plate. Afterwards, the absorbance was read at 570 nm using an EL_x800 Universal Microplate Reader (Bio-Tek Instruments Inc., Vermont, United States of America).

2.3.1.2 xCELLigence real-time label-independent approach

Real-time cell electronic awareness based on impedance determination is used in cell biology to monitor cell proliferation (176, 183). The xCELLigence method is a system based assay developed by Roche Applied Science (Penzberg, Germany) to demonstrate cell growth, adhesion and morphology in real-time utilizing a label-independent manner and was employed to confirm whether the dosage exerts optimal antiproliferative activity (176). This system measures electrical impedance across the micro-electrodes integrated on the bottom of tissue culture 96-well plates therefore allowing real-time and continuous cellular analysis as cells attach and proliferate. The change in impedance was expressed as the cell index and is an indication of cell number, cellular attachment and morphology. By plotting cell index values over time, a precise real time cellular analysis profile was generated (183).

A) Materials

The xCELLigence system which includes the real-time cell analyzer (RTCA) SP Station, RTCA Analyzer and RTCA Control Unit created by ACEA Biosciences, Inc. (San Diego, United States of America), were kindly provided by Roche Products (Pty) Ltd. (Randburg, Johannesburg, South Africa) as a demonstration model and disposable E-Plate 96 microtitre plates were purchased from Roche Products (Pty) Ltd. The e-plate 96 is a specialized disposable device that differs from the standard 96-well plate by the incorporation of gold cell sensor arrays in the bottom of each well that allows for the measurement of electrical impedance created by cellular events (184). This is accomplished by sensor electrodes that measure impedance to allow for physiological changes on cellular level on the electrodes. Approximately 80% of the wells are coated by the circle-on-line electrodes which are optimised for 15-40°C with relative humidity 98% without condensation (184).

B) Method

The RTCA SP Station was connected to the RTCA control unit and the xCELLigence system was tested by Resistor plate verification prior to placing the xCELLigence system inside the incubator at a humidified atmosphere at 37°C and 5% CO_2. Background quantification was done by adding 100 µl of the appropriate growth medium to the wells and subsequently the plate was calibrated using RTCA software package 1.2. Cells were seeded at 5 000 cells per well and was then placed on a rotator for 30 min at room temperature and samples were placed in the xCELLigence

system that was linked to the incubator in a humidified atmosphere at 37°C and 5% CO_2 (176, 184). The xCELLigence system monitored cell adhesion and proliferation for 24 h to allow for attachment. Thereafter, cells were exposed to 0.2-1 µM EMBS concentration series. As the cells were proliferating, the electrical impendence created by the cells were converted to cell index values corresponding to each well. Cell index values are directionally proportionate to cell number, size and attachment (176). Subsequently, cell adhesion and proliferation were determined for the next 72 h.

2.3.2 Cell viability and metabolism

2.3.2.1 Spectrophotometry (quantification of lactate dehydrogenase)

Lactate dehydrogenase (LDH) is a soluble cytosolic enzyme that catalyzes the interconversion of lactate and pyruvate. LDH cannot be measured extracellularly unless the cell membrane has been damaged (178). Cells release LDH during injury or cell damage, following the loss of membrane integrity consequential from either apoptosis or necrosis. LDH activity can therefore be used as an indicator of cell membrane integrity and serves as a general means to assess cytotoxicity resulting from exposure to chemical compounds. This LDH colorimetric assay is based on the reduction of the tetrazolium salt 3-(4,5-dimethylthiazol-2-Yl)-2,5-diphenyltetrazolium bromide (MTT) in a NADH-coupled enzymatic reaction to a reduced form of MTT which exhibits an absorption maximum at 565 nm. The purple colour intensity is directly proportional to the enzyme activity.

A) Materials

Lactate dehydrogenase assay kit was supplied by BIOCOM biotech Pty (Ltd) (Clubview, Gauteng, South Africa).

B) Methods

Cells were seeded in 96-well plates at a cell density of 5 000 cells per well with an overnight attachment policy (incubated at 37°C at 5% CO_2). Subsequently, cells were exposed to EMBS. Various controls were included in the experiment according to the supplier's manual. The background control consisted of growth medium only and represents the LDH represent in the growth medium. The low control referred to cells resuspended in growth medium referring to the LDH released by unexposed cells in propagated in growth medium (178). The high control contained cells resuspended in growth medium with cell lysis solution added to the cells shortly before the experiment

is terminated (according to the manufacturer's instructions). Medium (200 µl) was transferred and centrifuged at 5 000 revolutions per min (rpm) for 10 min. Afterwards, 10 µl was transferred to a clear 96-well plate. LDH reaction mix (100 µl) (mixed according to the kit pamphlet instructions) was added to the sample. After 90 min of incubation at room temperature, the absorbance was read at 460 nm, with a reference wavelength of 630 nm by means of EL_x800 Universal Microplate Reader (Bio-Tek Instruments Inc., Vermont, United States of America).

2.3.2.2 Spectrophotometry (NAD^+/NADH and $NADP^+$/NAPPH quantification)

Energy transformation induced by EMBS was evaluated by quantifying NAD^+/NADH and $NADP^+$/NADPH. In the salvage pathway nicotinamide and nicotinic acid are converted to nicotinamide mononucleotide (NMN) or nicotinic acid mononucleotide (NaMN) by means of the phophoribosyl transferases (186). NMN and NaMN are then converted to NAD^+ and NaAD. The latter is converted to NAD^+ by utilizing NAD^+ synthase. In the *de novo* pathway quinolinic acid generated from L-tryptophan (mammals) or L-aspartate (plants) is converted to NaMN by quinolinic acid phosphoribosyltransferase. NaMN is then converted to NAD^+ by means of NAD^+ synthase (186).

NAD^+ is required for the production of NADH, $NADP^+$ and NADPH (149, 185, 186). $NADP^+$ acts as a precursor for the formation of NADPH. Major biological functions of NAD^+ involve cellular respiration, acting as an electron source in the biosynthesis of fatty acids, steroids and DNA, being a substrate of NADPH oxidase that generates RO and calcium homeostasis (186). Calcium homeostasis is mediated by NAD^+ by means of production of cyclic ADP-ribose that inhibits ryanodine receptor-mediated calcium channels and activates the melastin-related transient receptor potential (TRPM2) resulting in calcium influx.

NADPH is of vital importance in neutralizing hydrogen peroxide, reactivating catalase and is involved in the conversion of glutathione disulfide (GSSG). The latter is imperative for the functioning of several antioxidant enzymes (glutathione peroxidase and glutathione *S*-transferase). Cellular metabolism is dependent on NAD^+ and NADH, since NADH is an electron donor for the electron transport chain. NAD^+ acts as

coenzyme in three rate-limiting steps in the tricarboxylic acid cycle. NAD^+ is a cofactor for the glycolytic enzyme GAPDH and NAD^+ also modulates the pyruvate conversion to lactate. NADH is capable of inhibiting the voltage-dependent anion channels (186).

A) Materials

NAD^+/NADH quantification kit and $NADP^+$/NAPPH quantification kits were acquired from BIOCOM biotech Pty (Ltd) (Clubview, Gauteng, South Africa).

B) Methods

NAD^+/NADH quantification

Cells were seeded at a density of 500 000 cells per 25 cm^2 flask and were incubated overnight. Afterwards cells were exposed EMBS for 24 h. Cells were trypsinized and resuspended in 1 ml growth medium. Cells were counted and 200 000 cells were utilized for each assay. Cells were extracted by adding 400 µl NADH/NAD^+ extraction buffer. Samples were left on ice for 20 min and then for 10 min at room temperature. The freeze/thaw cycle was repeated twice. Samples were votexed for 10 s and thereafter centrifuged at 14000 rpm for 5 min. The extracted NADH/NAD^+ supernatant were transferred to a new tube. Using NADH standards provided by the NAD^+/NADH quantification kit, a standard curve was created (according to supplier's instruction). Extracted samples (50 µl) were transferred into a sterile 96-well plate. Remaining extracted samples were left in a water bath at 60°C for 30 min and centrifuged (2000 rpm). Decomposed samples (50 µl) were transferred in duplicate to sterile wells. NAD cycling mix (100 µl) (mixed according to supplier's instructions) was added to samples and incubated for 5 min at room temperature. NADH developer (10 µl) was subsequently be added to all samples. After 60 min the absorbance was determined at 450 nm.

$NADP^+$/NADPH quantification

Cells (500 000) were seeded in a 25 cm^2 flask incubated overnight. Subsequently, cells were exposed EMBS and appropriate controls were included. After 24 h cells were trypsinized and resuspended in 1 ml growth medium. Cells were counted in order to obtain 100 000 cells per assay. $NADP^+$/NADPH extraction buffer (400 µl) was added; samples were left on ice for 20 min and then for 10 min at room temperature. This procedure was repeated twice. Samples were votexed for 10 s and thereafter centrifuged at 14000 rpm for 5 min. The extracted NADPH/$NADP^+$ supernatant was

transferred to a new tube. Using NADPH standards provided by the $NADP^+$/NADPH quantification kit, a standard curve was created (according to supplier's instruction). Extracted samples (50 µl) were transferred into a sterile 96-well plate. Remaining extracted samples were left in a water bath at 60°c for 30 min and then centrifuged (2000 rpm). Decomposed samples (50 µl) were transferred in duplicate into sterile wells. NADP cycling mix (100 µl) (mixed according to supplier's instructions) was added to all samples and incubated for 5 min at room temperature. NADPH developer (10 µl) was added to all samples. After 60 min, absorbance was read at 450 nm on the EL_x800 Universal Microplate Reader available from Bio-Tek Instruments Inc. (Vermont, United States of America).

2.3.3 Morphology

2.3.3.1 Polarization-optical transmitted light differential interference contrast

Polarization-optical transmitted light differential interference contrast (PlasDIC) is a contrast method used to view morphology. Unlike conventional differential interference contrast (DIC), linearly polarized light is only generated after the objective. PlasDIC is a system produced by Zeiss, which is made out of a slit aperture in the condenser front focal plane, a combination of polarizer (polarizers that are cemented to the Wollaston prisms), prism and analyzer that is interleaved in the objective back focal plane (BFP) (53, 54). PlasDIC displays the required phase profile which is relative to the product of the section thickness and the refractive index difference between the environment and the average refractive index of quartz. PlasDIC has high-quality DIC imaging of individual cells, cell clusters and thick individual cells in plastic cell-culture vessels possible for the first time (178, 179).

A) Materials

No additional material required

B) Methods

Cells were photographed before and after exposure using the Axiovert 40 CFL microscope (Carl Zeiss, Goettingen, Germany).

2.3.3.2 Light microscopy (haematoxylin and eosin staining)

Haematoxylin and eosin staining method was used to determine the *in vitro* influence of EMBS on cell morphology and mitotic indices were determined. Haematoxylin and

eosin staining allows for the identification of different mitotic phases and interphase (178, 179). In addition, apoptotic- and autophagic characteristics were also identified. This staining technique therefore provides qualitative and quantitative information. Haematoxylin is a natural compound originating from haematoxylin campechianum. Haematoxylin is oxidised, forming haematein and combines with aluminium ions to produce its staining capability (187). Positively-charged metal-haematein binds to the negatively charged phosphate pertaining to the cell nucleus and stains it blue. Eosin is fortified with ploxine to enhance the staining (187).

Materials

Bouin's fixative was purchased from Sigma-Aldrich ((St. Louis, United States of America). Haematoxylin, eosin, ethanol, xylol and Entellam® fixative were purchased from Merck (Munich, Germany).

Method

Cells (500 000) per well were seeded on sterile coverslips in 6-well plates and incubated overnight. Cells were then exposed to EMBS for 24 h and the appropriate controls respectively. Coverslips were transferred to staining dishes and cells were fixed with Bouin's fixative for 30 min. Bouin's fixative was discarded and 70% ethanol was added for 20 min to coverslips at room temperature before they were rinsed with tap water. Mayer's haematoxylin was added to the coverslips for 20 min. Coverslips were rinsed with tap water for 2 min. Afterwards 70% ethanol was added to the coverslip followed by 1% eosin for 5 min. Eosin was discarded and coverslips were consecutively rinsed twice for 5 min with 70%, 96%, 100% and xylol. Coverslips were mounted on microscope slides with resin and left to dry. Photos were taken with a Zeiss Axiovert MRc microscope (Zeiss, Oberkochen, Germany). Mitotic indices were also determined from the haematoxylin and eosin-stained cells. Quantitative data for mitotic indices were obtained by counting 1000 cells on each slide of the biological triplicates and expressing data as a percentage of cells in each phase of mitosis, interphase and abnormal cells. Distinction was made between mitotic cells (prophase, metaphase, anaphase and telophase), cells present in interphase and abnormal cells which displayed hallmarks of apoptosis and autophagy (178).

2.3.3.3 Transmission electron microscopy

Transmission electron microscope (TEM) was used to view and identify chromatin condensation, nuclear fragmentation, membrane blebbing and apoptotic bodies formed by apoptosis. TEM was conducted to identify characteristics of autophagy, namely the autophagic vacuolization of the cytoplasm. These vacuoles are large double-membrane vesicles containing degenerating sequestered cytoplasmic constituents (188, 189). Apoptotic characteristics were also noted such as rounding of the cell, retraction of pseudopodes, cytoplasmic and nuclear condensation (pyknosis), chromatin condensation, nuclear fragmentation (karyorrhexis), plasma membrane blebbing and engulfment by resident phagocytes (188, 189).

A) Materials

Aqueous osmium tetroxide, glutaraldehyde, phosphate buffer quetol, Reynolds' lead citrate, aqueous uranyl acetate were purchased by the Electron Microscopy Unit of the University of Pretoria from Merck Co. (Munich, Germany). The JOEL JEM 2100F transmission electron microscope (Electron Microscopy unit, University of Pretoria, South Africa) was used for viewing the prepared samples.

B) Methods

Cells were seeded in a 25 cm^2 flask at a density of 500 000 cells per flask with an overnight attachment policy. Subsequently, medium was discarded and cells were exposed to EMBS and appropriate controls were included. After 24 h, cells were trypsinized and resuspended in 1 ml medium. Cells were then fixed with 2.5% glutaraldehyde in 0.075 M phosphate buffer for 1 h, rinsed thrice with 0.075 M phosphate buffer, fixed with osmium tetroxide for 30 min, rinsed thrice with distilled water and dehydrated with increasing ethanol concentrations (30%, 50%, 70%, 90%, and 100%). Cells were then infiltrated with 50% quetol in ethanol for 1 h and then with 100% quetol for 4 to 6 h (178, 179). Ultra-thin sections were prepared using a microtome and contrasted by means of 4% uranyl acetate-staining for 10 min and rinsed with water. Images were taken using TEM (Electron Microscopy Unit, University of Pretoria, Pretoria, South Africa).

2.3.3.4 Scanning electron microscopy

Scanning electron microscopy (SEM) was used where high resolution images demonstrated the effects of EMBS on external morphology. The sample is coated by a layer of electron dense material where electrons are emitted from a cathode and are

accelerated towards an anode. After emission, low secondary electrons initiated within a few nanometers from the exterior and are detected by means of a scintillator-photomultiplier. The resulting signal is rendered into a two-dimensional intensity distribution that can be viewed as a digital image (190, 191).

A) Materials

Aqueous osmium tetroxide, glutaraldehyde, phosphate buffer and gold were purchased by the Electron Microscopy unit of the University of Pretoria from Merck Co. (Munich, Germany). The Cryo- Scanning electron microscope (JEOL 840 with Cryostage) of the Electron Microscopy Unit (University of Pretoria, Pretoria, South Africa) was utilised for viewing the samples.

B) Methods

MCF-7, MDA-231 and MCF-12A cells were seeded at 500 000 cells per well on heat-sterilized coverslips in 6-well plates. After 24 h attachment, cells were exposed to EMBS and incubated for 24 h. Cells were fixed in 2.5% glutaraldehyde in 0.075 M phosphate buffer for 1 h and rinsed 3 times for 5 min each with 0.075 M phosphate buffer. Cells were fixed in 0.25% aqueous osmium tetroxide for 30 min and rinsed three times in distilled water in a fume cupboard. Samples were dehydrated with increasing concentrations of ethanol (30%, 50%, 70%, 90%, 100%, 100%, 100%). Samples were dried utilizing critical point drying whereby the samples are mounted in a chamber and liquid Carbon dioxide (CO_2) was supplied to the chamber until it is full. Ethanol was then expelled from the chamber by opening a valve and thereby releasing CO_2 dissolved ethanol. The valve was closed and the sample was left in liquid CO_2 for 1 h. The vessel was then warmed to 34°C so that the CO_2 became a gas. Pressure was released slowly and the sample was completely dried. The dried coverslips were mounted on a stub and sprayed with a thin layer of gold. The samples were viewed with a Cryo-SEM (JEOL 840 with Cryostage).

2.3.3.5 Fluorescent microscopy (apoptosis, autophagy and necrosis detection)

A triple staining fluorescent microscopy method was employed to visualize induction of autophagy by EMBS. Autophagy literally means ‘self-eating when translated from the original Greek word (192). Autophagy is the evolutionary conserved multistep lysosomal pathway by which the cellular components are disintegrated to sustain an equilibrium of synthesis and degradation in the metabolism of eukaryotic cells (193,

194). This triple staining method included utilising propidium iodide, hoechst 33342 and acridine orange. Propidium iodide is a fluorescent dye that is unable to penetrate an intact membrane and therefore stains the nucleus of cells that have lost their membrane's integrity due to necrotic processes (195). Hoechst 33342 is a fluorescent dye that can penetrate intact cell membranes of viable cells and cells undergoing apoptosis and stain the nucleus (196). Acridine orange is lysosomotropic fluorescent compound that moves freely across cell membranes when uncharged. However, acridine orange accumulates in its protonated form in acidic compartments and thus serves as a tracer for acidic vesicular organelles including autophagic vacuoles and lysosomes (194).

A) Materials

Acridine orange, bisbenzimide (Hoechst 33342) and propidium iodide were purchased from Sigma-Aldrich (St. Louis, United States of America).

B) Methods

Cells (300 000) were seeded in 6-well plates and incubated overnight. Cells were exposed to EMBS for 24 h. Hoechst 33342 solution (0.5 ml) (3.5 µg/ml in phosphate buffered saline (PBS)) was added to the medium to provide a final concentration of 0.9 µM and cells were incubated for 25 min at 37°C. Subsequently, 0.5 ml of acridine orange solution (4 µg/ml in PBS) was added to the medium to give a final concentration of 1 µg/ml. Samples were incubated for 5 min at 37°C and 0.5 ml of propidium iodide solution (40 µg/ml in PBS) was added to the medium to provide a final concentration of 12 µM. Cells were washed three times with PBS. Photos were taken with appropriate filters in a dark room to prevent quenching. A Zeiss Axiovert CFL40 microscope and Zeiss Axiovert MRm monochrome camera (Zeiss, Oberkochen, Germany) were used employing a Zeiss filter 2 for Hoechst 33342 stained (blue) cells and a Zeiss filter 9 for acridine orange-stained (green) cells and a Zeiss filter 15 for propidium iodide-stained (red) cells.

2.3.4 Flow cytometry and ethanol fixation (cell cycle progression)

Flow cytometry was employed to measure the DNA content of cells exposed to EMBS and control cells to monitor the effect on cell cycle progression of MCF-7, MDA-MB-231 and MCF-12A cells. The latter was accomplished by means of ethanol fixation and propidium iodide staining of cells. Propidium iodide determined the amount of DNA in

attendance correlating with stages of the cell cycle during cell division (175). In flow cytometry a laser beam of a single frequency is directed onto a hydrodynamically focused stream of fluid. A number of detectors are aimed at the point where the stream passes through the light beam; one in line with the light beam (forward scatter (FSC)) and several perpendicular to it side scatter (SSC) and one or more fluorescent detectors (197). Each suspended particle passing through the beam scatters the light. Fluorescent chemicals in the particle may be excited into emitting light at a lower frequency than the light source (198). This combination of scattered and fluorescent light is detected by the detectors. By analyzing fluctuations in brightness at each detector (one for each fluorescent emission peak) it is possible to deduce the size, quantity and fluorescent intensity (DNA content when stained with propidium iodide) of cells. FSC correlates with cell volume and SSC depends on inner complexity of the particle *e.g.* amount of DNA, shape of nucleus, etc.

A) Materials

99.9% ethanol was supplied by Merck Co. (Munich, Germany). Propidium iodide was purchased from Sigma-Aldrich (St. Louis, United States of America).

B) Methods

Exponentially growing MCF-7, MDA-MB-231 and MCF-12A cells were seeded at 500 000 cells per 25 cm^2 flask. After 24 h attachment, cells were exposed to EMBS. Cells were trypsinized and resuspended in 1ml growth medium. Cells ($1x10^6$) were centrifuged for 5 min at 300 x g. The supernatant was discarded and cells were resuspended in 200 µl of ice-cold PBS containing 0.1% FCS. Ice-cold (4 ml) 70% ethanol was added in a drop wise manner and cells were stored at 4ºC for 24 h. After 24 h, the cells were pelleted by centrifugation (300 x g) for 5 min. The supernatant was removed and cells were resuspended in 1 ml of PBS containing propidium iodide (40 µg/ml) and incubated at 37ºC and 5% CO_2 for 45 min. Propidium iodide fluorescence (relative DNA content per cell) was measured with a fluorescence activated cell sorting (FACS) FC500 System flow cytometer (Beckman Coulter South Africa (Pty) Ltd) equipped with an air-cooled argon laser excited at 488 nm. Data from at least 10 000 events were analyzed with CXP software (Beckman Coulter South Africa (Pty) Ltd). Data from cell debris (particles smaller than apoptotic bodies) and clumps of 2 or more cells were removed from further analysis. Cell cycle distributions were calculated with Cyflogic 1.2.1 released 2008/11/19 (Perttu Terho & Cyflo Ltd) by assigning relative

DNA content per cell to sub-G_1, G_1, S and G_2M fractions. Propidium iodide molecules emit light at 617 nm therefore, data obtained from the log forward scatter detector nr 3 (FL3 log, detects 600 nm emissions) were represented as histograms on the *x*-axis.

2.3.5 Apoptosis

2.3.5.1 Flow cytometry utilizing annexin V- fluorescein isothiocyanate

The presence of apoptosis was evaluated and quantified using flow cytometry in combination with Annexin V-fluorescein isothiocyanate (FITC). One of the earliest indications of apoptosis is the externalization of the membrane phospholipid phosphatidylserine (PS) layer of the plasma membrane. Once exposed to the extracellular environment, binding sites on PS become available for Annexin V, a 35-36 kDa, Ca^{2+}-dependent, phospholipid binding protein with a high affinity for PS. Annexin V-FITC binds in the presence of calcium ions with high affinity to the negatively charged phospholipids including phosphatidylserine (199, 200). Viable cells preserve an asymmetric division of several phospholipids between inner- and outer leaflets of the plasma membrane (201).

Phosphatidylserine is mainly located in the inner membrane leaflet facing the cytosol. In apoptosis the calcium-dependent phospholipids scramblase activity is activated which results in the scrambling the aminophospholipids over the inner and outer membrane leaflets (199, 200). The latter leads to the loss of the plasma membrane asymmetry and the externalization of the phosphatidylserine layer of the cell membrane (199). Aminophospholipid flippase is responsible for the externalization of phosphatidylserine and phosphatidylethanolamine that provide binding sites for Annexin V (199). Propidium iodide was excluded from the plasma membrane of viable cells and only entered and stained the DNA of unviable cells (199). Thus Annexin V-FITC in conjunction with propidium iodide utilizing flow cytometry allowed identification of different stages of apoptosis (early and late) and necrosis.

A) Materials

The Annexin V-FITC Kit was purchased from BIOCOM biotech Pty (Ltd) (Clubview, Gauteng, South Africa).

B) Methods

Exponentially growing MCF-7, MDA-MB-231 and MCF-12A cells were seeded at 500 000 cells per 25 cm^2 flask. After 24 h attachment, cells were exposed to EMBS. Cells were trypsinized and 1 x 10^6 cells were resuspended in 1 ml of 1x Binding Buffer and centrifuged at 300 x g for 10 min. The supernatant was removed and cells were resupended in 100 µL of 1x Binding Buffer. Annexin V-FITC (10 µl) was added and samples were incubated for 15 min in the dark at room temperature. After 15 min, cells were washed by adding 1 ml of 1x Binding Buffer and thereafter cells were centrifuged at 300 x g for 10 min. The supernatant was pipetted off and cells were resuspended in 500 µl of 1x Binding Buffer solution. Immediately prior to analysis, 5 µl of propidium iodide (100 µg/ml) was added and gently mixed. Propidium iodide fluorescence (oncotic cells) and annexin V fluorescence (apoptotic cells) were measured with FACS FC500 System flow cytometer (Beckman Coulter South Africa (Pty) Ltd) equipped with an air-cooled argon laser excited at 488 nm. Data from at least 10 000 events were analyzed with CXP software (Beckman Coulter South Africa (Pty) Ltd). Data from cell debris (particles smaller than apoptotic bodies) and clumps of 2 or more cells were removed from further analysis. Propidium iodide molecules emit light at 617 nm and FITC emit at 530 nm therefore, data obtained from the log forward scatter detector nr 1 (Fl Lin, detects 515-545 nm emissions) and the log forward scatter detector nr 3 (Fl3 Lin, detects 600 nm emissions) were represented as a single dot-plot. FL3 log (propidium iodide) was represented on the *x*-axis and FL1 log (FITC) was represented on the *y*-axis. The FL3 log/FL1 log dot-plot was divided into for quadrants. The bottom-left quadrant was assigned to measure the viable cells, top left quadrant was assigned to cells in the early stages of apoptosis, the top-left quadrant was assigned to cells undergoing late apoptosis and the bottom-right quadrant was assigned to cells in the late stages of apoptosis which have become necrotic. Distributions of cells within the quadrants were calculated with Cyflogic 1.2.1 released 2008/11/19 (Perttu Terho & Cyflo Ltd).

2.3.5.2. Flow cytometry (mitochondrial membrane potential)

The mitocapture mitochondrial kit provided quantitive information apoptosis information where a cationic dye, 5,5',6,6'-tetrachloro-1,1',3,3'-tetraethylbenzimidazolylcarbocyanine iodide was used to detect the loss of the mitochondrial membrane potential. The reduction of the mitochondrial membrane

potential is an early feature during apoptosis due to the loss of the electrochemical gradient across the mitochondrial membrane (202). The mitochondrial membrane potential is dependent upon the mitochondrial permeability transition pore (PTP). The PTP consists of adenine nucleotide translocator protein, the voltage dependent anion channel, benzodiazepine receptor and cyclophilin D. The opening of PTP results in mitochondrial swelling and subsequent rupture of the intermembrane space leading cytochrome *c* release and apoptosis induction (203). In healthy cells, the dye concentrated in the mitochondrial matrix that formed red fluorescent aggregates. In any event that reduces the mitochondrial potential, such as apoptosis induced by sulphamoylated 2ME2 analogues, the dye remained in the cytoplasm in a green fluorescent monomeric form. The intensity of the fluorescence in cells was measured by cytometry analysis.

A) Materials

MitoCaptureTM Mitochondrial Apoptosis Detection Kit was purchased from BIOCOM biotech Pty (Ltd) (Clubview, South Africa).

B) Methods

Exponentially growing MCF-7 and MCF-12A cells were seeded at 500 000 cells per 25 cm^2 flask. After 24 h of attachment, medium was discarded and cells were exposed to EMBS and incubated for 24 h. Cells were trypsinized and centrifuged at 13 000 x g and resuspended in 1ml of diluted Mitocapture solution (1 µl mitocapture: 1 ml pretreated incubation buffer). Cells were incubated at 37°C, 5% CO_2 for 20 min and centrifuged thereafter at 500 x g. The supernatant was discarded, cells were resuspended in 1ml of prewarmed incubation buffer at 37°C. Cells were analyzed immediately after following the above-mentioned step using fluorescence activated cell sorting (FACS) FC500 System flow cytometer (Beckman Coulter South Africa (Pty) Ltd). Apoptotic cells were detected in the FITC channel (usually FL1) showing green fluorescence.

2.3.5.3. Spectrophotometry and flow cytometry (detection of caspase activation)

Caspases is a family of cysteinyl aspartate proteinases (cysteine proteases that cleave their substrates at specific aspartyl residues) and are instrumental to the execution of apoptosis (63, 202). Apoptotic caspases belongs to one of two categories; initiator caspases or effector / executioner caspase (64). Initiator caspases that trigger apoptosis include caspases 2, 8, 9, and 10 (65). Effector caspases include caspases 3,

6, and 7 that execute the apoptotic cell death (66). Apoptosis was detected by means of kits that detect caspases 6, caspase 7 (effector caspases) and caspase 8 (an initiator caspase). There are three caspase-dependent cell death pathways including the mitochondrial pathway (intrinsic), death receptor pathway (extrinsic) and the endoplasmic-specific pathway. Although the intrinsic and extrinsic cell death pathways act independently to initiate the cell death in some cellular networks, in most tumorigenic cells there is a delicate crosstalk between these two pathways which results in the activation of executioner caspases (204).

A) Materials

Caspase 6 colorimetric assay kit, the Flice/Caspase 8 colorimetric assay and the rabbit polyclonal antibody for anti-active caspase 7 and the anti-rabbit antibody conjugated to Dylight™ 488 were acquired from BIOCOM biotech Pty (Ltd) (Clubview, Gauteng, South Africa). The Fixation buffer, permeabilization buffer and the assay buffer from the FlowCellet™ Bcl-2 activation dual detection kit was supplied by Microsep (Pty) Ltd (Johannesburg, Gauteng, South Africa).

B) Methods

Caspase 6 and caspase 8

Cells (500 000) were seeded with an overnight attachment policy (30, 31). After 24 h of exposure to EMBS, cells were trypsinized and centrifuged at 12000 rpm. Subsequently, 500 000 cells were resuspended in 50 µl of chilled cell lysis buffer and incubated on ice for 10 min. Cells were centrifuged at 10,000 x g for 1 min. The supernatant was transferred to a fresh tube and put on ice. After determining the protein concentration using the BCA protein assay (Thermo Fisher Scientific, Johannesburg, SA), 100 µg protein/50 µl cell lysis buffer was mixed with 50 µl 2X reaction buffer (containing 10mM DTT). Afterwards 5 µl 4mM Ac-Leu-Glu-His-Asp-p-nitroanilide (Ac-VEID-*p*NA) (caspase-6-specific substrate), Ac-Ile-Glu-Thr-Asp-p-nitroanilide (Ac-IETD-*p*NA) (caspase-8-specific substrate) (200 µM final concentration) was added and incubated at 37°C for 120 min. Samples were read at 405 nm on the EL_x800 Universal Microplate Reader available from Bio-Tek Instruments Inc. (Vermont, United States of America).

Caspase 7

Cells were seeded at 500 000 cells per flask and after 24 h attachment cells were exposed to EMBS with appropriate controls. Subsequently, cells were trypsinised and

500 000 cells were centrifuged and medium discarded. Cells are then resuspended in wash buffer and centrifuged again. The supernatant was removed and cells were resuspended in fixation buffer (0.1% formaldehyde) and incubated for 20 min at room temperature. Afterwards, the supernatant was removed; cells were resuspended in assay buffer (1% bovine serum albumin (BSA)) and centrifuged. Cells were then resupended and resuspended in 500 µl ice-cold permeabilization buffer (100% methanol) and left on ice for 10 min. Samples were then centrifuged and the sediment was resuspended in assay buffer. Cells were centrifuged and resuspended in 100 µl assay buffer with 15 µg/ml primary antibody (rabbit anti-active caspase 7). Cells were then incubated on ice for 90 min. Subsequently, 900 µl assay buffer was added to samples. After centrifugation (2000 rpm), samples were washed twice with 500 µl assay buffer, centrifuged and resuspended in 100 µl assay buffer with 0.2 µg/ml anti-rabbit antibody conjugated to Dylight^{TM} 488 fluorochrome. Samples were incubated on ice for 60 min in the dark. Assay buffer (900 µl) was added; samples were centrifuged and washed twice with 500 µl assay buffer. Fluorescence was then measured using the FL1 channel by means of the fluorescence activated cell sorting (FACS) FC500 System flow cytometer equipped with an air-cooled argon laser excited at 488 nm that was supplied by Beckman Coulter South Africa (Pty) Ltd. (Pretoria, Gauteng, South Africa). Data from at least 10 000 events were analyzed with CXP software (Beckman Coulter South Africa (Pty) Ltd).

2.3.6 Flow cytometry using rabbit polyclonal anti-LC3B conjugated to DyLight 488 (autophagy induction)

The Rabbit polyclonal anti-LC3B conjugated to DyLight 488 was used to detect autophagy induction. The detection of the conversion of LC3-I to LC3-II is a useful and sensitive marker for identifying autophagy in mammalian cells (117, 118). LC3B antibody allowed for autophagy detection and confirmation (results provided by light microscopy and Hoechst 33342, propidium iodide and acridine orange staining) in mammalian cells during fluorescence microscopy by binding to the autophagosome membrane.

A) Materials

Formaldehyde, methanol, triton X-100, propidium iodide and bovine serum albumin (BSA) were purchased from Sigma-Aldrich (St. Louis, United States of America). Rabbit

polyclonal anti-LC3B conjugated to DyLight 488 was supplied by BIOCOM biotech Pty (Ltd) (Clubview, South Africa).

B) Methods

Exponentially growing MCF-7, MDA-MB-231 and MCF-12A cells were seeded at 500 000 cells per 25 cm^2 flask. After 24 h attachment the medium was discarded and cells were exposed to EMBS. Cells were washed with cold PBS and pelleted. Cells were fixed with 3 ml 0.01% formaldehyde in PBS for 10 min at 4˚C. Cells were centrifuged and resuspended in 200 µl PBS, followed by 1 ml ice-cold methanol (-20˚C) for 15 min at 4˚C. Afterwards, cells were washed twice with cold PBS. Cells were stained with the 0.5 ml antibody cocktail (0.05% triton X-100, 1% BSA, 40 µg/ml propidium iodide and 0.5 µg/ml conjugated rabbit polyclonal anti-LC3B antibody) prepared in PBS for 2 h at 4˚C. Cells were washed trice with PBS/0.05% triton X-100/1% BSA and analyzed with flow cytometry. Data from at least 10 000 – 30 000 events were analyzed by means of Cyflogic version 1.2.1 software (Pertu Therho, Turko, Finland).

2.3.7 Crosstalk between autophagy and apoptosis

2.3.7.1 Reactive oxygen species (ROS)

In the following experiments ROS generation induced by EMBS was investigated. Increased ROS production results in release of cytochrome *c* that binds to apoptosis activating factor 1(apaf-1) in the presence of and ATP and leads to the activation of caspase 9 that triggers apoptosis (146). Studies have reported mitochondrial ROS play an essential role in survival and cell death by means of autophagy. Low ROS levels potentially promote survival by autophagy induction in order to redistribute intracellular resources under starvation, while increased ROS production promotes controlled autophagic cell death when survival is unachievable (150). 2,7-Dichlorofluorescein diacetate (DCFDA), a non-fluorescent probe, which upon oxidation by ROS and peroxides, is converted to the highly fluorescent derivative DCF. The latter was used to detect hydrogen peroxide (205). Superoxide generation was evaluated using hydroethidine (HE). HE is oxidized by superoxide to a red fluorescing compound (145, 205).

A) Materials

DCFDA, HE and PBS was acquired from BIOCOM biotech Pty (Ltd) (Clubview, South Africa).

B) Methods

Hydrogen peroxide detection

Exponentially growing MCF-7, MDA-MB-231 and MCF-12A cells were seeded at 500 000 cells per 25 cm^2 flask. After 24 h of attachment, medium was discarded, cells were exposed to EMBS. Cells were trypsined, washed with PBS and trypsinized. Cells (1000 000) were resuspended in 1 ml PBS. DCFDA stock solution (1 µl, 10 mM) was added to the cells and samples were incubated for 25 min at 37°C. Cells were analysed using a fluorescence activated cell sorting (FACS) FC500 System flow cytometer (Beckman Coulter South Africa (Pty) Ltd). Data from at least 10 000-30 000 events were analyzed by means of Cyflogic version 1.2.1 software (Pertu Therho, Turko, Finland).

Superoxide detection

Exponentially growing MCF-7, MDA-MB-231 and MCF-12A cells were seeded at 500 000 cells per 25 cm^2 flask. After 24 h of attachment, medium was discarded and cells were exposed to EMBS. Cells were trypsinized, washed with PBS and centrifuged. Cells (1000 000) were resuspended in 1 ml PBS. HE stock solution (1 µl, 10 mM) was added and samples were incubated for 15 min at 37°C. Cells were analysed using a fluorescence activated cell sorting (FACS) FC500 System flow cytometer (Beckman Coulter South Africa (Pty) Ltd). Data from at least 10 000 – 30 000 events were analyzed by means of Cyflogic version 1.2.1 software (Pertu Therho, Turko, Finland).

2.3.8.2 Expression of p53

The apoptosis-autophagy crosstalk was investigated by means of demonstrating the effect of EMBS on p53 and murine double minute 2 (Mdm2). The tumor suppressor p53 protein is essential for genetic integrity. In response to DNA damage wild type p53 coordinates events resulting in cell cycle arrest, senescence and apoptosis. In undisturbed mammalian cells, p53 is maintained at low levels due to continuous ubiquitination (208, 209, 210).

(A) Materials

ImmunoSet p53/MDM2 Complex ELISA development set, RIPA cell lysis buffer, TMB substrate and plates (ImmunoSet pack) were purchased from BIOCOM biotech (Ltd) (Clubview, Gauteng, South Africa.

(B) Methods

Cells were seeded at a density of 5 000 cells per 96-well. After 24 h, cells were exposed to EMBS. After the exposure period, 100 µl of assay buffer (mixed according to suppliers' instructions) was added to the control wells. Standards (100 µl) and samples prepared in assay buffer were added to sterile wells. The plate was sealed and incubated for 1 h at room temperature. The wells were emptied and washed with 400 µl wash buffer (3 X). The detection antibody (100 µl) (mixed according to suppliers' instructions) was added to each sample, except for the blank and the plate was sealed and left for 1 h at 4°C. The wells was emptied and washed with 400 µl wash buffer, wash was repeated thrice. TMB solution (100 µl) was pipetted into each well and the plate was sealed for 30 min at room temperature. Subsequently, 1N hydrochloric acid was added and absorbance was read at 450 nm using EL_x800 Universal Microplate Reader (Bio-Tek Instruments Inc., Vermont, United States of America).

2.3.8.3 Bcl-2 expression

The crosstalk between autophagy and apoptosis was also investigated by demonstrating Bcl-2 expression. Bcl-2 is a anti-apoptotic protein belonging to the B-cell lymphoma-2 (BCL-2) family that manages apoptosis induction by regulating the mitochondrial membrane potential (211, 212, 213).

(A) Materials

The Flow Collect Bcl-2 activation dual detection kit was purchased from Merck Millipore (Ltd) (Massachusetts, United States of America).

(B) Methods

Exponentially growing MCF-7, MDA-MB-231 and MCF-12A cells were seeded at 500 000 cells per 25 cm^2 flask. After 24 h of attachment, medium was discarded and cells were exposed to EMBS. Cells were trypsinized, washed with 1 X wash buffer, centrifuged at 2500 rpm for 3 min. Fixation buffer (0.5 ml) was added and samples were incubated at room temperature for 20 min. Cells were centrifuged at 2500 rpm for 3 min and resuspended in 0.5 ml 1 X assay buffer. After centrifugation (2500 rpm) cells were resuspended in ice-cold 1 X permeabilization buffer and samples were left on ice

for 10 min. Samples were centrifuged at 2500 rpm, resuspended in 0.5 ml assay buffer and centrifuged again. Cells were stained using 5 µl 20 X antibody (as described by suppliers) and incubated in the dark for 60 min. Subsequently, 900 µl 1 X assay buffer was added to the samples and cells were centrifuged. Thereafter, cells were resuspended in 1 ml 1 X assay buffer and samples were analyzed using a fluorescence activated cell sorting (FACS) FC500 System flow cytometer (Beckman Coulter South Africa (Pty) Ltd). Data from at least 10 000 - 30 000 events were analyzed by means of Cyflogic version 1.2.1 software (Pertu Therho, Turko, Finland).

2.4 Statistical planning

Qualitative data were obtained from PlasDIC, TEM, light microscopy and fluorescent microscopy. Quantitative data were supplied by means of cell number determination, lactate dehydrogenase assay, NAD^+/NADH quantification kit, $NADP^+$/NADPH quantification kit, mitotic indices, flow cytometry and ELISA assays. Data for mitotic indices were obtained by counting 1000 cells on each slide of the biological replicates (repeated three times) and expressing data as a percentage of cells in each phase of mitosis, interphase and abnormal cells. Three independent experiments (cell number determination conducted with six replicates) were conducted where the average and standard deviation were calculated. Data were statistically analysed for significance using the factorial design approach of analysis of variance (ANOVA)-single model. This was followed by treatment comparison for possible effects of interactions between cell line types between time. Averages were represented in bar charts, with T-bars referring to standard deviations. *P*-values < 0.05 were regarded as statistically significant and were indicated by an asterisk (*).Flow cytometry analysis involved at least 10 000 events and was repeated thrice. Flow cytometry data were analyzed using Cyflogic version 1.2.1 software (Pertu Therho, Turko, Finland). Data analysis was descriptive representing effectiveness of EMBS as an anticancer agent and Stata 12 was used for analysing outcomes.

2.5 Logistics

All the required equipment were available and all relevant techniques and protocols were standardized in the Department of Physiology (University of Pretoria). The cell culture laboratory of the Department of Physiology at the University of Pretoria was

used to conduct the research project. TEM and SEM were conducted at the Electron Microscopy Unit at the University of Pretoria. Flow cytometry was done at the Department of Pharmacology (University of Pretoria). Professor AM Joubert was consulted on all the required techniques.

2.6 Ethical Approval

This research protocol was approved by the Research Ethics Committee (209/2012).

Chapter 3

3. Results

3 Antiproliferative activity

3.1 Spectrophotometry (crystal violet)

Crystal violet staining permits for the quantification of the cell number in monolayer cultures as a function of the absorbance of the dye taken up by the cells (180, 181, 182, 214). Staining nuclei of fixed cells with the crystal violet allows for rapid, accurate and reproducible quantification of cell numbers in cultures grown in 96-well plates measured spectrophotometrically at 570 nm corresponds to cell numbers (180, 181, 182). A time-dependent study was conducted with time intervals of 24 h, 48 h and 72 h.

EMBS exposure (24 h) decreased MCF-7 cell growth to 75% at 0.2 μM, 65% at 0.4 μM, 61% at 0.6 μM, 57% at 0.8 μM and 58% at 1 μM when compared to cells propagated in growth medium (Figure 3.1). EMBS exposure (24 h) decreased MDA-MB-231 cell growth to 70% at 0.2 μM, 69% at 0.4 μM, 61% at 0.6 μM, 57% at 0.8μM and 56% at 1 μM when compared to cells propagated in growth medium. EMBS exposure (24 h) decreased MCF-12A cell growth to 73% at 0.2 μM, 60% at 0.4 μM, 42% at 0.6 μM, 427% at 0.8 μM and 25% at 1 μM when compared to cells propagated in growth medium. Exposure to EMBS for 48 h and 72 h demonstrated the same antiproliferative activity in the MCF-7 cell line when compared to 24 h EMBS exposure (Figure 3.2 and Figure 3.3). Exposure to EMBS for 48 h decreased MDA-MB-231 cell growth to 32% at 0.2 μM, 30% at 0.4 μM, 26% at 0.6 μM, 22% at 0. 8μM and 20% at 1 μM when compared to cells propagated in growth medium. EMBS exposure (48 h) decreased MCF-12A cell growth to 78% at 0.2 μM, 71% at 0.4 μM, 37% at 0.6 μM, 28% at 0.8 μM and 5% at 1 μM when compared to cells propagated in growth medium. Exposure to EMBS for 72 h demonstrated minor growth recovery in MDA-MB-231 and MCF-12A cell lines.

Deducing the optimal exposure period and concentration focused on the demonstration that exposure to 0.4 μM EMBS for 24 h resulted in 60-65% growth inhibition in all three cell lines. However, this inhibition of cell proliferation reached a plateau effect in the tumorigenic cell lines. Thus, for all subsequent experiments, cell lines were exposed to

0.4 µM EMBS for 24 h to determine the effect on morphology and induction of autophagy, as well as apoptosis.

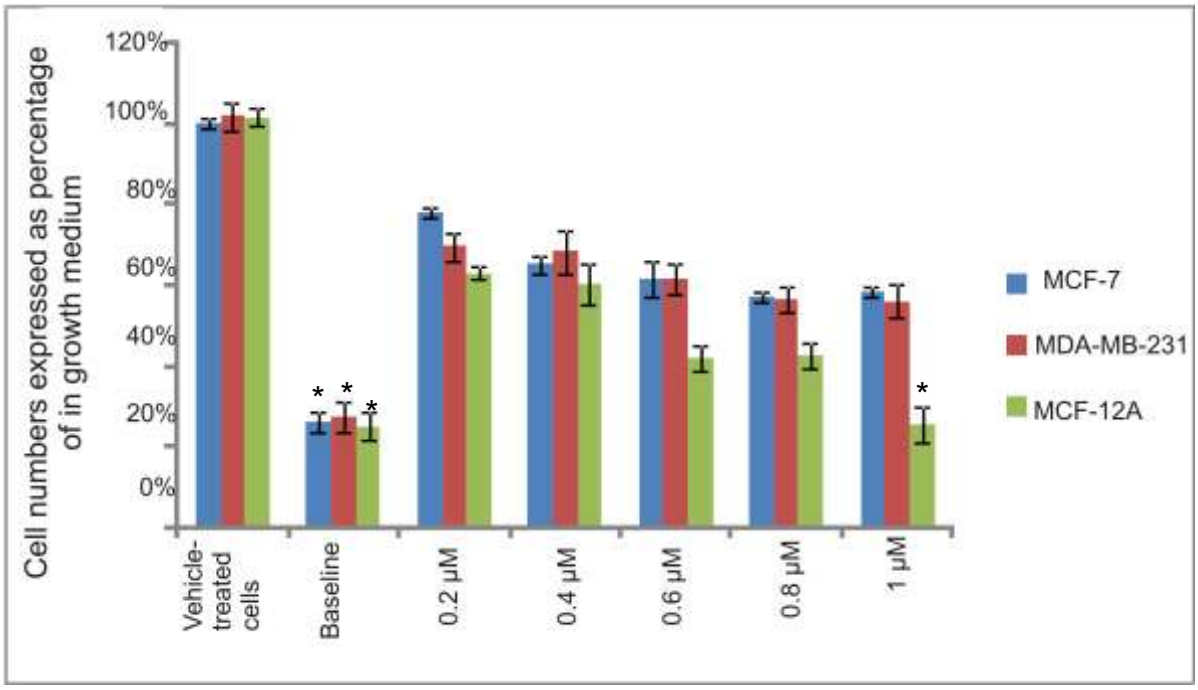

Figure 3.1: 24 h EMBS exposure to the MCF-7 cell line, MDA-MB-231 and the MCF-12A cell line resulted in significant growth inhibition in all three cell lines. EMBS exposure reduced MCF-7 cell growth to 75% at 0.2 µM, 65% at 0.4 µM, 61% at 0.6 µM, 57% at 0.8 µM and 58% at 1 µM when compared to cells propagated in growth medium. MDA-MB-231 cell growth was lowered to 70% at 0.2 µM, 69% at 0.4 µM, 61% at 0.6 µM, 57% at 0.8 µM and 56% at 1 µM when compared to cells propagated in growth medium. EMBS exposure (24 h) decreased MCF-12A cell growth to 73% at 0.2 µM, 60% at 0.4 µM, 42% at 0.6 µM, 42% at 0. 8µM and 25% at 1 µM when compared to cells propagated in growth medium. *(*An * indicates *P*-value < 0.05).

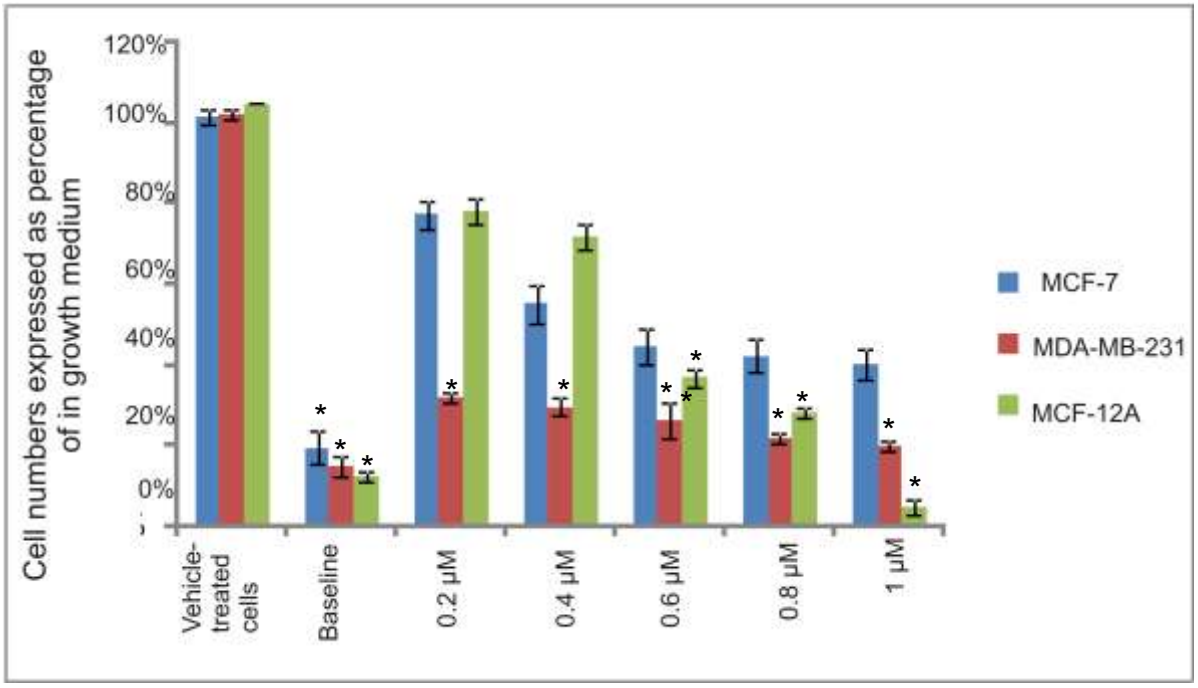

Figure 3.2: 48 h EMBS exposure to the MCF-7 cell line, MDA-MB-231 and the MCF-12A cell line resulted in significant growth inhibition in all three cell lines. MCF-7 cell growth did not decline after 24 h exposure and remained constant. MDA-MB-231 cell growth was decreased statistically significantly at all concentrations when compared to cells propagated in growth medium. EMBS exposure decreased MCF-12A cell growth to 78% at 0.2 µM, 71% at 0.4 µM, 37% at 0.6 µM, 28% at 0.8 µM and 5% at 1 µM when compared to cells propagated in growth medium. *(*An * indicates *P*-value < 0.05).

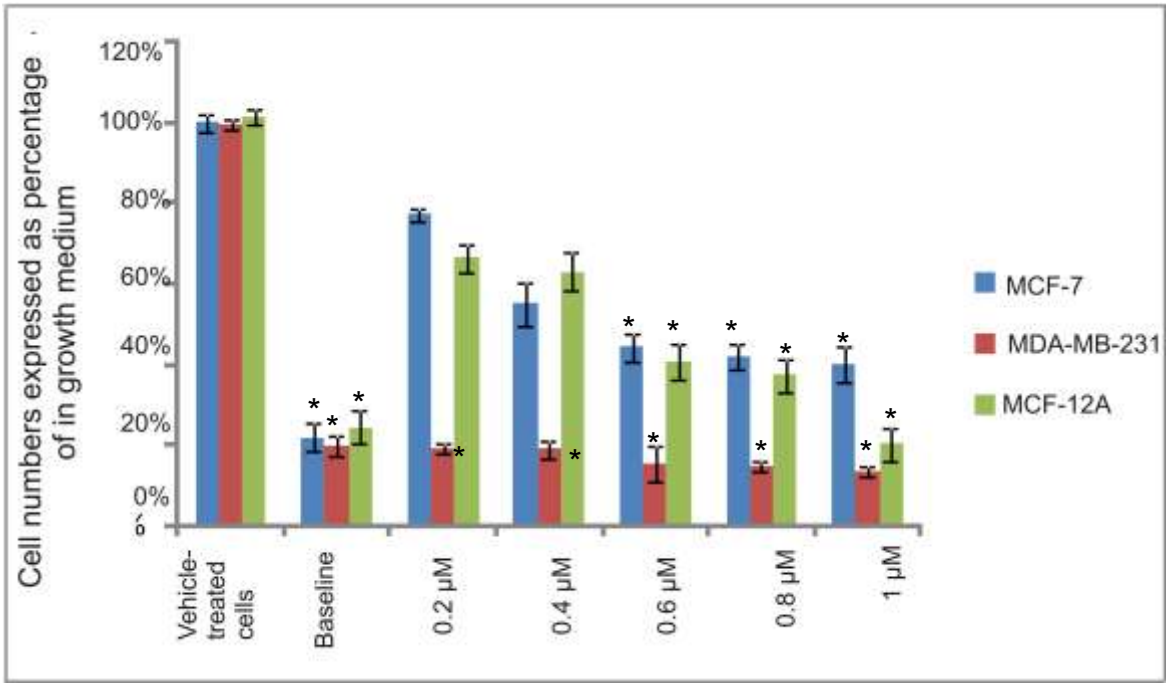

Figure 3.3: 72 h EMBS exposure to the MCF-7 cell line, MDA-MB-231 and the MCF-12A cell line resulted in minor growth recovery. However, MCF7 cell growth percentage remains unchanged after 24 h. *(*An * indicates *P*-value < 0.05).

3.1.2 xCELLigence real-time label-independent approach

The xCELLigence method (Roche Applied Science, Penzberg, Germany) was used to demonstrate cell growth, adhesion and morphology in real time utilizing a label-independent manner and was employed to confirm whether the selected dosage exerts optimal antiproliferative activity (176). The system quantifies electrical impedance across the micro-electrodes incorporated in the bottom of the tissue culture 96-well plates resulting in real-time and continuous cellular analysis as cells attach and proliferate. In addition, loss of attachment due to cell death results in a loss of electrical impedance and CI (215). The response of live cells to EMBS provided valuable proliferative and antiproliferative information which was not possible to achieve with any other end-point assays (183).

This novel real time label-independent approach quantified cell adhesion and cell proliferation of EMBS exposure to MCF-7, MDA-MB-231 and MCF-12A cells (Figure 3.4, Figure 3.5 and Figure 3.6). Cell proliferation was significantly inhibited in all cell lines (0.2-1μM) decreasing the cell index in the MCF-7 and MDA-MB-231 cell line. The MCF-12A cell line recovered after 24 h of exposure.

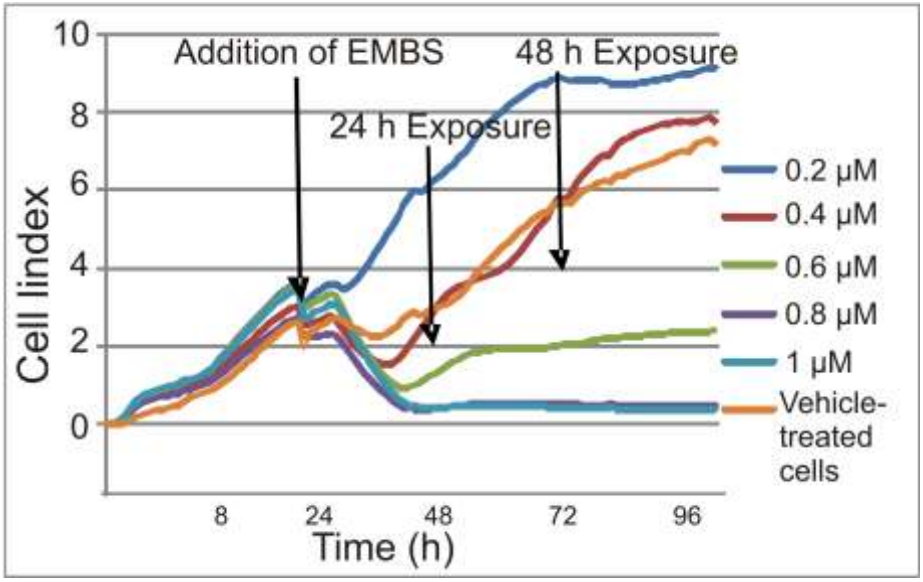

Figure 3.4: The xCELLigence method demonstrated the *in vitro* effects of EMBS on proliferation in the MCF-7 cell line. Cell proliferation was significantly inhibited at all concentrations in a concentration-dependent manner. *(P*-value < 0.05)

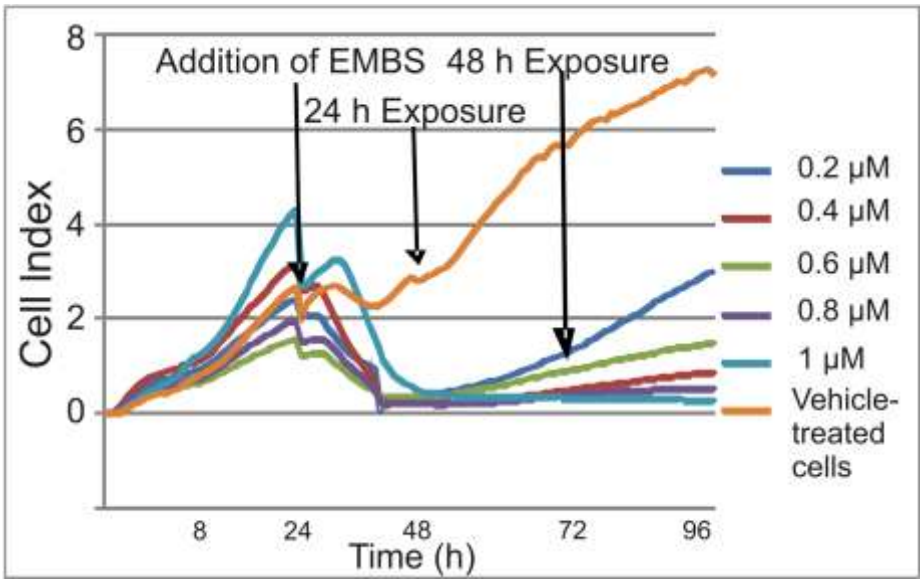

Figure 3.5: The xCELLigence method demonstrated the *in vitro* effects of EMBS on proliferation in the MDA-MB-231 cell line. Cell proliferation was significantly inhibited at all concentrations in a concentration-dependent manner. *(P*-value < 0.05)

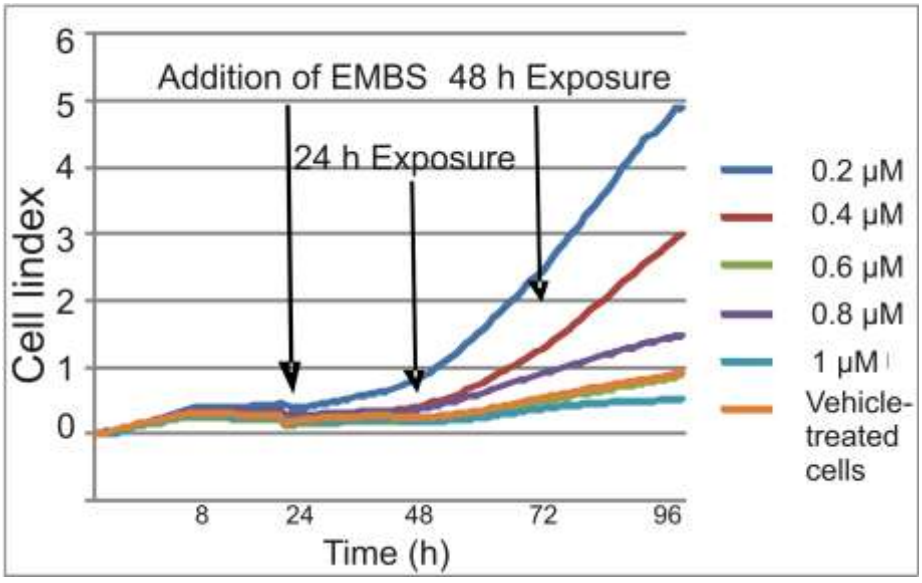

Figure 3.6: The xCELLigence method demonstrated the *in vitro* effects of EMBS on proliferation in the MCF-12A cell line. Cell proliferation was significantly inhibited at all concentrations in a concentration-dependent manner. However, after 24 h exposure cell growth recovers. *(P*-value < 0.05)

3.2 Cell viability and metabolism

3.2.1 Spectrophotometry (quantification of lactate dehydrogenase)

LDH release takes place either after injury or cell damage; following the loss of membrane integrity consequential from either apoptosis or necrosis Quantitative determination of lactate dehydrogenase (LDH) present in the medium is thus a

convenient cost effective parameter of cell viability (216). Cytotoxicity was determined by measuring the amount of LDH found in the medium after exposure to EMBS. Various controls were included in the experiment namely: background control, low control and high control. The background control consisted of growth medium. The low control refers to cells propagated in growth medium, and the high control refers to cells propagated in growth medium with cell lysis solution added to the cells shortly before the experiment is terminated (according to manufacturer's instructions).

A statistically insignificant (*P*-value > 0.05) increase in LDH levels was observed in the compound-treated cells when compared to the vehicle-treated cells (Figure 3.7).

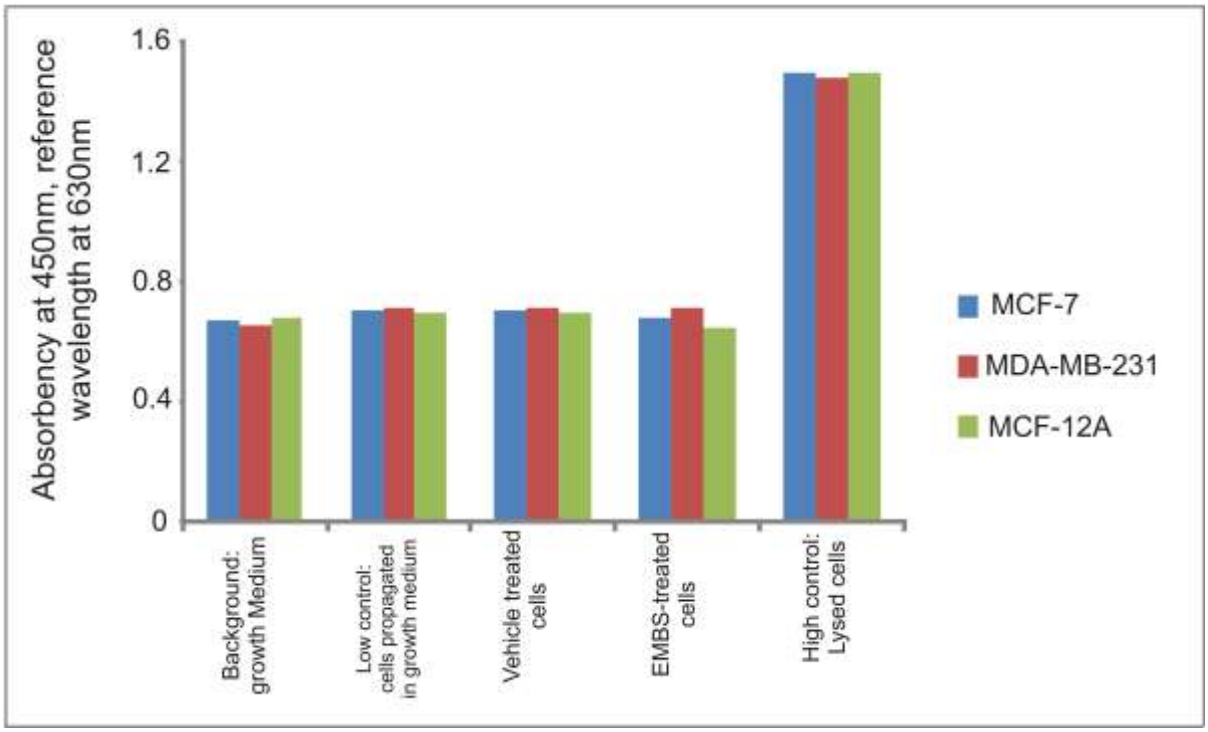

Figure 3.7: LDH levels of EMBS-treated MCF-7, MDA-MB-231 and MCF-12A cells compared to vehicle-treated cells after 24 h exposure. No statistically significant increase in LDH levels were observed in treated cells. Results demonstrate that EMBS were not toxic to the cells. The background control consisted of growth medium only. The low control refers to cells resuspended in growth medium and the high control to cells resuspended in growth medium with cell lysis solution added to the cells shortly before the experiment was terminated (according to the manufacturer's instructions).

3.2.2 Spectrophotometry (NAD^+/NADH and $NADP^+$/NAPPH quantification)

The energy transformation induced by EMBS was assessed by assessing production of NAD^+/NADH and $NADP^+$/NAPPH that indicates metabolic adjustments by means of a

variety of dehydrogenases involved in aerobic and anaerobic metabolism and controls posttranslational protein modification (216). Energy transformation and the redox state of the cells were investigated via NAD^+/NADH and $NADP^+$/NADPH quantification. However, no statistically significant (*P*-value > 0.05) changes in NAD^+/NADH and $NADP^+$/NADPH concentrations were demonstrated after 24 h exposure to 0.4 µM EMBS exposure (Figure 3.8 and Figure 3.9).

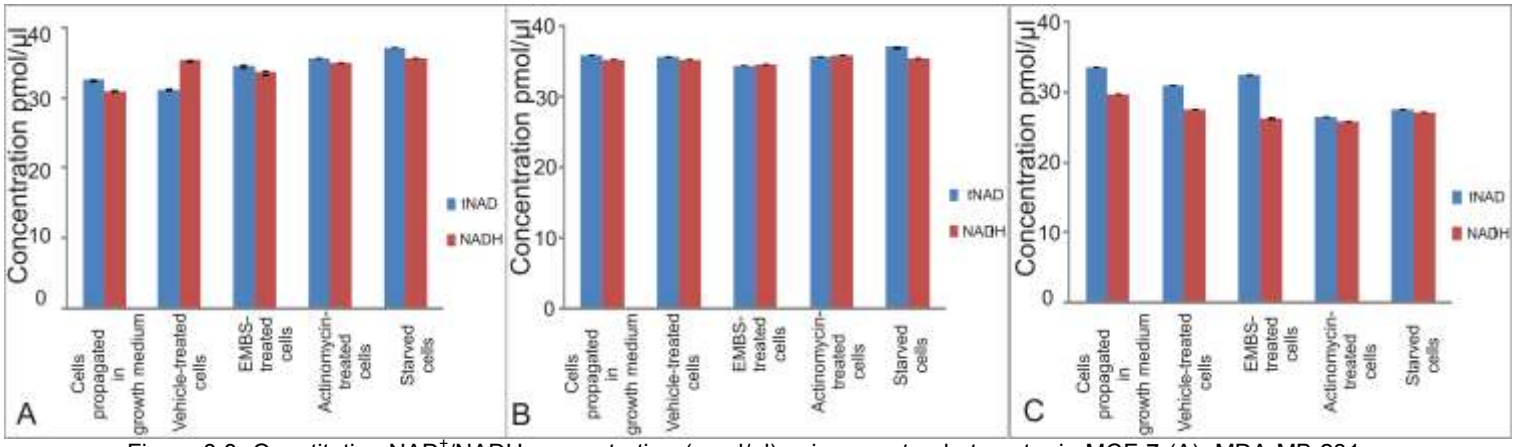

Figure 3.8: Quantitative NAD^+/NADH concentration (pmol/µl) using spectrophotometry in MCF-7 (A), MDA-MB-231 (B) and MCF-12A cells (C). No statistically significant changes in NAD^+/NADH concentration were observed in treated cells when compared to cells propagated in growth medium and vehicle-treated cells.

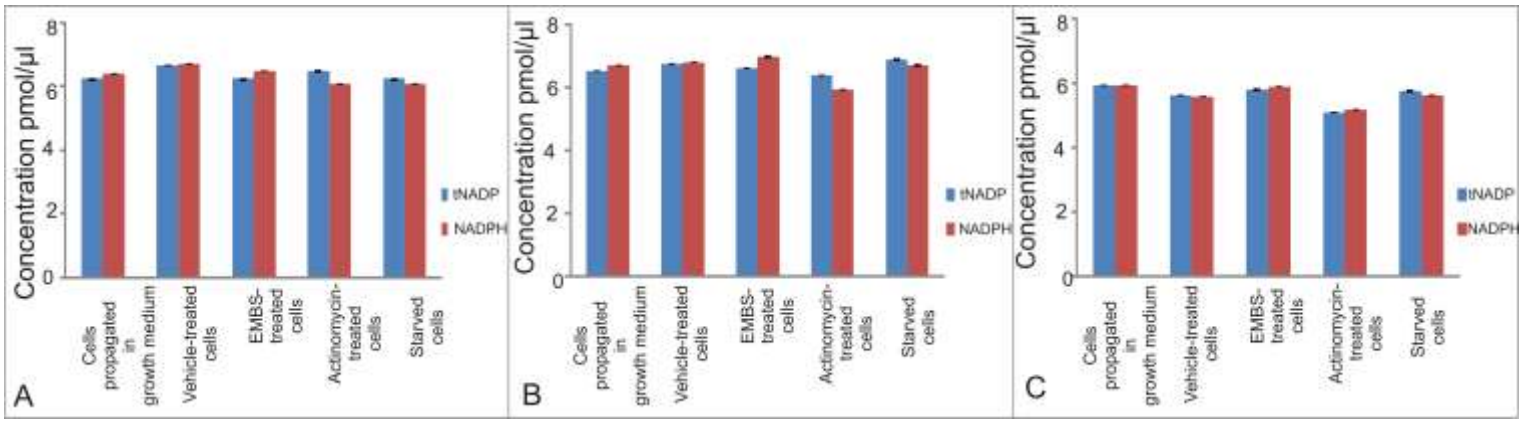

Figure 3.9: Quantitative $NADP^+$/NADPH concentration (pmol/µl) using spectrophotometry in MCF-7 (A), MDA-MB-231 and MCF-12A cells. No statistically significant changes in $NADP^+$/NADPH concentration were observed in treated cells when compared to cells propagated in growth medium and vehicle-treated cells.

3.3 Morphology

3.3.1 Polarization-optical transmitted light differential interference contrast

PlasDIC was utilized to view the effects on morphology exerted by EMBS. The latter allows for the initial investigation of characteristics with regard to apoptosis and

autophagy (178,179). Cells were photographed before exposure; furthermore, cells were also be photographed after exposure to EMBS (24 h; 0.4 µM).

PlasDIC photos of MCF-7, MDA-MB-231 and MCF-12A before exposure revealed no characteristics of distress (Figure 3.10). Cells propagated in growth medium and vehicle-treated cells revealed no abnormal morphology (Figure 3.11 and Figure 3.12). However, a decrease in cell density, rounded cells and the presence of apoptotic bodies were observed in all three cell lines after 24 h exposure to EMBS (Figure 3.13).

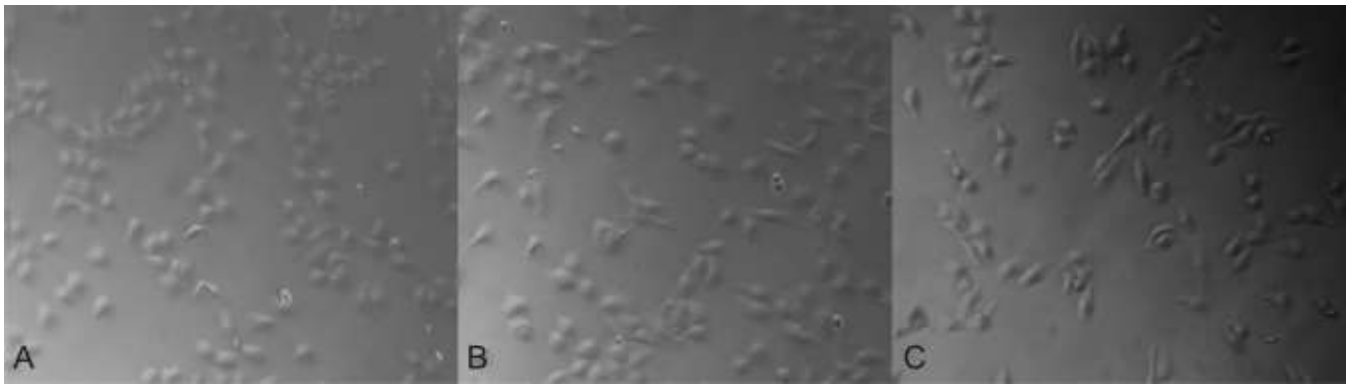

Figure 3.10: PlasDIC micrographs of MCF-7 cells (A), MDA-MB-231 cells (B) and MCF-12A cells (C) taken before exposure revealed cells with no signs of distress (20X magnification).

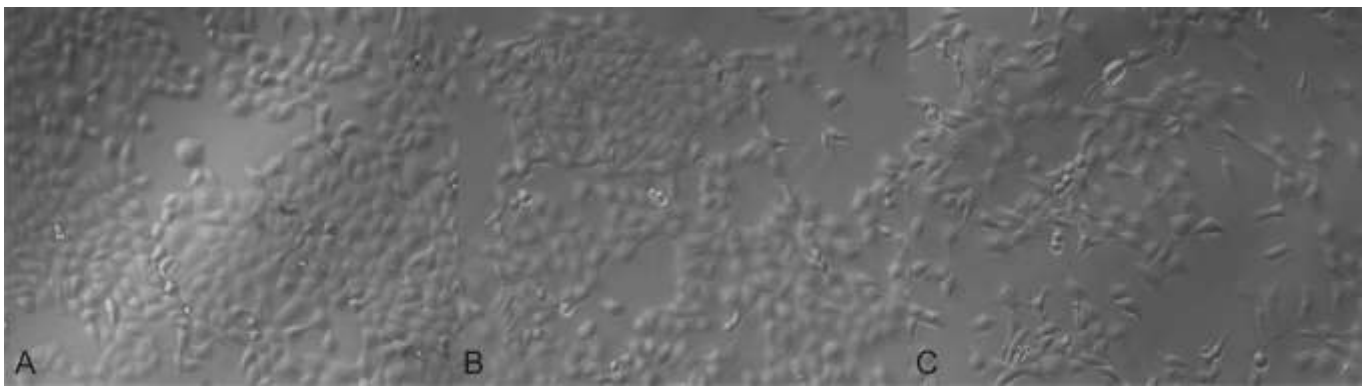

Figure 3.11: PlasDIC micrographs of medium propagated MCF-7 cells (A), MDA-MB-231 cells (B) and MCF-12A cells (C) demonstrated no abnormal morphology (20X magnification).

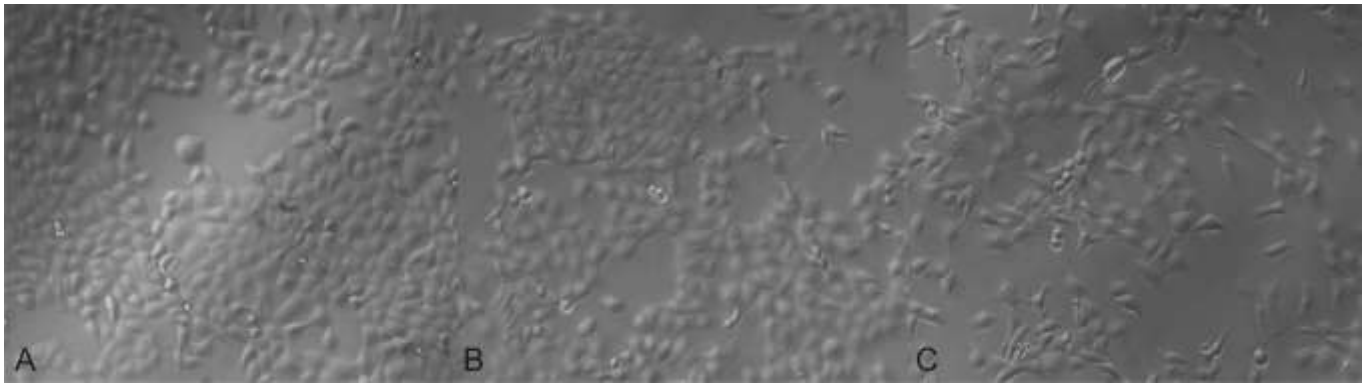

Figure 3.12: PlasDIC micrographs of vehicle-treated MCF-7 cells (A), MDA-MB-231 cells (B) and MCF-12A cells (C) demonstrated no irregular morphology (20X magnification).

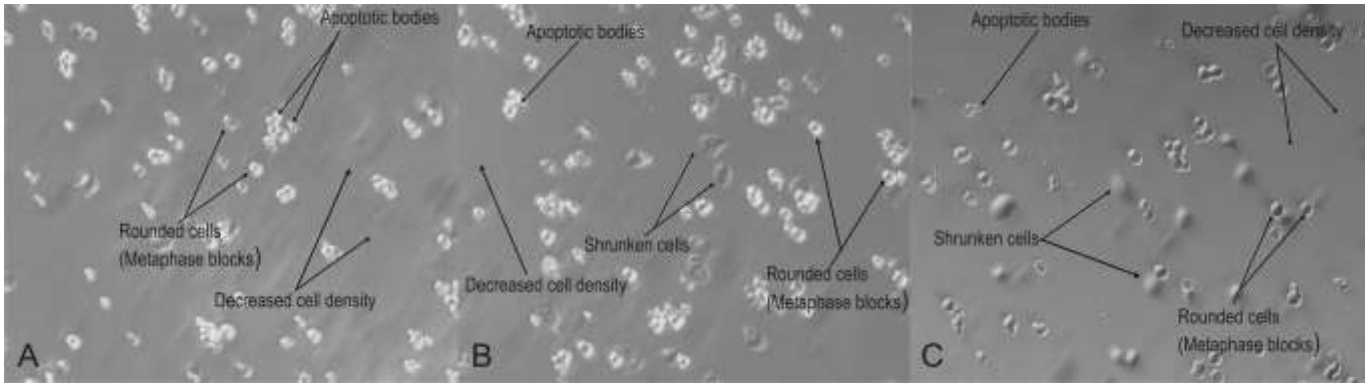

Figure 3.13: PlasDIC micrographs of EMBS-treated MCF-7 cells (A), MDA-MB-231 cells (B) and MCF-12A cells (C). Cells were exposed to 0.4 µM of EMBS for 24 h. EMBS-treated cells revealed decreased cell density, rounded cells and apoptotic bodies (20X magnification).

3.3.2 Light microscopy (haematoxylin and eosin staining)

Light microscopy was utilised to visualise the effects of EMBS on MCF-7, MDA-MB-231 and MCF-12A. Mitotic indices were determined to provide quantitative data by counting 1 000 cells for each sample (n=3). Data expressed the average percentage of cells in interphase, prophase, anaphase and telophase. Percentages of cells blocked in metaphase culminating in hallmarks of apoptosis were combined (218). This haematoxylin and eosin staining yielded both qualitative and quantitative information.

Haematoxylin and eosin-stained images of MCF-7, MDA-MB-231 and MCF-12A cells propagated in growth medium and vehicle-treated cells demonstrated no abnormal morphology with most cells occupying interphase (Figure 3.14 and Figure 3.15). Exposure to EMBS (0.4 µM; 24 h) resulted in decreased cell density and several cells blocked in metaphase and cell debris was observed when compared to cells

propagated in growth medium and vehicle-treated cells (Figure 3.16). Cells exposed to 0.1 µg/ml actinomycin for 24 h demonstrated severe decreased cell density. Several cells were blocked in metaphase and apoptotic bodies were present (Figure 3.17). Cells that were nutrient-deprived exhibited decreased cell density (Figure 3.18). Mitotic indices (quantitative data) revealed an increase in the number of apoptotic cells and an increase in the number of cells in metaphase in all three cell lines after exposure to 0.4 µM EMBS for 24 h (Figure 3.19 and Table 3.1).

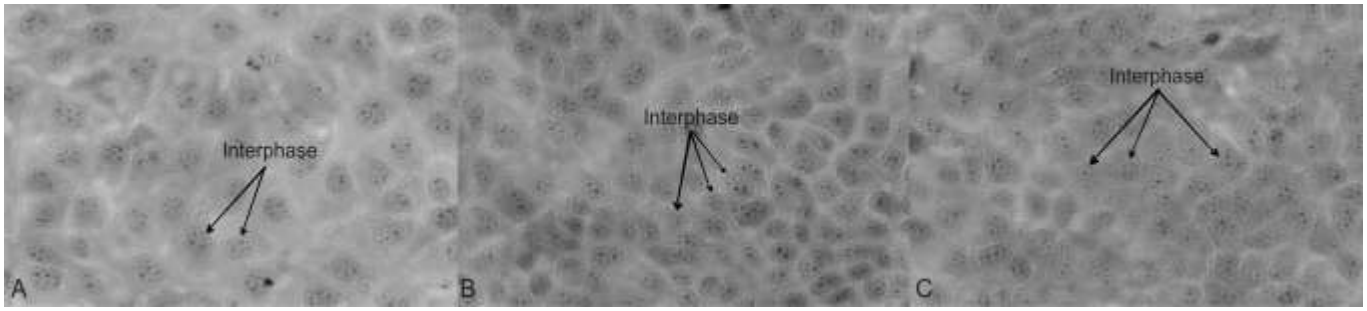

Figure 3.14: Haematoxylin and eosin-stained MCF-7 (A), MDA-MB-231 (B) and MCF-12A cells (C) propagated in growth medium demonstrated no abnormal morphology (20X magnification).

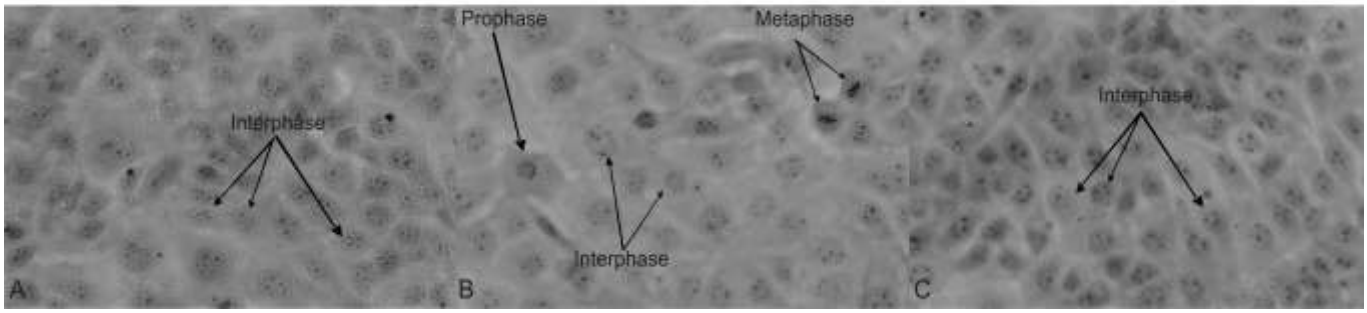

Figure 3.15: Haematoxylin and eosin-stained vehicle-treated MCF-7 (A), MDA-MB-231 (B) and MCF-12A cells (C) demonstrated no abnormal morphology (20X magnification).

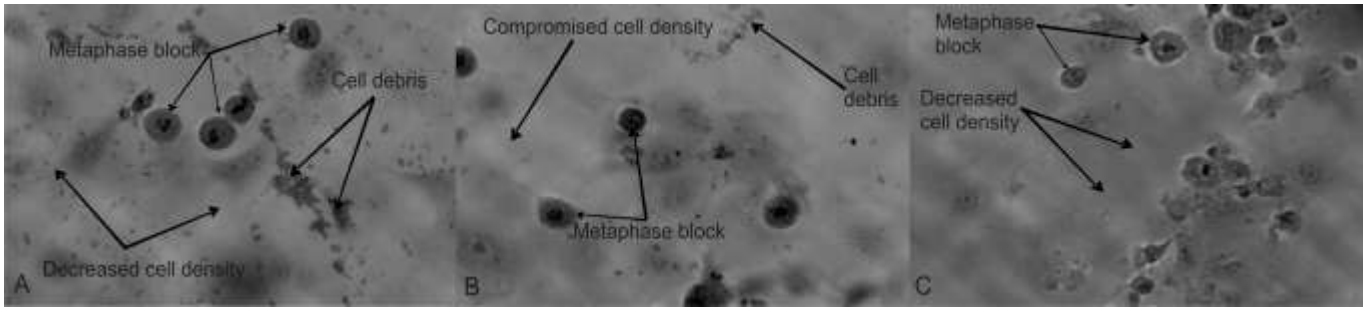

Figure 3.16: Haematoxylin and eosin-stained images of EMBS-treated MCF-7 (A), MDA-MB-231 (B) and MCF-12A cells (C). All three cell lines were exposed to 0.4 µM for 24 h and resulted in decreased cell density, cell debris and several cells blocked in metaphase culminating in apoptosis (20X magnification).

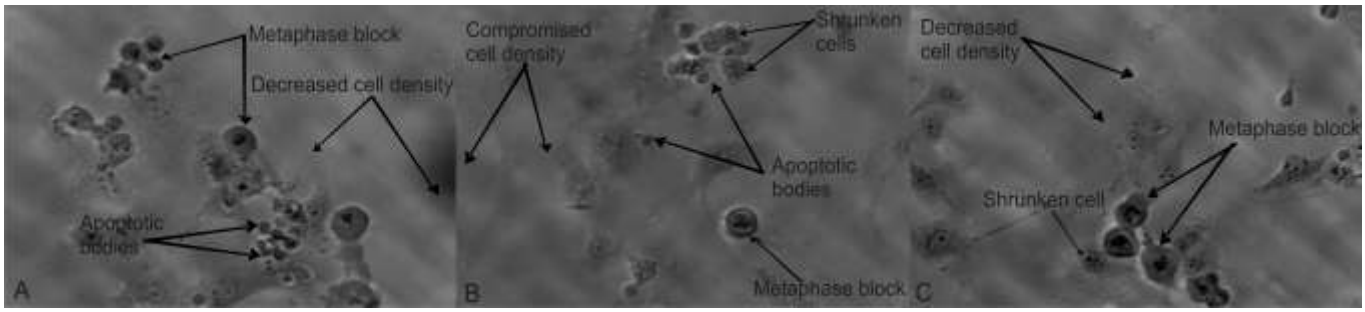

Figure 3.17: Haematoxylin and eosin-stained images of Actinomycin D-treated MCF-7 (A), MDA-MB-231 (B) and MCF-12A cells (C). Several hallmarks of apoptosis were observed including compromised cell density, apoptotic bodies, shrunken cells and cells blocked in metaphase (20X magnification).

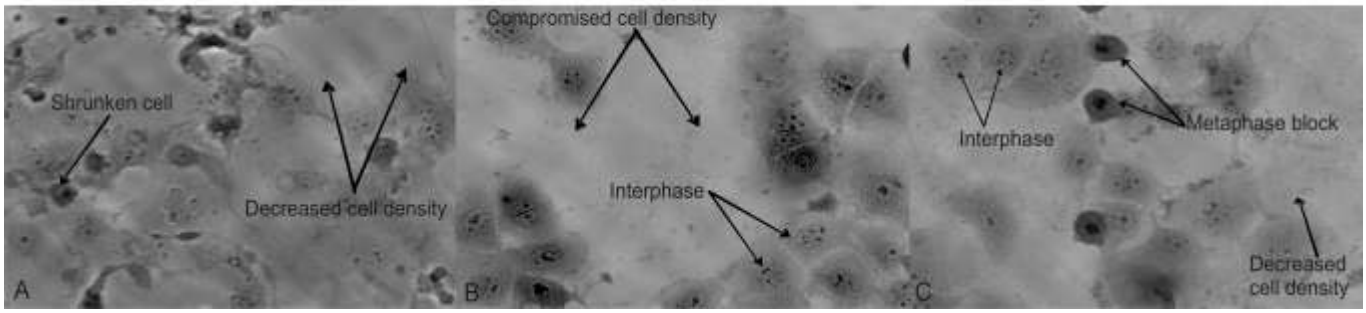

Figure 3.18: Haematoxylin and eosin-stained images of starved MCF-7 (A), MDA-MB-231 (B) and MCF-12A cells (C). Cells deprived of nutrients illustrated compromised cell density. MCF-7 starved cells were shrunken and starved MCF-12A cells displayed cells blocked in metaphase (20X magnification).

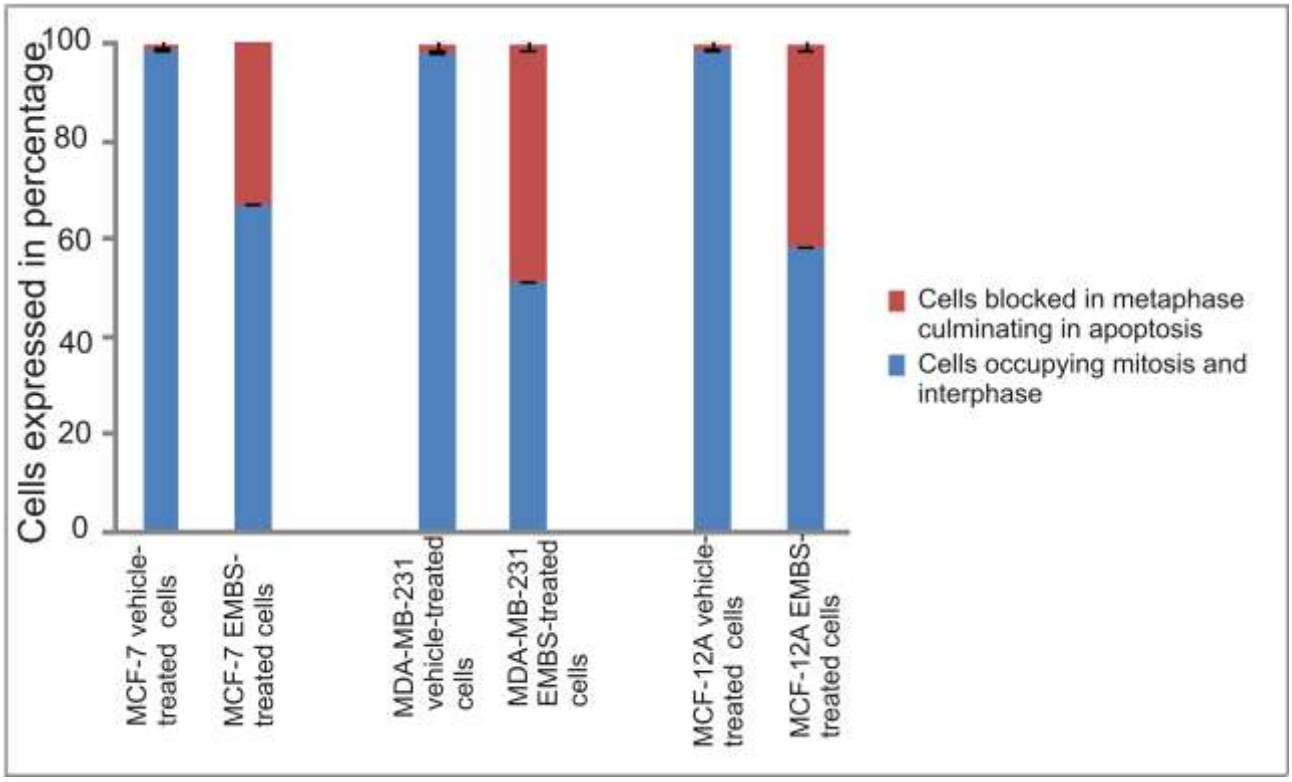

Figure 3.19: Mitotic indices of MCF-7, MDA-MB-231 and MCF-12A cells after exposure to EMBS expressed as a percentage of a thousand cells counted. Distinction was made between normal mitotic cells and abnormal mitotic cells, cells that presented with membrane blebbing and cells blocked in metaphase, culminating in apoptosis.

Table 3.1: Mitotic indices: percentage of cells in mitosis, interphase and cells featuring characteristics of apoptosis (an * indicates *P*-value < 0.05).

	Interphase	Prophase	Anaphase	Telophase	Cells blocked in metaphase culminating in apoptosis
MCF-7 cells Vehicle-treated cells	96.10±3%	1.30±0.8%	0.80±0.22%	0.80±0.044%	1±0.031%
MCF-7 cells EMBS-treated cells	55.6%±2% *	1.10±0.21%	0.10±0.23%	0.20±0.26%	43±2.16% *
MDA-MB-231 Vehicle-treated cells	94.30±2.3%	2.30±0.06%	1±0.02%	0.80±0.01%	1.60±0.05%
MDA-MB-231 EMBS-treated cells	48.2±3.1% *	1.90±0.08%	0.70±0.3%	0.30±0.03%	48.9±1.12% *
MCF-12A cells Vehicle-treated cells	95.50±4.2%	2.20±0.02%	0.90±0.02%	0.20±0.01%	1.20±0.01%
MCF-12A cells EMBS-treated cells	54.7±2.1% *	1.90±0.01%	0.90±0.01%	0.80±0.01%	41.7±0.012% *

3.3.3 Transmission electron microscopy

Transmission electron microscopy (TEM) was employed to observe and rounding of the cell, retraction of pseudopodes, cytoplasmic and nuclear condensation (pyknosis), chromatin condensation, nuclear fragmentation (karyorrhexis), plasma membrane blebbing and engulfment by resident phagocytes which are all characteristics of apoptosis (188, 189). Characteristics of autophagy, namely the autophagic vacuolization of the cytoplasm were also identified. These vacuoles are large double-membrane vesicles containing degenerating sequestered cytoplasmic constituents (188, 189).

TEM images of MCF-7, MDA-MB-231 and MCF-12A cells propagated in growth medium and vehicle-treated cells revealed no abnormal morphology (Figure 3.20 and Figure 3.21). Hallmarks of apoptosis including shrunken cells apoptotic bodies were

observed in EMBS-treated MCF-7, MDA-MB-231 and MCF-12A cells (Figure 3.22). In addition, vacuoles were observed suggesting autophagy induction by EMBS. MCF-7, MDA-MB-231 and MCF-12A cells treated with 0.1 µg/ml actinomycin D as a positive control for apoptosis and cells with induced starvation as a positive control for autophagy resulted in severely compromised cells (Figure 3.22).

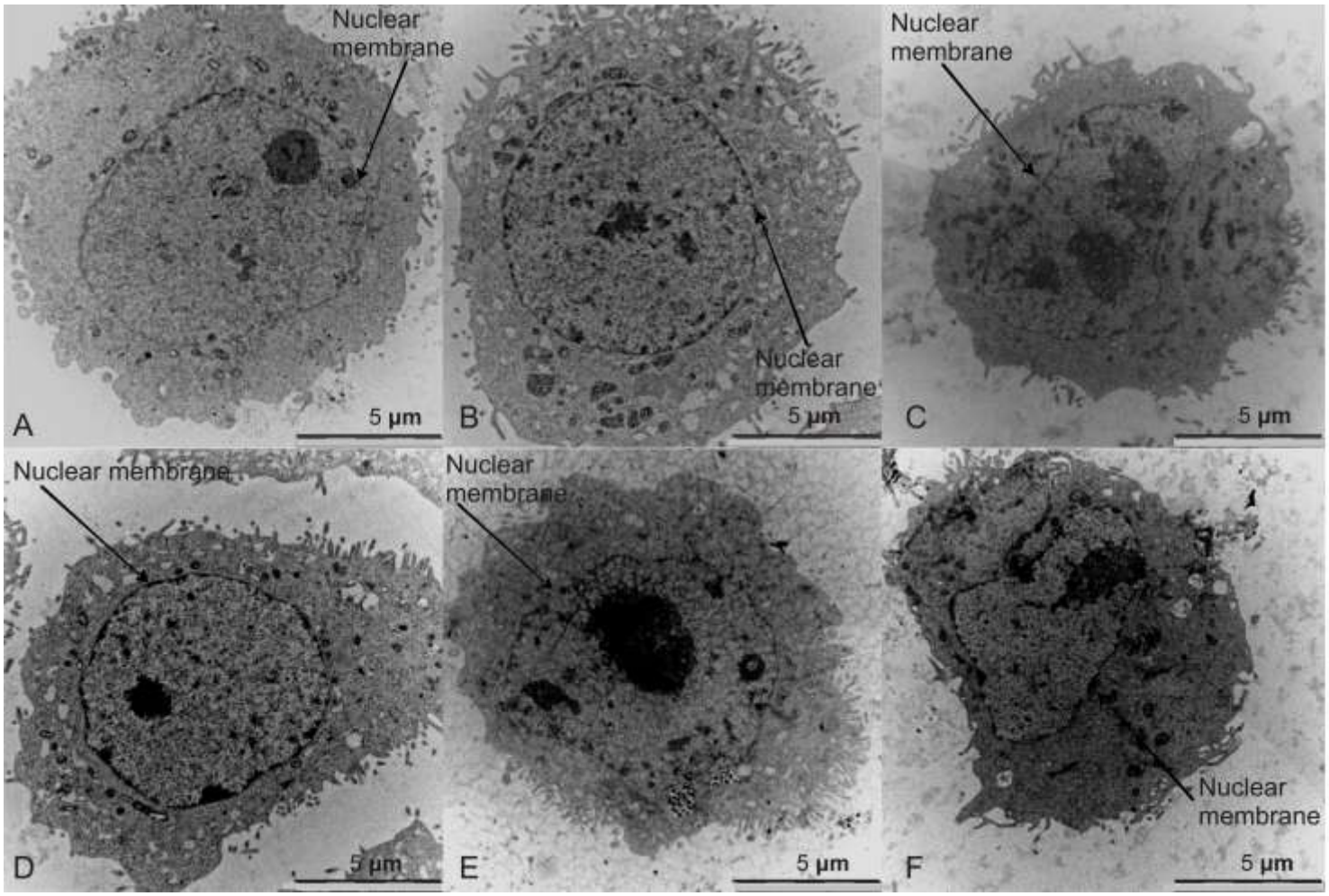

Figure 3.20: TEM images of MCF-7 (A), MDA-MB-231 (B) and MCF-12A cells (C) propagated in growth medium demonstrated no abnormal morphology. In addition, vehicle-treated MCF-7 (D), MDA-MB-231 (E) and MCF-12A cells (F) exhibited no signs of distress (8000X magnification).

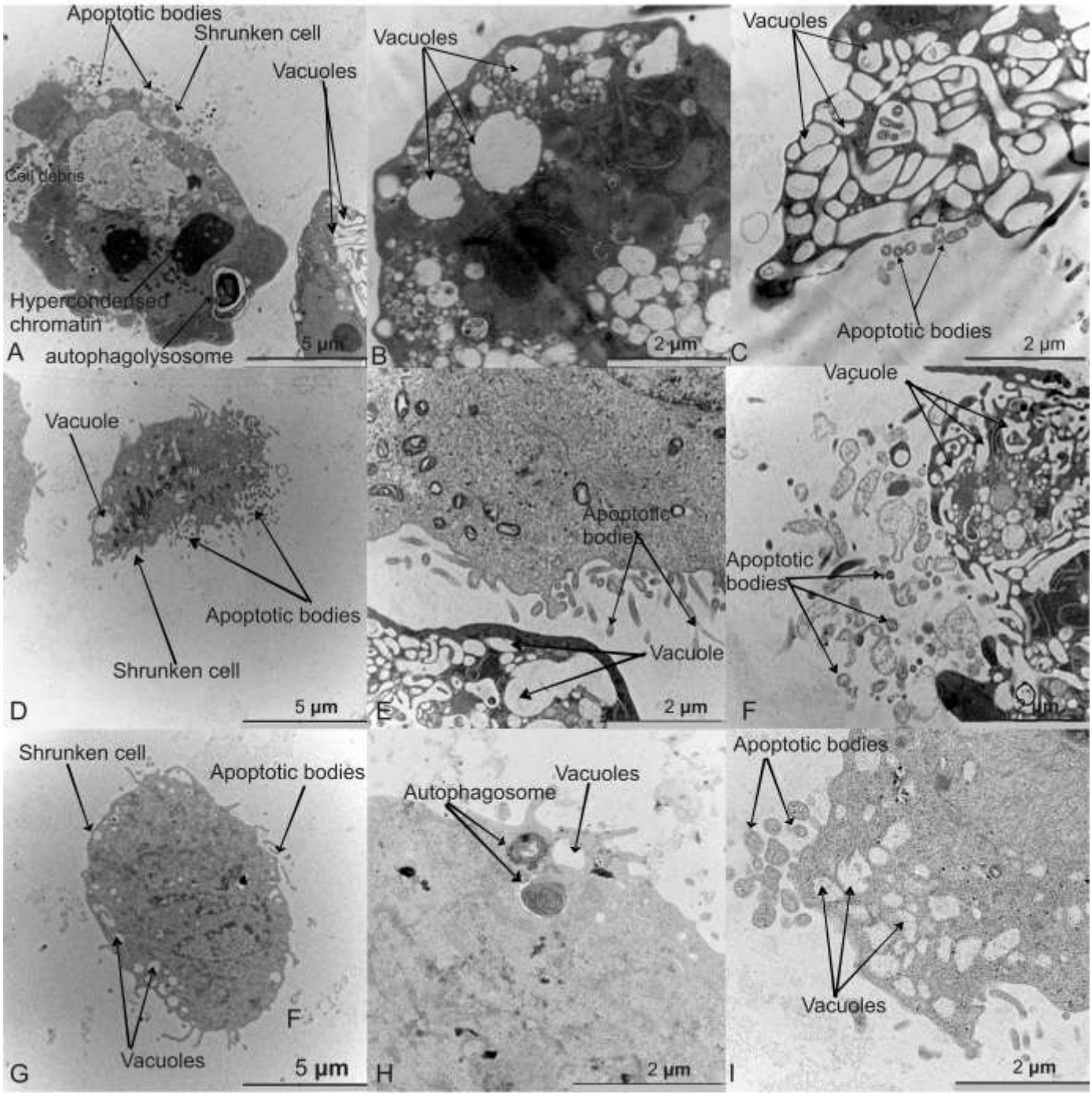

Figure 3.21: TEM images of EMBS-treated MCF-7 (A, B, C), MDA-MB-231 (D, E, F) and MCF-12A cells (G, H, I). All three cell lines were exposed to 0.4 µM for 24 h and demonstrated shrunken cells, intracellular vacuoles and apoptotic bodies (Images for A, D, G were obtained at 8000X magnification and images for B, C, E, F, H, I were taken at 20 000X magnification).

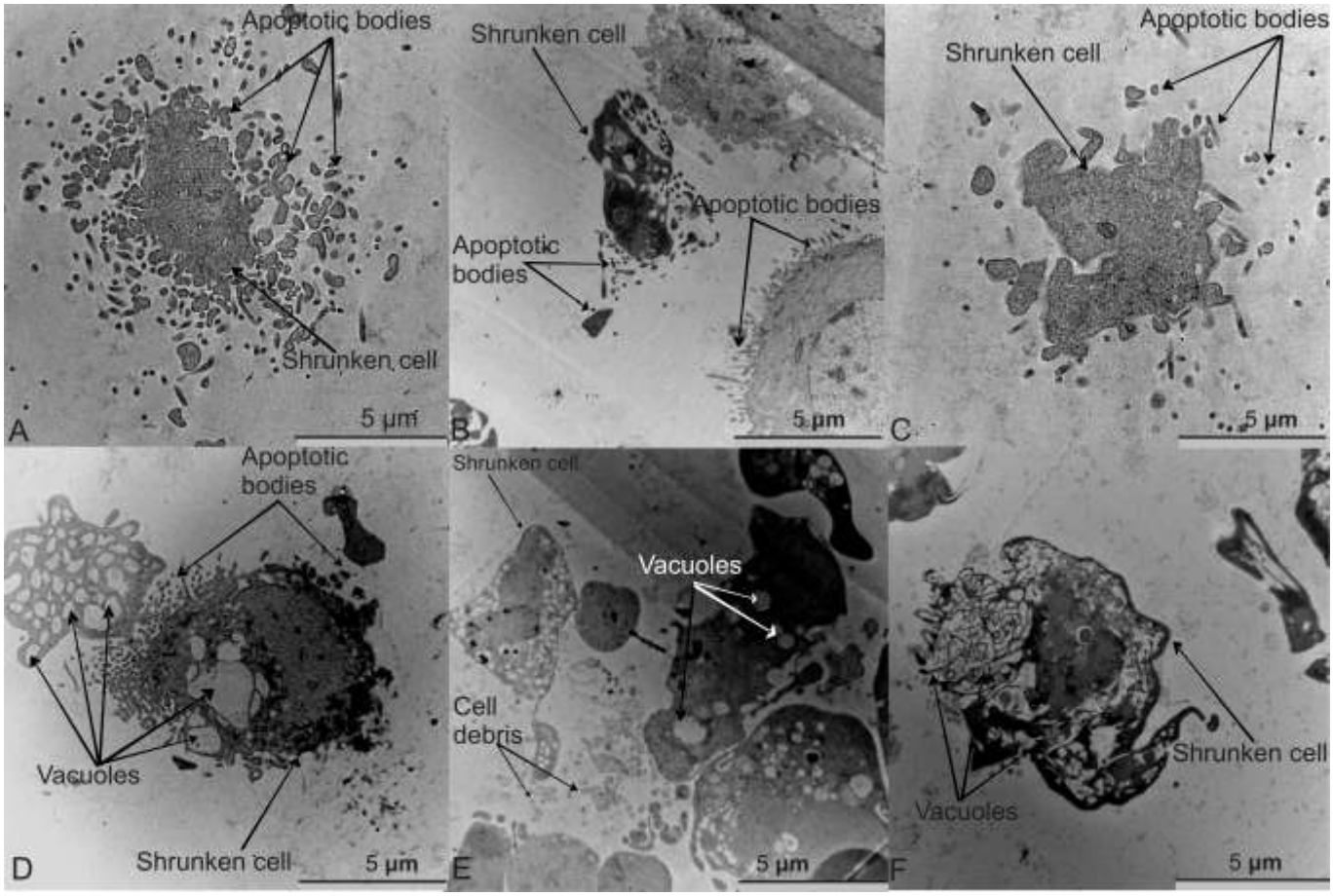

Figure 3.22: TEM images of Actinomycin D-treated MCF-7 (A), MDA-MB-231 (B), MCF-12A cells (C) and starved MCF-7 (D), MDA-MB-231 (E) and MCF-12A cells (F). Hallmarks of apoptosis were observed in the Actinomycin D-treated cells including apoptotic bodies and shrunken cells. Starved cells displayed vacuole formations suggesting autophagy induction (8000X magnification).

3.3.4 Scanning electron microscopy

Scanning electron microscopy (SEM) allowed for high resolution images of the cell's ultrastructure that displayed effects of EMBS on external morphology. SEM images of MCF-7, MDA-MB-231 and MCF-12A cells propagated in growth medium and vehicle-treated cells demonstrated no abnormal morphology (Figure 3.23). EMBS-treated cells exhibited shrunken cells, apoptotic bodies and cell debris suggesting the induction of apoptosis. The formations of intracellular vacuoles were also present implying cell death via autophagy. MDA-MB-231 and MCF-12A cells treated with 0.1 µg/ml actinomycin D as a positive control for apoptosis displayed shrunken cells, apoptotic bodies and cell debris.

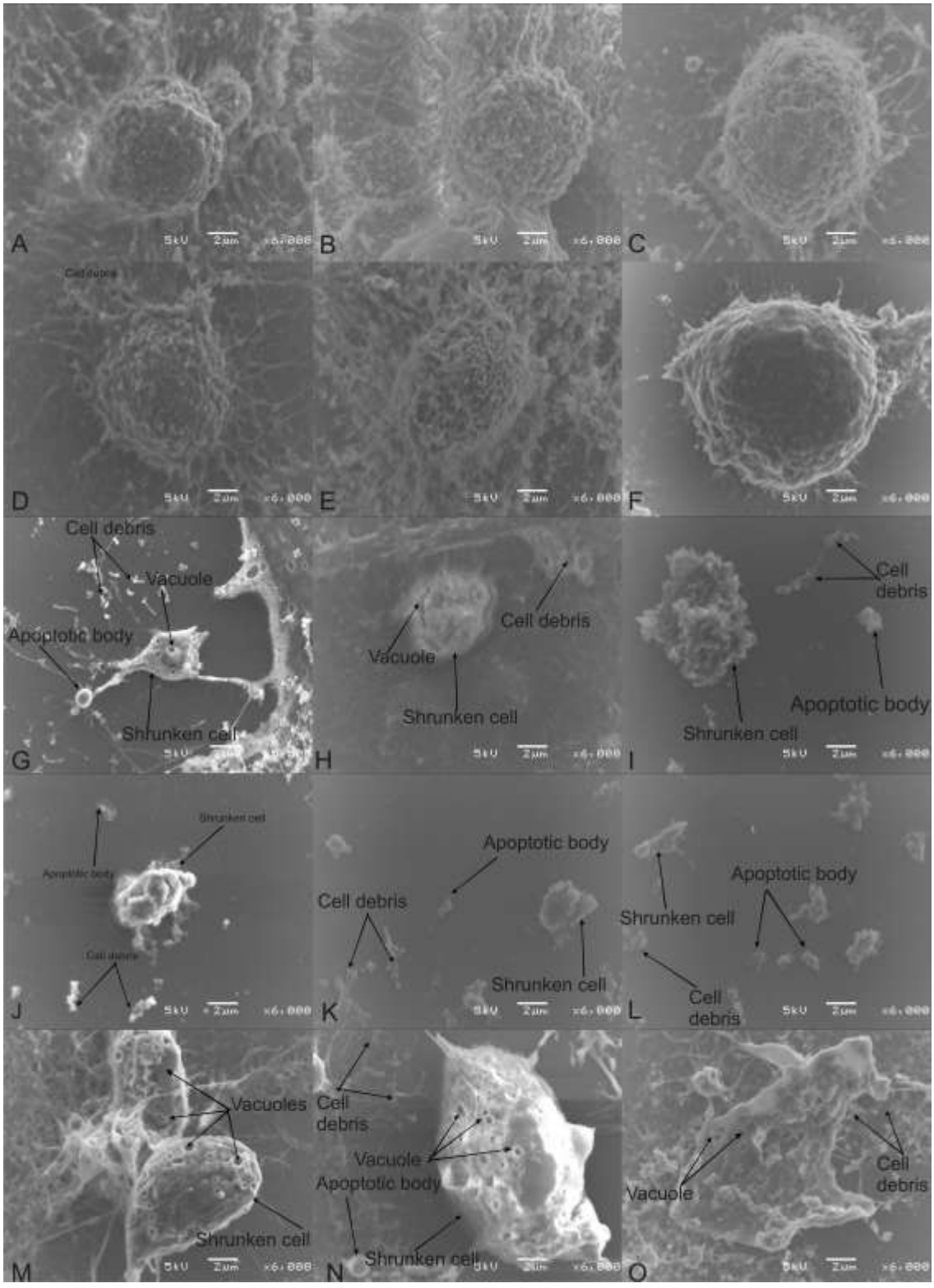

Figure 3.23: SEM images of MCF-7 (A), MDA-MB-231 (B) and MCF-12A cells (C) propagated in growth medium demonstrated no abnormal morphology. Vehicle-treated MCF-7 (D), MDA-MB-231 (E) and MCF-12A cells (F) exhibited no signs of distress. EMBS-treated MCF-7 (G), MDA-MB-231 (H) and MCF-12A cells (I) revealed apoptotic bodies, shrunken cells, cell debris and vacuole formation. MCF-7 (J), MDA-MB-231 (K) and MCF-12A cells were exposed to 0.1 µg/ml actinomycin D and were used as a positive control for apoptosis induction resulting in severely compromised cells with apoptotic bodies, shrunken cells and shrunken cells. Starved MCF-7 (M), MDA-MB-231 (N) and MCF-12A (O) used for autophagy induction revealed the formation of several vacuoles.

3.3.5 Fluorescent microscopy (apoptosis, autophagy and necrosis detection)

A triple staining fluorescent microscopy method employing Hoechst 33342 (blue) and propidium iodide (red) fluorescent dyes and acridine orange (green) were utilized employed to envisage the influence of EMBS on morphology, cell viability and autophagy induction. Although Hoechst 33342 and propidium iodide both stain the DNA, only Hoechst is membrane permeant and stains DNA blue. Propidium iodide is membrane impermeable and only stains the nucleus of cells where the membrane is compromised due to oncotic or necrotic processes (219). Acridine orange is a lysosomotropic fluorescent compound that accumulates in acidic compartments, autophagic vacuoles and lysosomes (220). Cells undergoing autophagy has an increased tendency for acridine orange staining when compared to viable cells, however acridine orange is not a specific marker for autophagy and therefore additional techniques were subsequently included to further verify the appearance of increased autophagic activity.

Vehicle-treated cells demonstrated confluency with Hoechst 33342 staining the nucleus and DNA (Figure 3.24). Increased lysosomal staining was evident in EMBS-treated cells indicating increased acidity and the presence autophagic vesicles and lysosomes. This suggests cell death via autophagy induction.

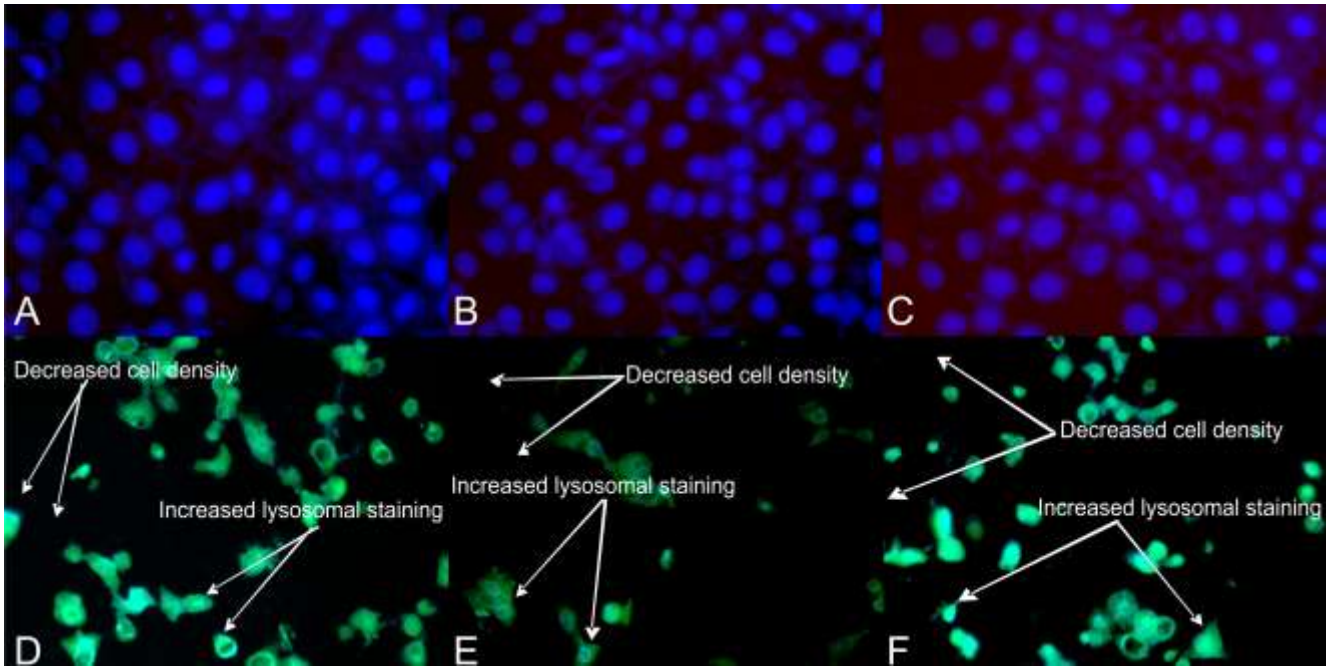

Figure 3.24: Fluorescent microscopy of vehicle-treated MCF-7 (A), MDA-MB-231 (B) and MCF-12A cells (C) were confluent. Fluorescent staining of EMBS-treated MCF-7 (D), MDA-MB-231 and MCF-12A (E) revealed decreased cell density and increased lysosomal staining indicating acidic vesicles and possible autophagy induction (20X magnification).

3.4 Flow cytometry and ethanol fixation (cell cycle progression)

Flow cytometry using propidium iodide staining and ethanol fixation permitted for quantification of cell cycle distribution, G_2M block and the presence of apoptosis indicated by the existence of a sub-G_1 phase after exposure to EMBS MCF-7, MDA-MB-231 and MCF-12A cells. Cell cycle progression of MCF-7, MDA-MB-231 and MCF-12A cells propagated in growth medium and vehicle-treated cells revealed less than 2% of cells in the sub-G_1 fraction (Figure 3.25 and Table 3.2). EMBS exposure resulted in a statistically significant an (*P*-value < 0.05) increased sub-G_1 peak in MCF-7 (36%), MDA-MB-231 (28%) and MCF-12A cells (33%) when compared to cells propagated in growth medium and vehicle-treated cells. Furthermore, EMBS exposure produced a statistically significant (*P*-value < 0.05) increase of MCF-7 (50%), MDA-MB-231(63%) and MCF-12A cells (52%) present in the G_2M phase accompanied with a decrease in cells occupying the G_1 and S phase when compared to cells propagated in growth medium and vehicle-treated cells.

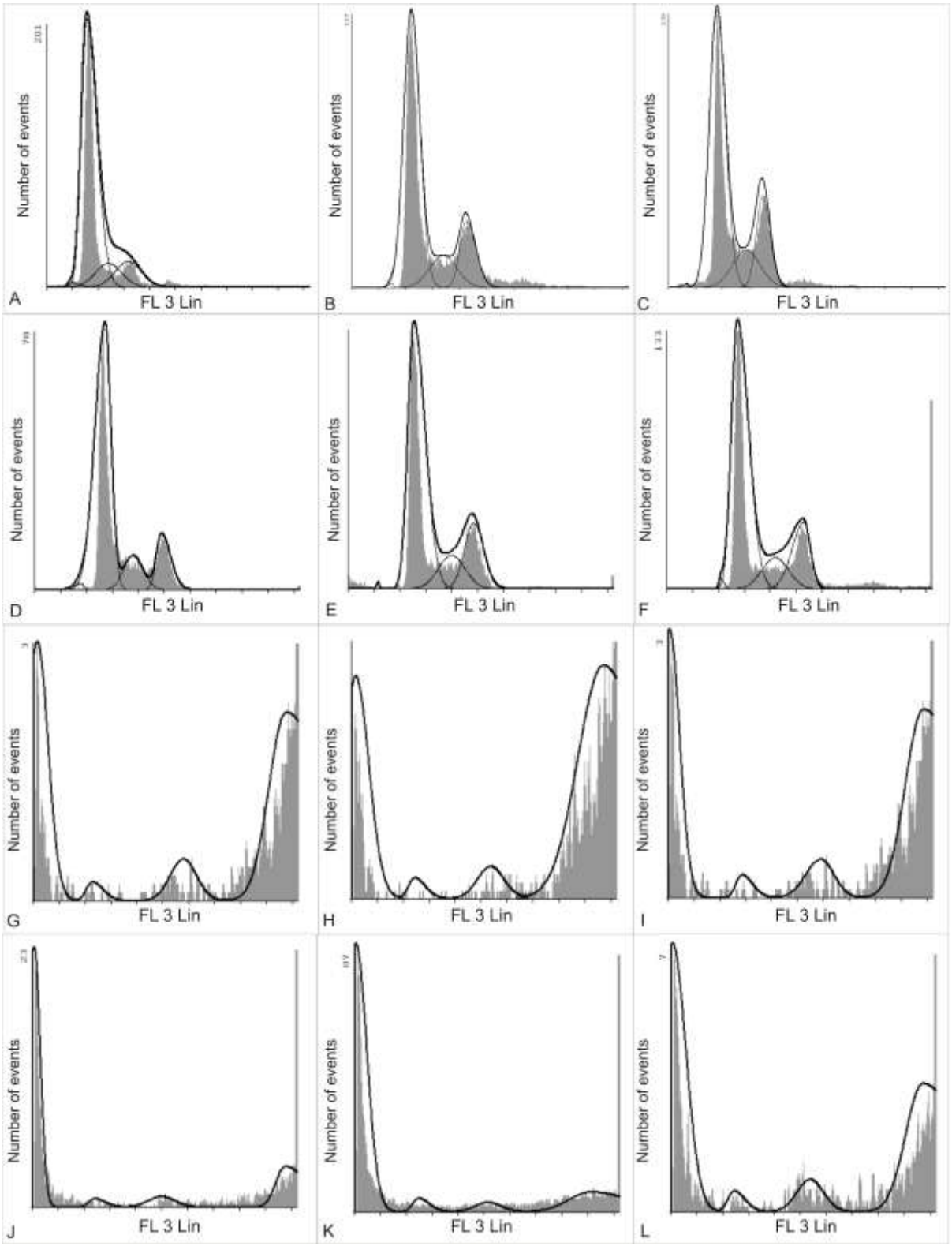

Figure 3.25: Cell cycle progression revealed that 0.96% of MCF-7 cells propagated in growth medium (A) was present in Sub-G_1, 75% in G_1, 12% in the S phase and 12% in the G_2M phase. MDA-MB-231 cells propagated in growth medium (B) presented with 0.31% present in Sub-G_1, 70% in G_1 phase, 14% in the S phase and 17% in the G_2M phase. MCF-12A cells propagated in growth medium (C) presented with 0.25% present in Sub-G_1, 66% in G_1, 15% in the S phase and 19% in the G_2M phase. MCF-12A vehicle-treated cells (D) presented with 1% present in Sub-G_1, 74% in G_1, 12% in the S phase and 14% in the G_2M phase. MDA-MB-231 vehicle-treated cells (E)

presented with 0.64% present in Sub-G_1, 69% in G_1 phase, 15% in the S phase and 15% in the G_2M phase. MCF-12A vehicle-treated cells (F) presented with 0.64% present in Sub-G_1, 69% in G_1 phase, 15% in the S phase and 15% in the G_2M phase. Cell cycle progression data demonstrated that EMBS exposure resulted in a statistically significant increases of MCF-7 cells (36%) (G), MDA-MB-231 cells (28%) (H) and MCF-12A cells (33%) (I) present in Sub-G_1 phase accompanied with an increase in MCF-7 cells (50%), MDA-MB-231 (63%) and MCF-12A (52%) present in the G_2M phase. MCF-7 (J), MDA-MB-231 (K) and MCF-12A cells (L) exposed to 0.1 µg/ml actinomycin D used as a positive control for apoptosis induction resulted in apoptosis induction and an increase of cells occupying the G_2M phase.

Table 3.2: Cell cycle progression (an * indicates *P*-value < 0.05).

	Sub G_1	G_1	S	G_2M
MCF-7 cells propagated in growth medium	0.96±0.01 %	75.29±0.12 %	11.43±0.00 1%	12.31±0.03 6%
MCF-7 cells vehicle-treated cells	1.16±0.1%	73.53±0.25 %	11.43±0.6 %	13.86±1.2 %
MCF-7 cells EMBS-treated cells	36± 2.1 % *	3.14±2.1%	10.92±3.2 %	50% ±0.01*
MCF-7 cells Actinomycin D-treated cells	62.7±0.1% *	4.46±0.005 %	8.72±0.002 %	24.13±1.1 %
MDA-MB-231 cells propagated in growth medium	0.31±2.1%	69.17±1.3 %	13.86±0.05 %	16.65±0.5 %
MDA-MB-231 vehicle-treated cells	0.64±0.5%	68.95±2.23 6%	15.16±0.9 %	15.23±1%
MDA-MB-231 EMBS-treated cells	27.9±0.8% *	2.66±0.66 %	6.45±0.86 %	63±0.96% *
MDA-MB-231 Actinomycin D-treated cells	71±1.25% *	4.97±2.2%	5.38±1.3%	18.69±0.69 %
MCF-12A cells propagated in growth medium	0.25±1.2%	65.99±2.58 %	15.12±2.89 %	18.62±0.89 %
MCF-12A vehicle-treated cells	0.78±1.2%	68.33±0.38 %	12.42±0.21 %	18.45±0.77 %
MCF-12A EMBS-treated cells	32.5±0.89 % *	4.14±4.2%	11.69±5.8 %	51.7±1.89 % *
MCF-12A Actinomycin D-treated cells	45.4±1% *	4.06±1.58 %	9.85±2.01 %	40.7±0.89 % *

3.5 Apoptosis

3.5.1 Flow cytometry utilizing annexin V- fluorescein isothiocyanate

Flow cytometry utilizing fluorescein isiothiocyanate conjugated annexin V and propidium iodide allow for the identification of cells undergoing early apoptosis, late apoptosis and necrosis in addition to the viable cells. This is due to the unique co-staining of annexin V. Propidium iodide, as previously mentioned, is membrane impermeable and only stains the nucleus of cells where the membrane is compromised (219). The surface expression of phosphatidylserine translocated from the inner membrane to the outer membrane is considered an early characteristic of apoptosis. The latter event was investigated by means of fluorescein isiothiocyanate conjugated Annexin V (200, 221).

Cell viability of cells propagated in growth medium and vehicle-treated cells remained above 98% (Figure 3.26 and Table 3.3). After exposure to EMBS (0.4 μM, 24 h), MCF-7 cell viability decreased to 66% with 0.1% present in early apoptosis, 22.21% in late apoptosis and 12.25% in necrosis. After exposure to EMBS (0.4 μM, 24 h) MDA-MB-231 cell viability decreased to 65% with 0.68% present in early apoptosis, 21.61% in late apoptosis and 12.31% in necrosis. After exposure to EMBS (0.4 μM, 24 h) MCF-12A cell viability decreased to 66% with 17% present in early apoptosis, 11.44% in late apoptosis and 5.11% in necrosis.

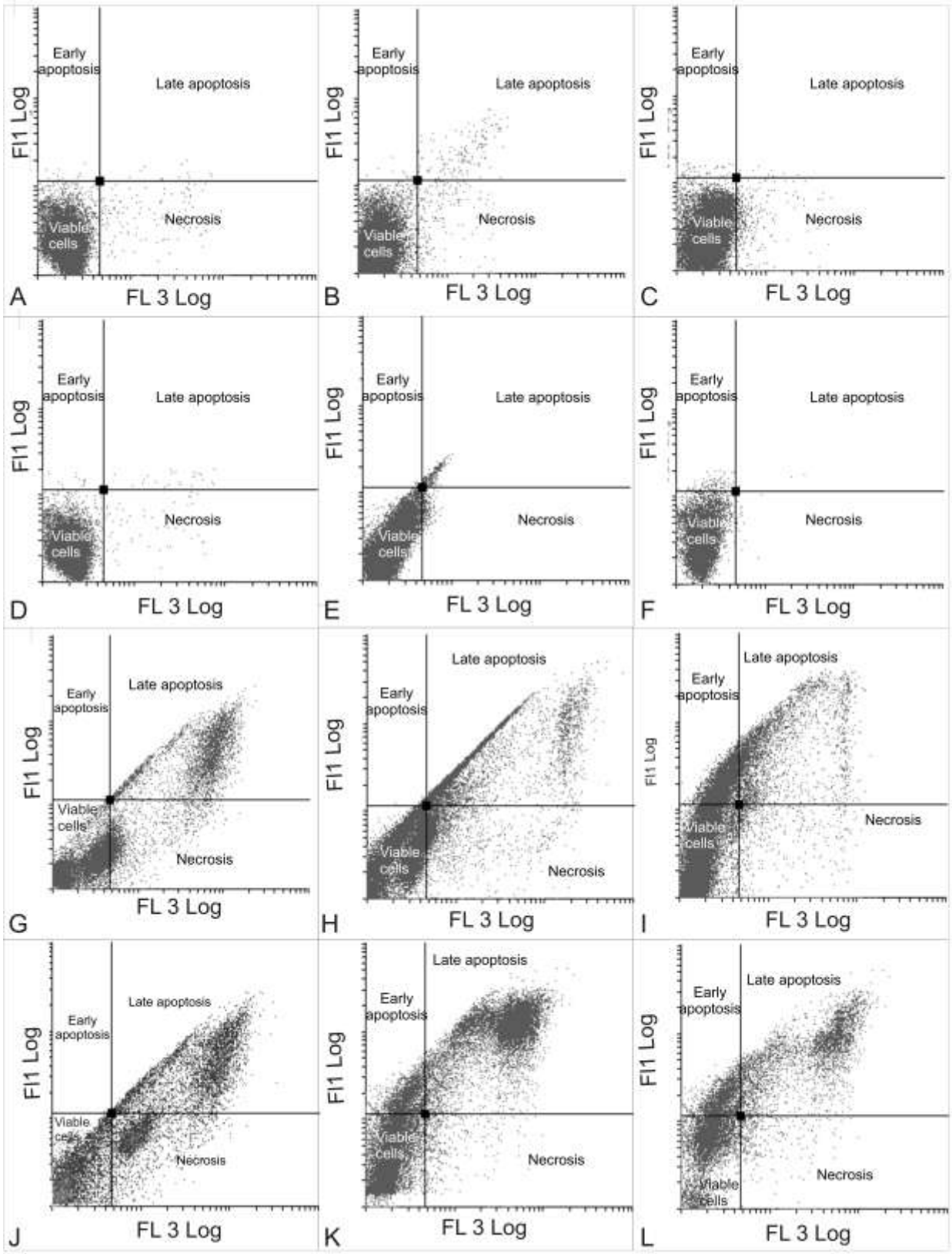

Figure 3.26: Flow cytometry investigation using annexin-V-FITC revealed cell viability of more than 98% for the MCF-7 (A), MDA-MB-231 (B), MCF-7 cells (C) propagated in growth medium and vehicle-treated MCF-7 (D), MDA-MB-231 (E) and MCF-12A cells (F). Treated cells were exposed to 0.4 µM for 24 h. EMBS-treated MCF-7 (G), MDA-MB-231 (H) and MCF-12A cells (I) revealed a decrease in cell viability to 65-66% accompanied by an increase in cells

undergoing late apoptosis and necrosis. In addition, EMBS-treated MCF-12A cells also experienced an increase of cells undergoing early apoptosis. MCF-7 (J), MDA-MB-231 (K) and MCF-12A cells (L) exposed to 0.1 µg/ml actinomycin D resulted in decreased cell viability and apoptosis induction.

Table 3.3: Flow cytometry using annexin V-FITC demonstrating viable cells, cells in early apoptosis, cells in late apoptosis and necrotic cells (an * indicates *P*-value < 0.05).

	Viable cells	Cells occupying early apoptosis	Cells occupying late apoptosis	Necrotic cells
MCF-7 cells propagated in growth medium	98.8±1.2%	0.2±0.2%	0.1±0.002%	0.9±0.6%
MCF-7 vehicle-treated cells	99.3±0.9%	0.3±0.99%	0.1±0.65%	0.3±1.9%
MCF-7 EMBS-treated cells	65.5±1.8% *	0.0±0.6%	22.21±1.23% *	12.3±0.89%
MCF-7 Actinomycin D-treated cells	49.3±2.1% *	0.0±1.8%	30.11±% *	20.5±% *
MDA-MB-231 cells propagated in growth medium	98.2±0.58%	0.1±0.005%	0.9±0.002%	0.8±0.003%
MDA-MB-231 vehicle-treated cells	98.6±4.2%	0.0±0.002%	0.6±0.006%	0.9±0.02%
MDA-MB-231 EMBS-treated cells	65.4%±3.8 *	0.7±0.08%	21.6±2.8% *	12.3±1.25%
MDA-MB-231 Actinomycin D-treated cells	48.4%±4.2 *	9.3±0.06%	40.3±0.004% *	1.9±0.002%
MCF-12A cells propagated in growth medium	98.1±4.3%	0.3±0.5%	0.0±0.002%	1.6±0.00%
MCF-12A vehicle-treated cells	98.6±1.5%	1.1±0.003%	0.0±0.002%	0.2±0.001%
MCF-12A EMBS-treated cells	66.13±3.6% *	17.4±0.002%	11.4±0.02%	5.1±0.001%
MCF-12A Actinomycin D-treated cells	46.57±4.2% *	32.71±1.01% *	17.6±0.069%	3.1±0.002%

3.5.2. Flow cytometry (mitochondrial membrane potential)

Possible apoptosis induction was demonstrated by measuring the mitochondrial membrane potential using Mitocapture Mitochondrial Apoptosis Detection Kit employing flow cytometry. In cells with no disturbances within the mitochondria Mitocapture accumulates in the mitochondria showing a bright red fluorescence. The apoptotic cells MitoCapture cannot aggregate in the mitochondria as a consequence of the reduced mitochondrial transmembrane potential and therefore resides in the cytoplasm giving off a green fluorescence (222).

Cells propagated in growth medium and vehicle-treated cells demonstrated high cell viability with less than 2% of cells revealing a reduction in the mitochondrial membrane potential (Figure 3.27). Exposure to 0.4 µM EMBS for 24 h resulted in a statistically significant increased number of MCF-7 (22%), MDA-MB-231 (26%) and MCF-12A cells (21%) with a reduction in the mitochondrial membrane potential (Figure 3.28). Cells exposed to actinomycin D used as a positive control for apoptosis demonstrated a statistically significant number of cells presenting a reduced mitochondrial membrane potential.

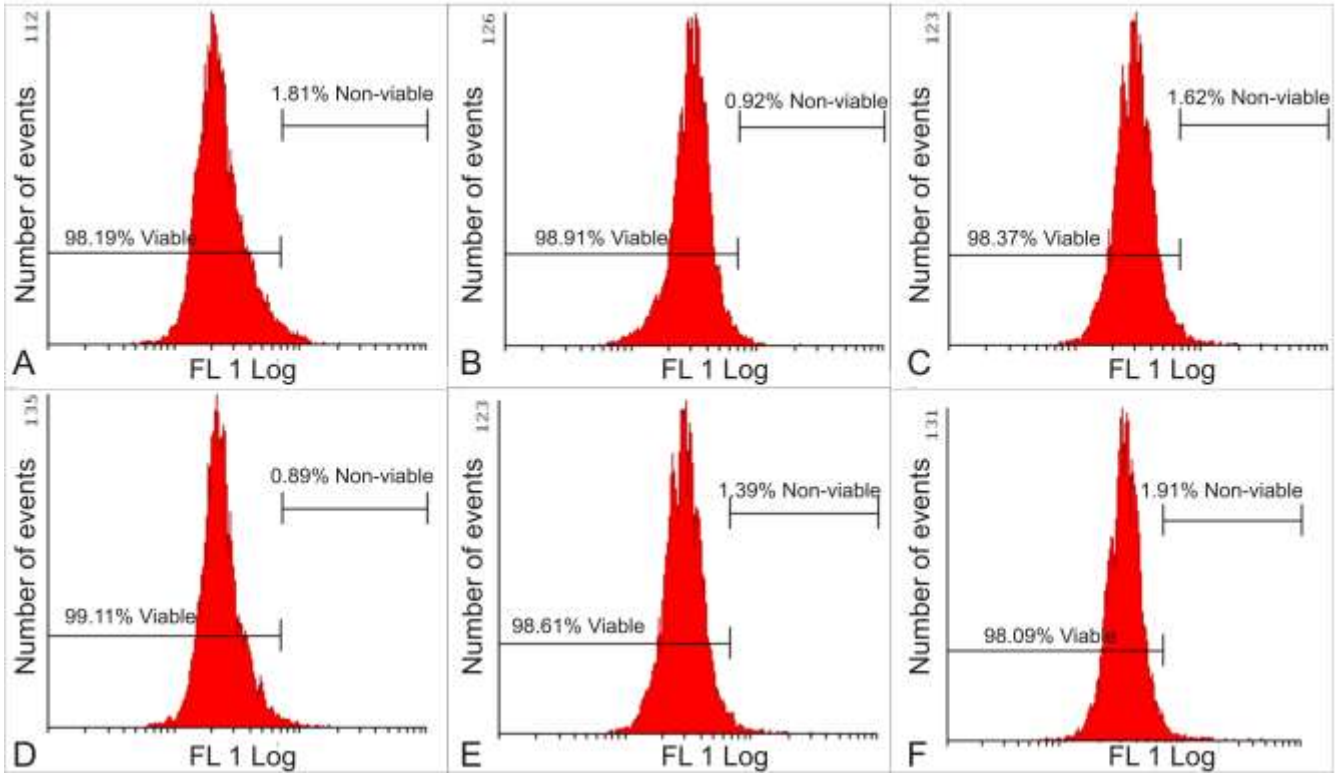

Figure 3.27: Flow cytometry investigation of mitochondrial membrane potential demonstrated cell viability above 98% for the MCF-7 (A), MDA-MB-231 (B) and MCF-12A cells (C) propagated in growth medium and vehicle-treated MCF-7 (D), MDA-MB-231 (E) and MCF-12A cells (F).

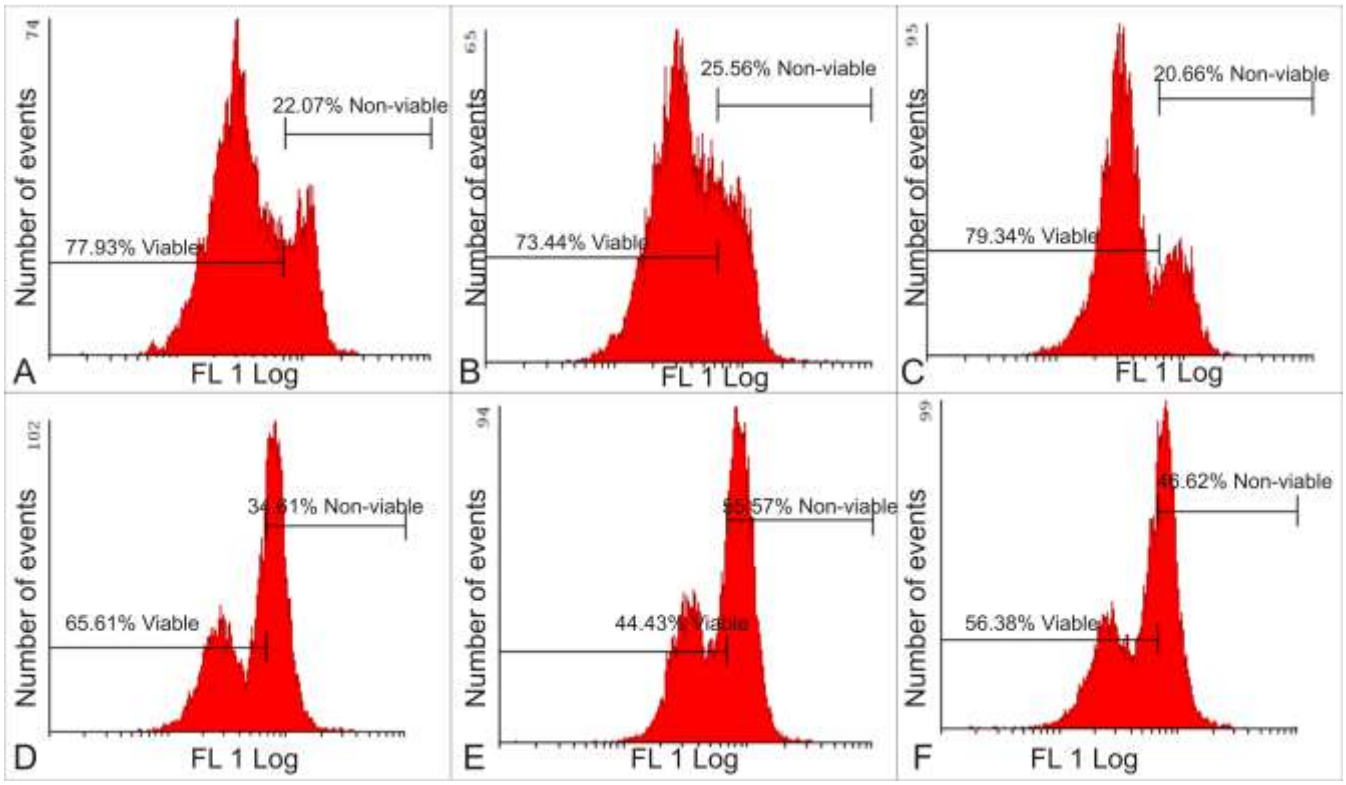

Figure 3.28: Flow cytometry investigation of mitochondrial membrane potential demonstrated a significant decrease in cell viability of MCF-7 (A), MDA-MB-231 (B) and MCF-12A cells (C). EMBS-treated MCF-7 (22%), MDA-MB-231 (26%), MCF-12A cells (21%) had a reduction in the mitochondrial membrane potential when compared to cells propagated in growth medium and vehicle-treated cells. Actinomycin D-treated MCF-7 (D), MDA-MB-231 (E) and MCF-12A cells (F) showed an increase in the number of cells possessing a reduction in the mitochondrial membrane potential *(P*-value < 0.05).

3.5.3. Spectrophotometry and flow cytometry (detection of caspase activation) Apoptosis induction was also investigated by demonstrating the effect of EMBS on caspase activation in MCF-7, MDA-MB-231 and MCF-12A cells lines. This study specifically focused on the activation of initiator caspase 8 and effector caspases 6 and 7. This not only confirmed the induction of apoptosis by EMBS, but also the involvement of the extrinsic pathway. Data implicated that EMBS exposure resulted in increased caspase 6, caspase 7 and caspase 8 activity when compared to vehicle-treated cells. Caspase 6 colorimetric assay indicated that MDA-MB-231 cells were more pronouncedly affected followed by MCF-7 when compared to vehicle-treated cells (Figure 3.29). The latter was also indicated regarding caspase 8 utilizing caspase 8 colorimetric assay when compared to vehicle-treated cells (Figure 3.30). Cells propagated in growth medium and vehicle-treated cells showed minimal caspase 7 activity up to 1% (Figure 3.31). EMBS exposure resulted in elevated caspase 7 activity

in MCF-7 (28%), MDA-MB-231 (25%) and MCF-12A cells (23%) when compared to cells propagated in growth medium and vehicle-treated cells (Figure 3.32).

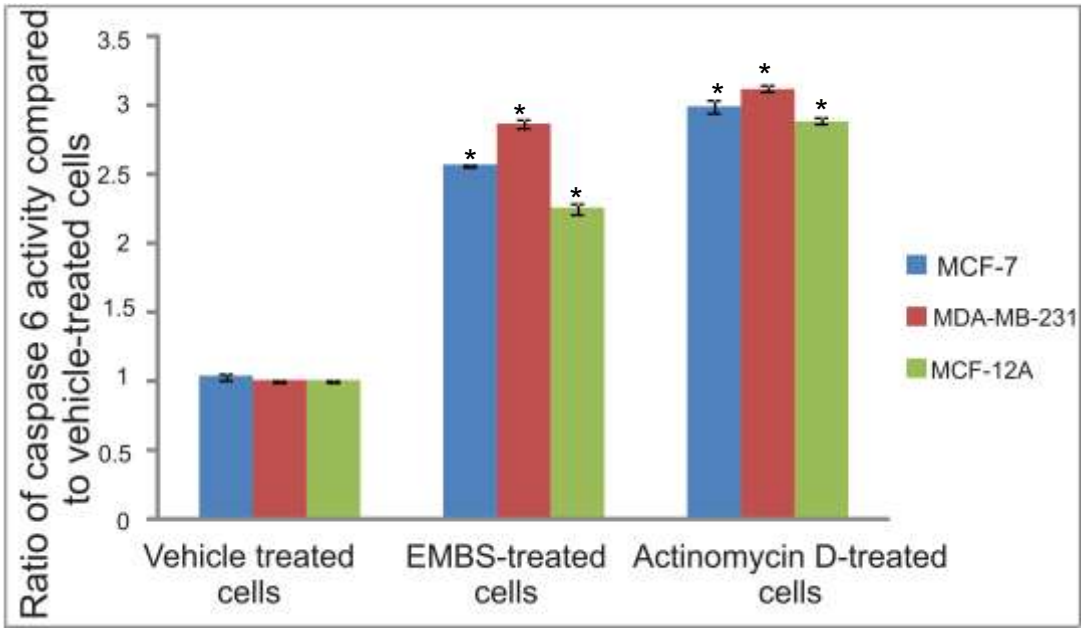

Figure 3.29: Caspase 6 activity ratios of EMBS- and actinomycin D-treated cells compared to vehicle-treated cells. EMBS-treated MDA-MB-231 cells possessed the highest caspase 6 activity, followed by MCF-7 and MCF-12A. Actinomycin D-treated cells were used as a positive control for apoptosis and caspase activation and displayed significant elevated caspase 6 activity when compared to vehicle-treated cells (an * indicates *P*-value < 0.05).

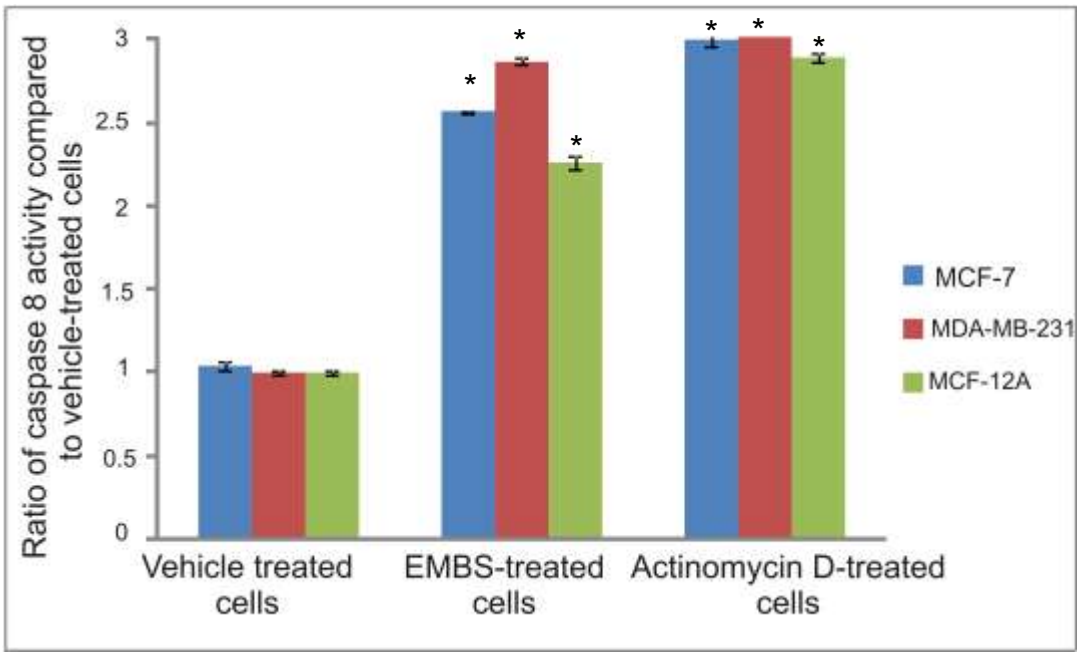

Figure 3.30: Caspase 8 activity ratios of EMBS- and actinomycin D-treated cells compared to vehicle-treated cells. EMBS-treated MDA-MB-231 cells possessed the highest caspase 8 activity, followed by MCF-7 and MCF-12A. Actinomycin D-treated cells were used as a positive control for apoptosis and caspase activation and displayed significant elevated caspase 8 activity above 2.5-fold when compared to vehicle-treated cells *(P*-value < 0.05).

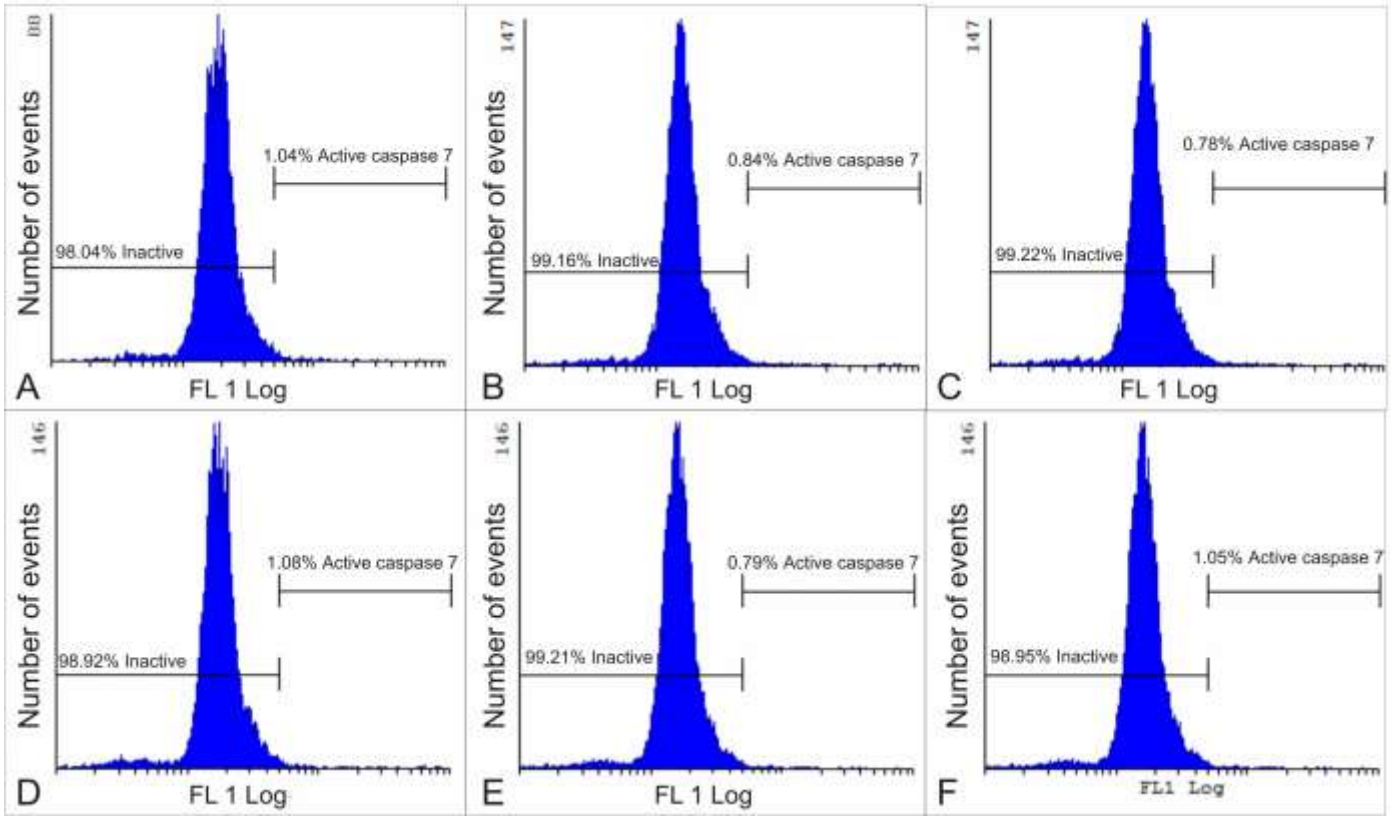

Figure 3.31: Flow cytometry investigation demonstrated caspase 7 activity up to 1% for the MCF-7 (A), MDA-MB-231 (B), MCF-12A cells (C) propagated in growth medium and vehicle-treated MCF-7 (D), MDA-MB-231 (E) and MCF-12A cells (F).

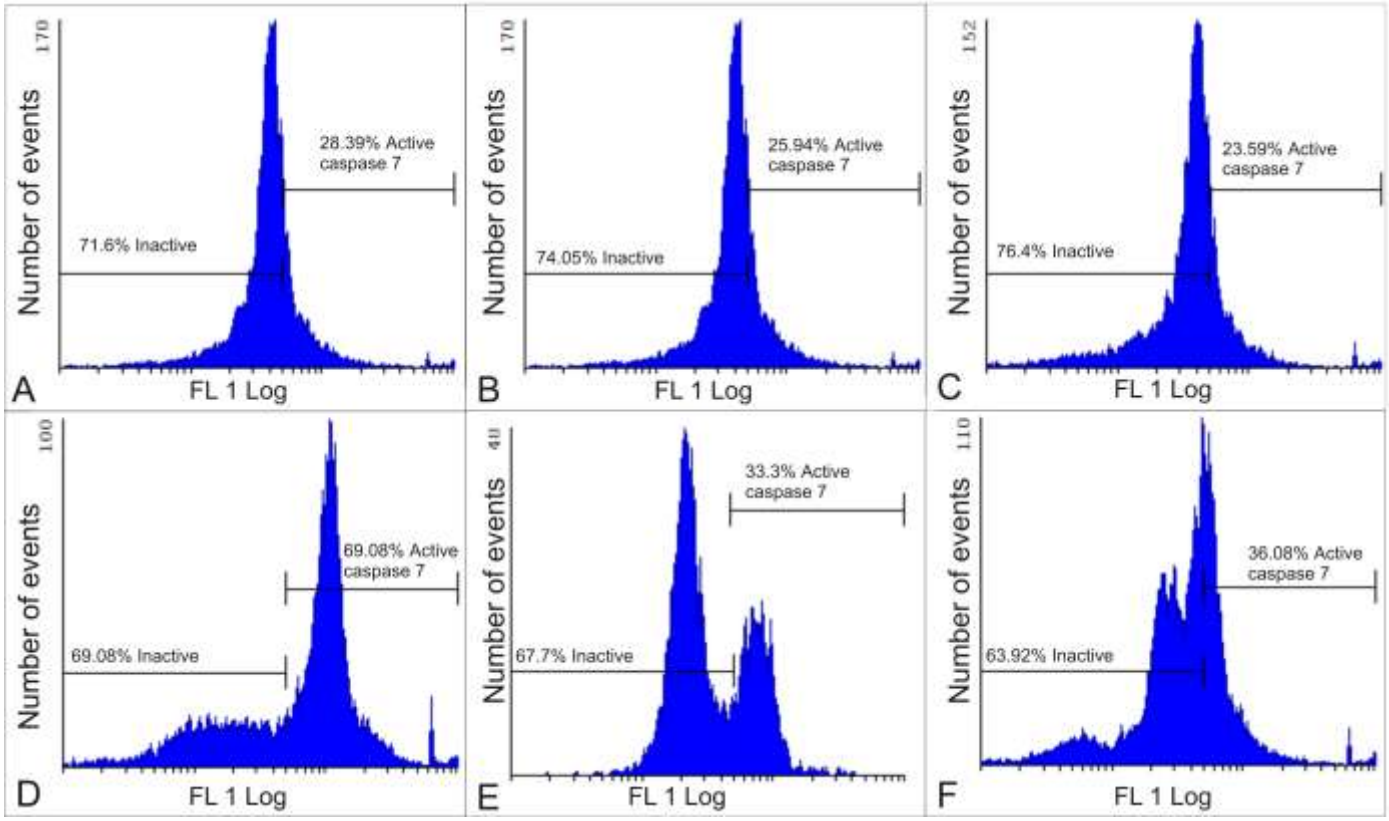

Figure 3.32: Flow cytometry investigation demonstrated a significant increase in caspase 7 activity of MCF-7 (A), MDA-MB-231 (B) and MCF-12A cells (C) after exposure to 0.4 µM EMBS when compared to cells propagated in growth medium and vehicle-treated cells. Actinomycin D-treated MCF-7 (D), MDA-MB-231 (E) and MCF-12A cells (F) showed an increase in the number of cells with increased caspase 7 activity when compared to cells propagated in growth medium and vehicle-treated cells *(P*-value < 0.05)..

3.6 Autophagy induction (rabbit polyclonal anti-LC3B conjugated to DyLight 488)

LC3 is the corresponding mammalian protein of yeast ATG8 that is required for autophagosome mammalian protein identified that stably associates with the autophagosome membranes. LC3-I is cytosolic; however, LC3-II is membrane bound and enriched in the autophagic vacuole fraction (223). LC3-II may thus be used to estimate the abundance of autophagosomes prior to their destruction through fusion with lysosomes. The anti-LC3B antibody allows for autophagy identification and confirmation (results provided by light microscopy and Hoechst 33342, propidium iodide and acridine orange staining) in the breast tumorigenic and non-tumorigenic cell lines during flow cytometry.

Autophagy induction of cells propagated in growth medium and vehicle-treated cells were demonstrated to be minimal and below 1% (Figure 3.33). Increased autophagy

induction was detected in EMBS-treated MCF-7 (28%), MDA-MB-231 (34%) and MCF-12A cells (32%) when compared to cells propagated in growth medium and vehicle-treated cells (Figure 3.34). Starved cells that were nutrient deprived (2 PBS: 1 growth medium) revealed significant (*P*-value < 0.05) autophagy induction (71% in the MCF-7 cell line, 87% in the MDA-MB-231 cell line and 80% in the MCF-12A cell line) when compared to cells propagated in growth medium and vehicle-treated cells.

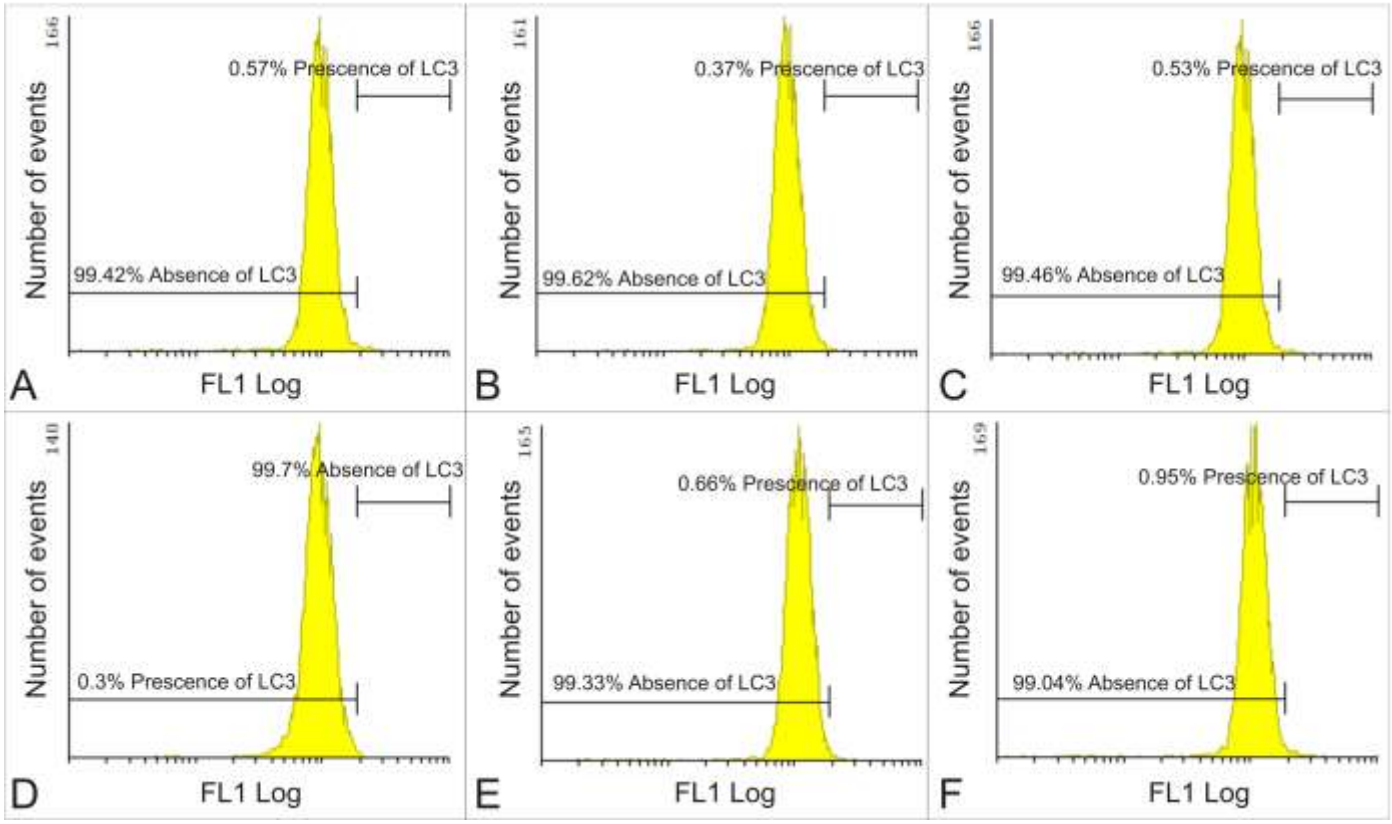

Figure 3.33: Autophagy investigation demonstrated statistically insignificant autophagy induction in MCF-7 (A), MDA-MB-231 (B), MCF-12A cells (C) propagated in growth medium and vehicle-treated MCF-7 (D), MDA-MB-231 (E) and MCF-12A cells (F).

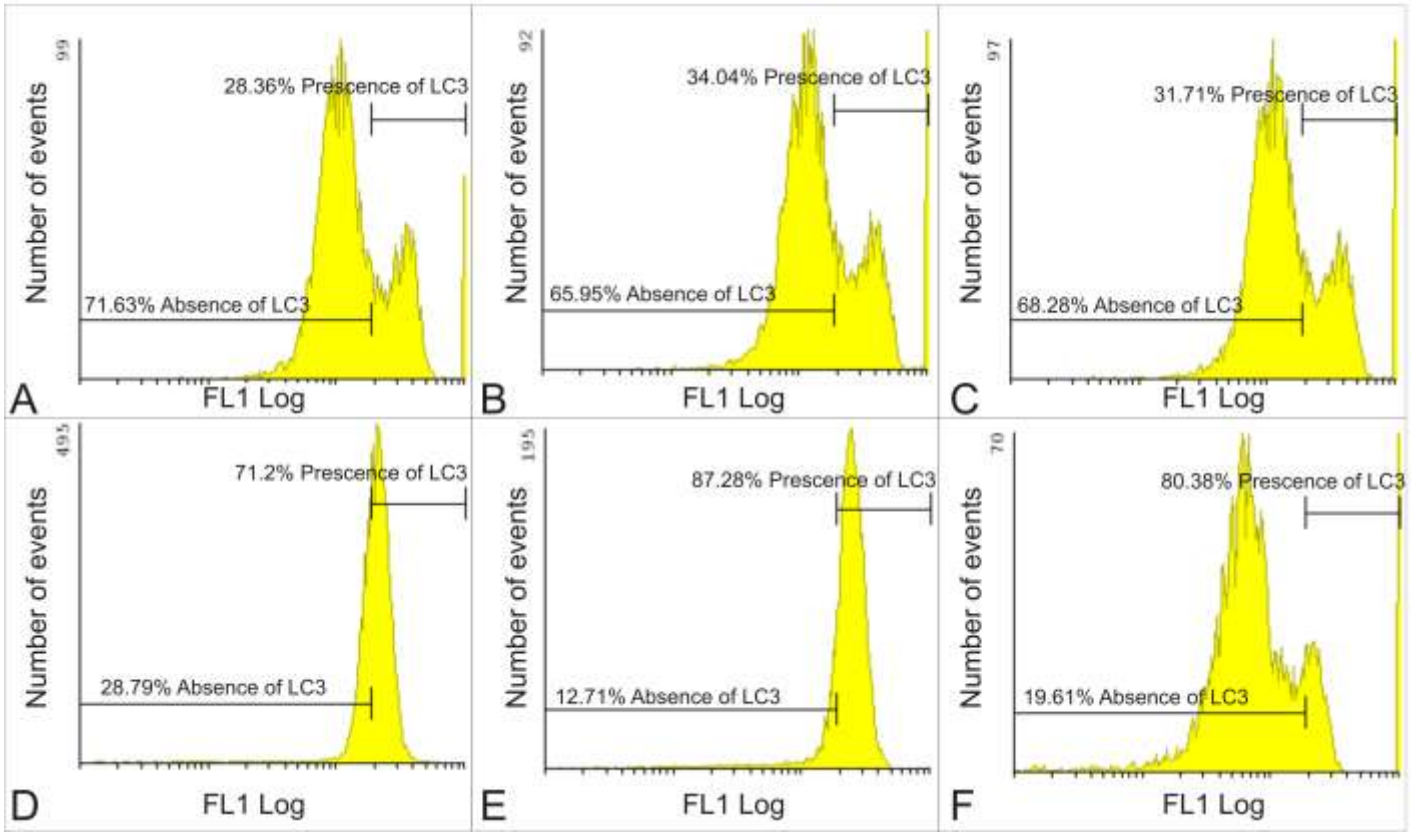

Figure 3.34: Autophagy quantification indicated a statistically significant increase in autophagy activity of MCF-7 (A), MDA-MB-231 (B), MCF-12A cells (C) after exposure to 0.4 μM EMBS when compared to cells propagated in growth medium and vehicle-treated cells. Starved cells where cells were nutrient deprived (3 PBS: 1 growth medium) revealed statistically significant autophagy induction when compared to cells propagated in growth medium and vehicle-treated cells *(P*-value < 0.05).

3.7 Crosstalk between autophagy and apoptosis

3.7.1 Flow cytometry (reactive oxygen species (ROS))

Hydrogen peroxide production

Hydrogen peroxide was quantified using 2,7-dichlorofluorescein diacetate (DCFDA), a non-fluorescent probe that passively diffuses into cells, which upon oxidation by ROS and peroxides, is converted to the highly fluorescent derivative DCF (224). Hydrogen peroxide detection using flow cytometry demonstrated the presence of less than 3% hydrogen peroxide in cells propagated in growth medium and vehicle-treated cells (Figure 3.35). After exposure to 0.4 μM EMBS for 24 h the hydrogen peroxide production increased in a statistically significantly manner in the MCF-7 cell line (40%), MDA-MB-231 cell line (46%) and MCF-12A cells (56%) when compared to cells propagated in growth medium and vehicle-treated cells (Figure 3.36). Treatment with hydrogen peroxide used as a positive control resulted in statistically significant

increased hydrogen peroxide levels in MCF-7 cells (80%), MDA-MB-231 cells (78%) and MCF-12A cells (76%).

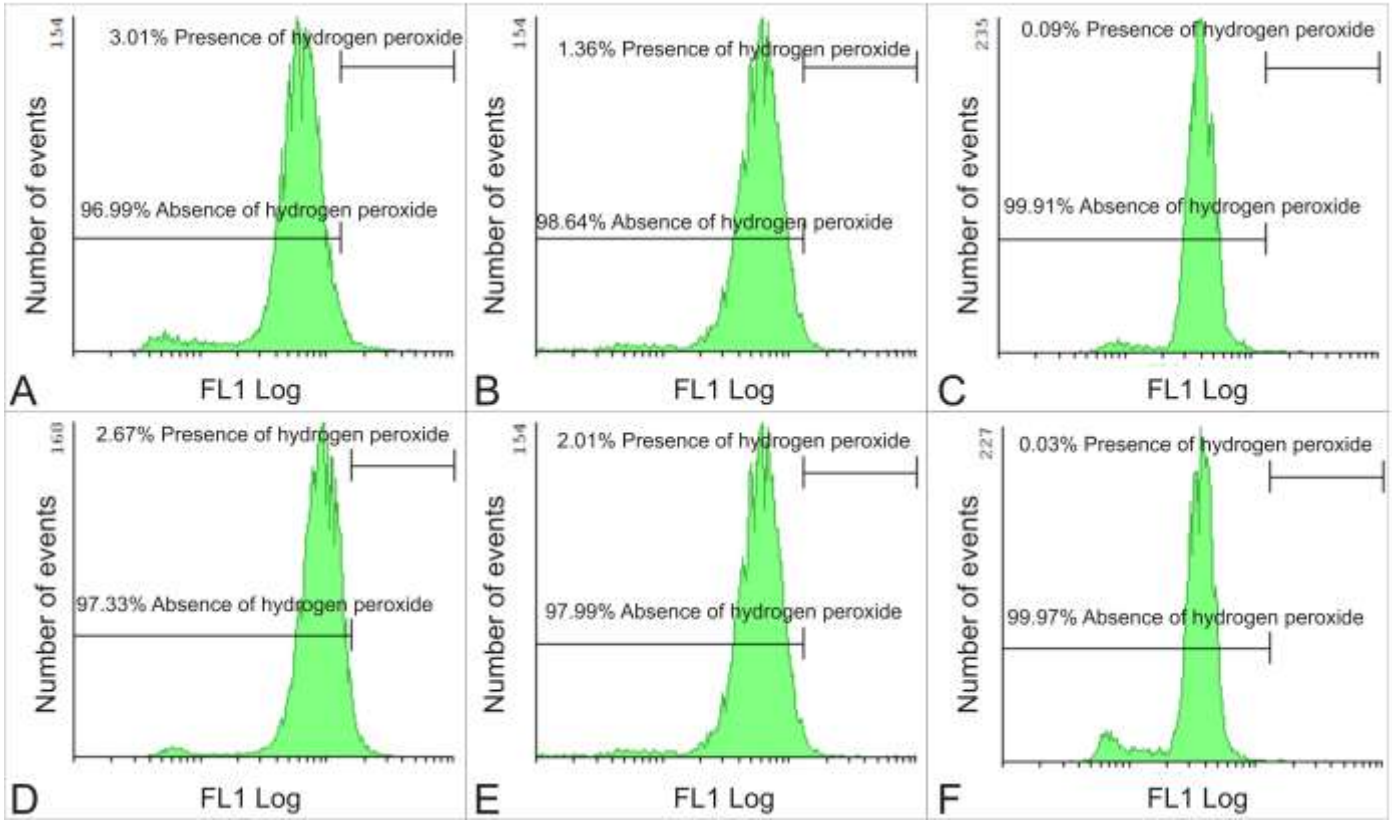

Figure 3.35: Flow cytometry investigation demonstrated insignificant hydrogen peroxide production of less than 3% in MCF-7 (A), MDA-MB-231 (B) and MCF-12A cells (C) propagated in growth medium and vehicle-treated MCF-7 (D), MDA-MB-231 (E) and MCF-12A cells (F).

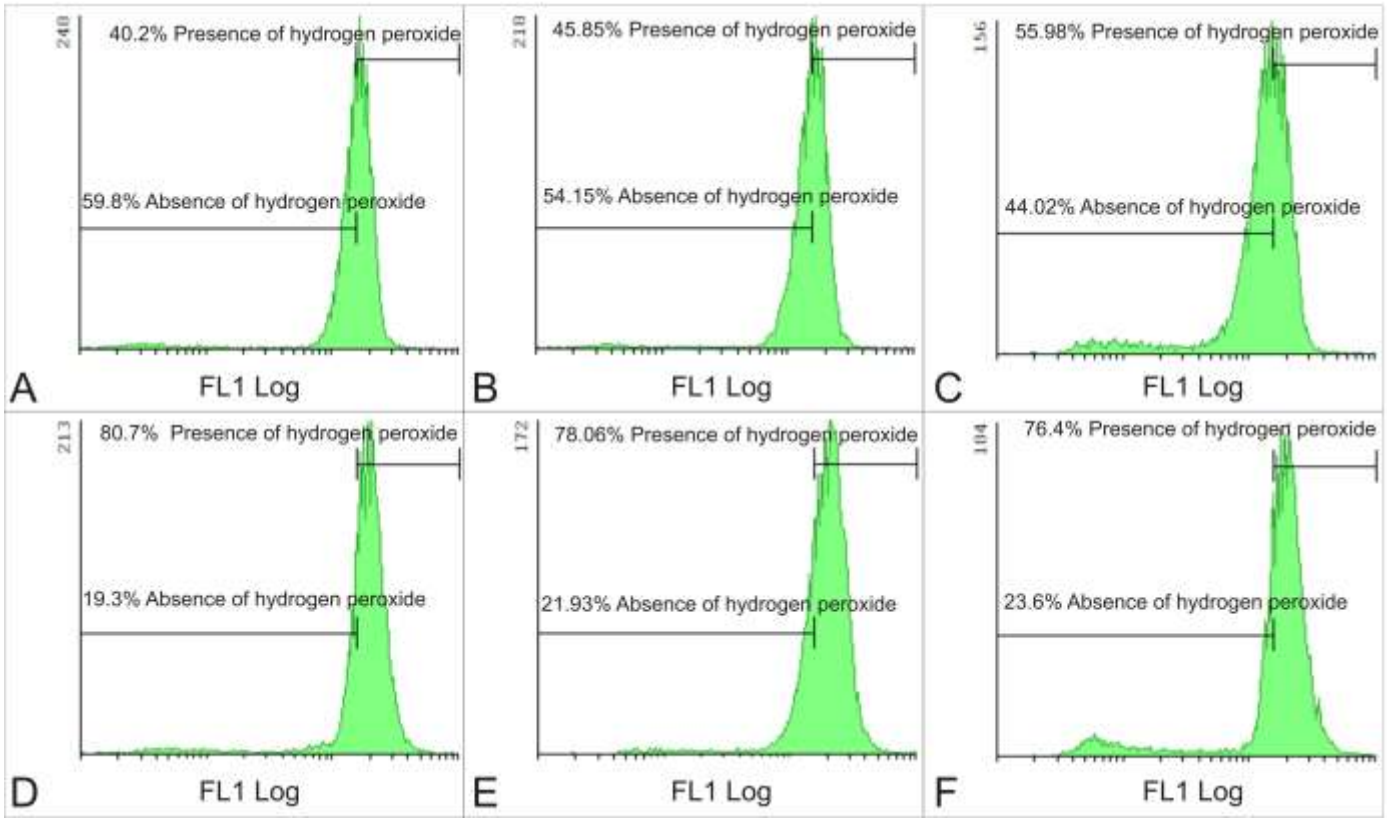

Figure 3.36: Flow cytometry investigation indicated a statistically significant increase in hydrogen peroxide production of MCF-7 (A), MDA-MB-231 (B) and MCF-12A cells (C) after exposure to 0.4 µM EMBS when compared to cells propagated in growth medium and vehicle-treated cells. Hydrogen peroxide production increased to 40% in MCF-7, 46% in MDA-MB-231 and 56% in MCF-12A cells when compared to cells propagated in growth medium and vehicle-treated cells. The positive control for this experiment included cells treated with hydrogen peroxide and demonstrated an increase in hydrogen peroxide production when compared to cells propagated in growth medium and vehicle-treated cells *(P*-value < 0.05).

Superoxide production

Hydroethidine is freely permeable and is oxidised to a red fluorescent compound, ethidium, by superoxide. Superoxide quantification was made possible by using flow cytometry and hydroethidine (225). Flow cytometry investigations revealed that cells propagated in growth medium and vehicle-treated cells produced minimal quantities of superoxide (Figure 3.37). After exposure to 0.4 µM for 24 h superoxide production increased to 27% in MCF-7 cells, 33% in MDA-MB-231 cells and 25% in MCF-12A cells.

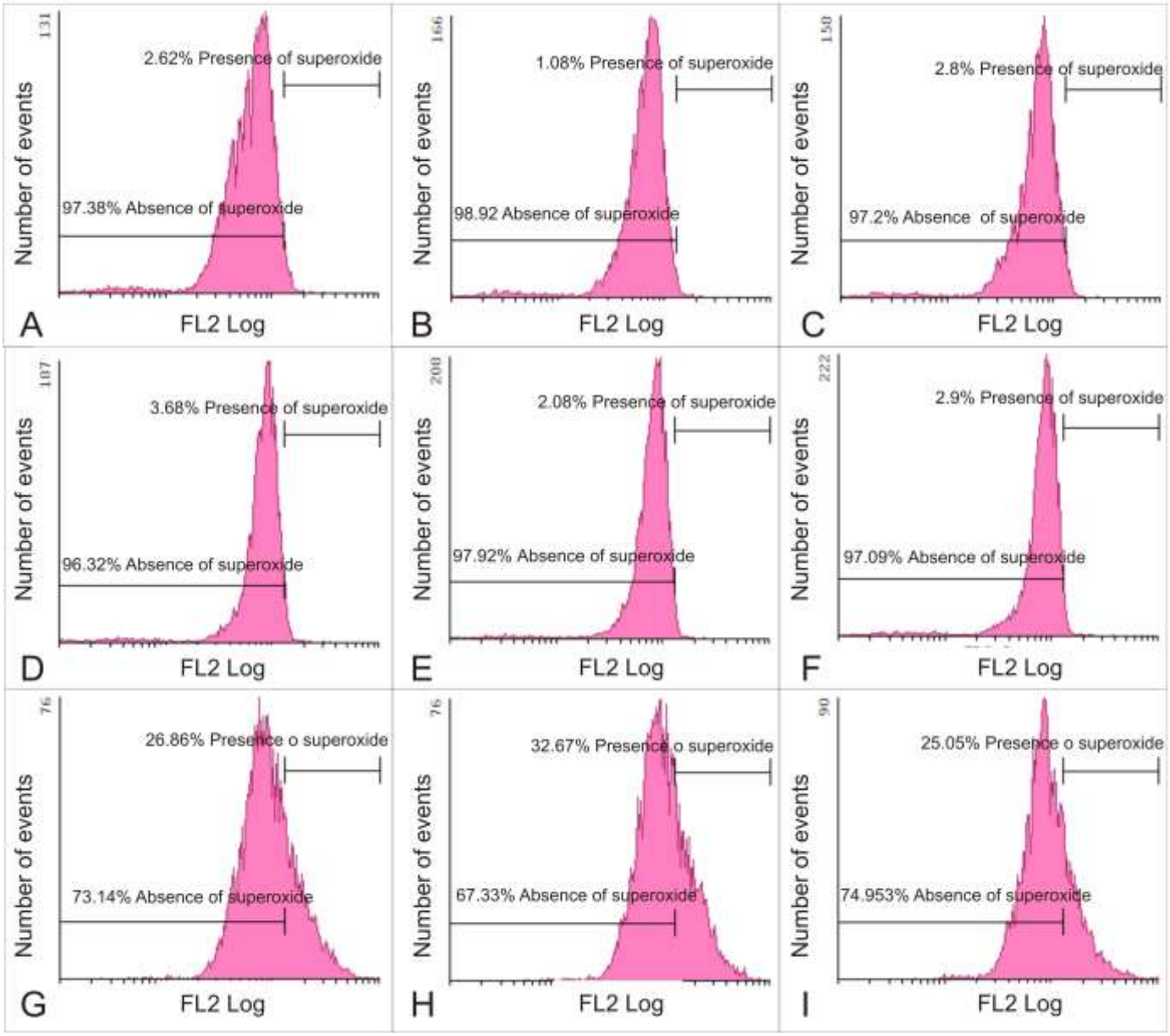

Figure 3.37: Flow cytometry investigation revealed minimal amounts of superoxide in MCF-7 (A), MDA-MB-231 (B) and MCF-12A cells (C) propagated in growth medium and vehicle-treated MCF-7 (D), MDA-MB-231 (E) and MCF-12A cells (F). Treated cells exposed to 0.4 µM for 24 h demonstrated a statistically significant increased superoxide production to 27% in MCF-7 (G), 33% in MDA-MB-231 (H) and 25% in MCF-12A cells (I) *(P*-value < 0.05).

3.8.2 Expression of p53

Cancer prevention is greatly dependent on the p53 tumor suppressor protein. This is due to the ability of p53 to eliminate damaged cells by apoptosis and is essential for regulation of cell proliferation (226). MDM2 binds and inhibits p53 and is overexpressed in various types of cancers (227). In addition, p53 also plays a vital role in autophagy induced by nutrient deprivation and genotoxic stress by inhibiting mTOR (228). Spectrophotometrical data indicated that EMBS exposure resulted in a statistically

significant increase in p53 expression when compared to cells propagated in growth medium and vehicle-treated cells (Figure 3.37). The p53 expression of MCF-7 cells were pronouncedly affected, followed by MDA-MB-231 cells and MCF-12A cells.

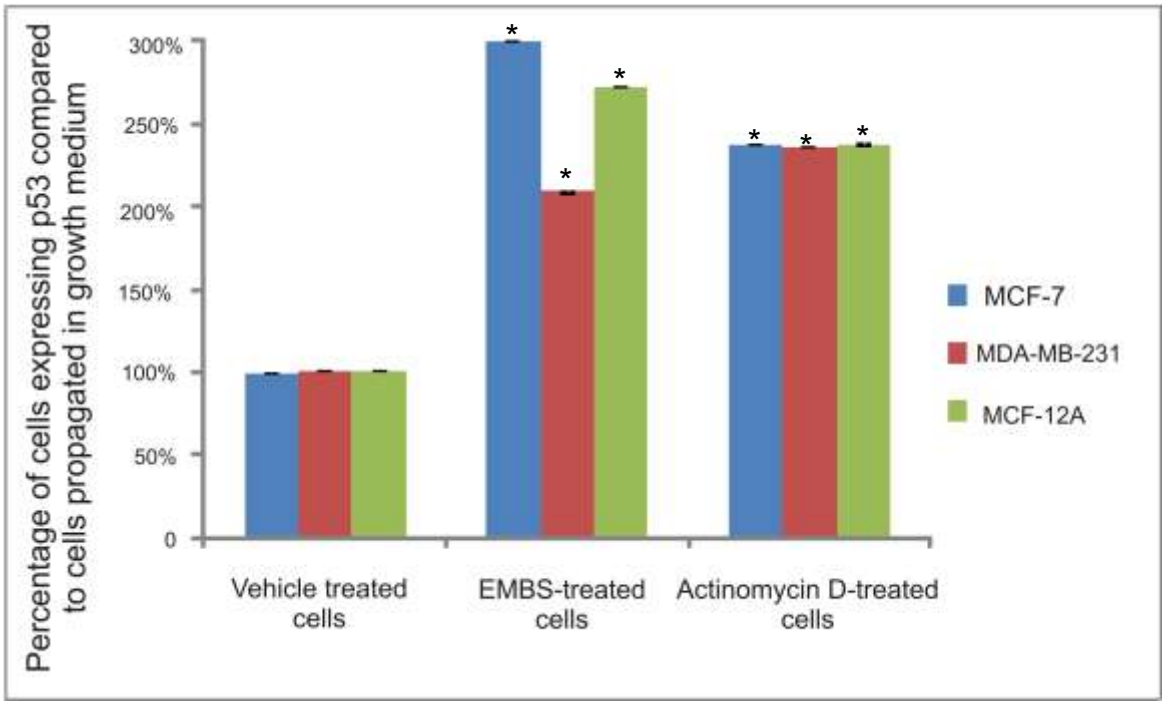

Figure 3.38: Expression of p53 was statistically significantly increased when exposed to 0.4 µM for 24 h. The p53 expression of EMBS-treated MCF-7 was increased more pronouncedly, followed by MCF-12A and MDA-MB-231 cells (an * indicates *P*-value < 0.05).

2.3.8.3 Bcl-2 expression

Bcl-2 expression and phosphorylation at serine 70 of Bcl-2 was investigated the Flow Collect Bcl-2 activation dual detection kit and flow cytometry. The Flow Collect Bcl-2 activation dual detection kit utilizes two antibodies to quantify Bcl-2 protein expression and the extent of Bcl-2 phosphorylated at Ser 70 (229).The Bcl-2 protein is an anti-apoptotic protein that prevents apoptosis by means of sequestering proforms of caspases or by preventing mitochondrial apoptogenic factors (cytochrome *c* and AIF) from entering the cytoplasm. In addition, the bcl-2 anti-apoptotic activity is regulated by phosphorylation at several serine and threonine residues including Ser70 (230). Bcl-2 Ser70 phosphorylation is required for the anti-apoptotic activity and reports indicate that this may delay apoptosis in G_2M arrested cells (231). Moreover, Bcl-2 interacts with Beclin-1 which is essential for autophagosome formation and autophagy induction (232).

Flow cytometry data of cells treated with EMBS revealed downregulated Bcl-2 expression and a decrease in pBcl-2(s70) phosphorylation when compared to cells propagated in growth medium and vehicle-treated cells (Figure 3.39 and Table 3.4). This corresponds with data of cells treated with actinomycin D that was used as a positive control for apoptosis. The latter showed downregulated Bcl-2 expression and a decrease in pBcl-2(s70) phosphorylation.

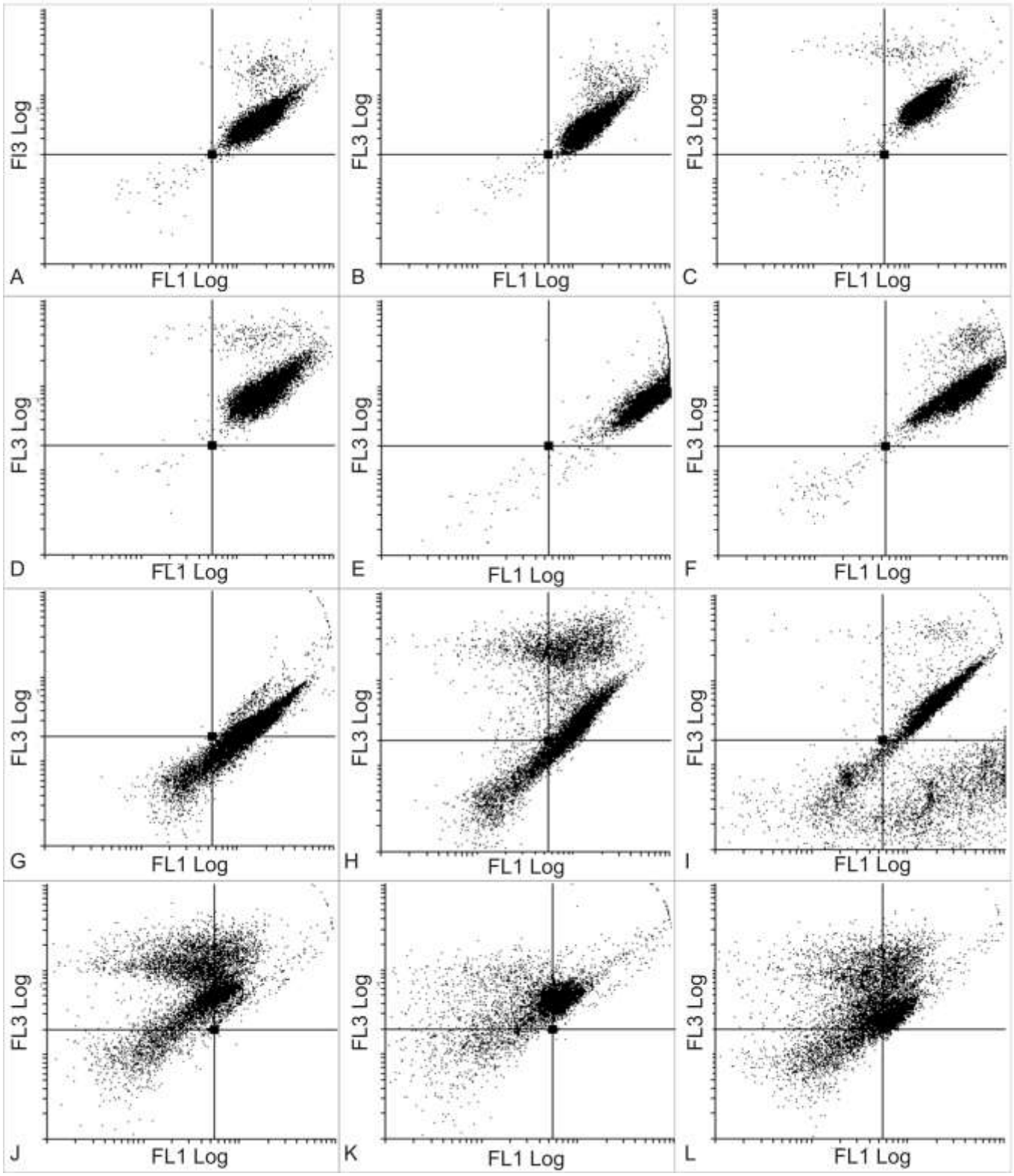

Figure 3.39: Flow cytometry investigation of Bcl-2 expression (FL1 Log) and pBcl-2(s70) phosphorylation (FL3 Log) of MCF-7 (A), MDA-MB-231 (B) and MCF-12A cells (C) propagated in growth medium and vehicle-treated MCF-7 (D), MDA-MB-231 (E) and MCF-12A cells (F). Treated cells were exposed to 0.4 μM for 24 h and demonstrated a downregulated expression of Bcl-2 and pBcl-2(s70) phosphorylation in MCF-7 (G), MDA-MB-231 (H) and MCF-12A cells (I). Actinomycin D-treated cells were used as a positive control for apoptosis and showed a decrease in Bcl-2 expression and Bcl-2(s70) phosphorylation in MCF-7 (J), MDA-MB-231 (K) and MCF-12A cells (L).

Table 3.4: Data regarding Bcl-2 expression and pBcl-2(s70) phosphorylation (an * indicates *P*-value < 0.05).

	Standard Bcl-2 expression and pBcl-2(s70) phosphory-lation	Down-regulated Bcl-2; standard pBcl-2(s70) phosphory-lation	Down-regulated Bcl-2 expression and pBcl-2(s70) phosphory-lation	Standard Bcl-2 expression; down-regulated pBcl-2(s70) phosphory-lation
MCF-7 cells propagated in growth medium	99.2±2.6%	0.1±0.001%	0.5±0.009%	0.1±0.00%
MCF-7 vehicle-treated cells	99.2±3.8%	0.6±0.002%	0.1±0.008%	0.0±0.00%
MCF-7 EMBS-treated cells	63.06±2.9% *	0.0±0.0%	14.2±0.3%	22.69±0.2% *
MCF-7 Actinomycin D-treated cells	36.53±1.7% *	54.38±1.5% *	9.0±4.2%	0.0±0.00%
MDA-MB-231 cells propagated in growth medium	99.3±3.1%	0.00.00%	0.4±0.00%	0.2±0.00%
MDA-MB-231 vehicle-treated cells	99.3±0.9%	0.0±0.00%	0.3±0.00%	0.3±0.008%
MDA-MB-231 EMBS-treated cells	61.75±1.6% *	9.5±0.007%	17.4±0.9%	11.4±0.7%
Actinomycin D-treated cells	27.78±1.1% *	65.13±2.4% *	7.1±0.04%	0.0±0.00%
MCF-12A cells propagated in growth medium	97.9±1.2%	1.6±0.002%	0.5±0.004%	0.0±0.03%
MCF-12A vehicle-treated cells	99.1±1.0%	0.1±0.00%	0.7±0.00%	0.0±0.00%
MCF-12A EMBS-treated cells	70.14±0.56% *	0.6±0.78%	10.9±0.4%	18.3±0.4%
MCF-12A Actinomycin D-treated cells	35.07±4.1% *	50.18±4.0% *	35.07±1.2% *	0.4±0.00%

Chapter 4

4. Discussion

The 17β-estradiol, 2ME2 possess antiproliferation activity and induces apoptosis without exerting any estrogenic activity (233). However, rapid breakdown due to metabolism in oxidative- and conjugation processes results in subsequent low bioavailability (234). Thus, 2ME2 failed to advance to United States Food and Drug Administration approval (235). The latter resulted in the *in silico* design and subsequent synthesis of several estradiol compounds in our laboratory (175). This *in vitro* study demonstrated the influence of a 17-beta estradiol analogue, EMBS, on proliferation, metabolism, morphology, reactive oxygen species and cell death induction via apoptosis and autophagy in adenocarcinoma receptor positive cell line (MCF-7), estrogen receptor negative metastatic cell line (MDA-MB-231) and a non-tumorigenic epithelial breast cell line (MCF-12A). Effects exerted by EMBS on the crosstalk between autophagy and apoptosis and the *in vitro* influence on non-tumorigenic MCF-12A cells were unreported prior to this *in vitro* study.

Cell growth studies by means of crystal violet staining indicated that EMBS exerts antiproliferative activity in an estrogen-independent manner in all three cell lines in a dose-dependent manner. MDA-MB-231 and MCF-12A cell lines were also affected in a time-dependent manner with cell growth drastically decreased after 48 h exposure with recovery of the MCF-12A cell lines after 72 h exposure. Antiproliferative activity exerted by EMBS reached a plateau when exposed to 0.4 μM for 24 h and thus all subsequent experiments were conducted at this concentration and exposure period. Antiproliferative activity exerted by EMBS was confirmed by means of the xCELLigence real-time approach. EMBS was previously found to exert antiproliferative activity within this concentration range in cell lines including lung adenocarcinoma cell line (HOP-62), human colorectal carcinoma cell line (HCT-116), human glioblastoma cell line (SF-539), melanoma cell line (UAVC-62), human ovarian adenocarcinoma cell line (OVCAR-3), renal carcinoma cell line (SN12-C), human prostate carcinoma cell line (DU-145) and breast tumorigenic cell line (MDA-MB-435) (236).

Panchapakesan, *et al.* (2011) reported that another 17β-estradiol methylated analogue, 17β-hydroxy/17-methylene estratrienes reduced cell growth in the HCT-116 cell line, large lung cancer cell line (NCIH-460), glioblastoma astrocytoma (U-251) and MDA-MB-435 cell line (237).

Research conducted in our laboratory demonstrated that other sulphamoylated estradiol analogues, 2-ethyl-3-*O*-sulphamoyl-estra-1,3,5(10) and 15-tetraen-17-ol, 2-ethyl-3-*O*-sulphamoyl-estra-1,3,5(10)16-tetraene, (8,9,13,14,17)-2-ethyl-17-hydroxy-13-methyl-7,8,9,11,12,13,14,15,16,17-decahydro-6H-cyclopenta[*a*]phenanthren-3-yl sulphamate possessed antiproliferation activity in a similar concentration range as this study demonstrated (175, 229, 238, 239). In addition, another sulphamoylated 2ME2 derivative, 2MEBM, inhibited cell growth in a dose-dependent manner (0.1-1μM) in the MCF-7 cell line, prostate cancer cell line (LNACaP), MDA-MB-231 cell line, human cervical adenocarcinoma cell line (HeLa), human ovarian carcinoma (A2780), androgen-sensitive human prostate adenocarcinoma cells (LNCaP) and the CAL51 human breast carcinoma cell line (167, 240, 241, 242, 243).

Cell viability, metabolism and energy production were investigated by demonstrating the *in vitro* influence EMBS exerts on membrane integrity by quantifying the LDH released by the cells and NAD^+/NADH and $NADP^+$/NAPPH production. No statistically significant changes were found in NAD^+/NADH and $NADP^+$/NAPPH production and LDH present when compared to vehicle-treated cells and other appropriate controls as discussed earlier. The lack of a substantial increase in LDH production found in the media indicates that EMBS did not have a cytotoxic effect and did not compromise the cell membrane enough to allow for acute leakage of LDH. This is supported by previous research that reported that 17β-estradiol exposure did not significantly increase LDH production in smooth muscle cells leaving cell viability unaffected and the cell membrane intact (244). In addition, studies from our laboratory verified that 2MEBM exposure in a non-tumorigenic breast cancer cell line (MCF-12A) and oesophageal cancer cell line (SNO) resulted in a statistical insignificant release of LDH. The latter indicates that 2MEBM refrained from damaging the cell membrane sufficiently to allow for LDH leaking and did not induce necrosis (178, 246, 247).

Recent reports, also from our laboratory, indicated that exposure to sulphamoylated analogues (2-ethyl-3-*O*-sulphamoyl-estra-1,3,5(10) 16-tetraene and 2-ethyl-3-*O*-sulphamoyl-estra-1,3,5(10)15-tetraene-3-ol-17one) and EMBS in human epithelial cervical cell line (HeLa) did not demonstrate a statistical significant LDH increase (214). LDH is released by the cell into the surrounding environment in the event of cell membrane damage. These studies suggest that exposure to sulphamoylated 2ME2 analogues does not result in sufficient cell membrane damage to allow for acute leakage of LDH.

Qualitative data regarding morphology were provided by means of PlasDIC, light microscopy, TEM, SEM and fluorescent microscopy. These techniques revealed several hallmarks of apoptosis after exposure to EMBS (0.4 μM; 24 h) including decreased cell density, apoptotic bodies, shrunken cells, hypercondensed chromatin and several cells trapped in metaphase culminating in apoptosis in all cell lines. Characteristics of autophagy induction were also found including vacuoles and autophagosomes. The same morphological findings were reportedly induced by 2-ethyl-3-*O*-sulphamoyl-estra-1,3,5(10)16-tetraene, 2-ethyl-3-*O*-sulphamoyl-estra-1,3,5 (10)15-tetraene-3-ol-17one and EMBS in human epithelial cervical cell line (HeLa) (214). Light microscopy, TEM and PlasDIC demonstrated the induction of apoptosis and autophagy by 2MEBM illustrating apoptotic bodies, shrunken cells and vacuoles in MCF-7 cells (178). The latter is supported by visualization of apoptotic bodies, shrunken cells and cells blocked in metaphase in the oesophageal cancer cell line (SNO) (247).

Influence of EMBS on apoptosis induction was quantified by means of mitotic indices, cell cycle progression, Annexin V-FITC, changes in mitochondrial membrane potential and caspase activation. Mitotic indices revealed an increase in cells possessing abnormal morphology associated with apoptosis and the number of cells in metaphase culminating in apoptosis. This was confirmed by flow cytometry using propidium iodide (cell cycle progression) that revealed a significant induction in apoptosis and an increase in the number of cells occupying the G_2M phase. Reduction of mitochondrial membrane potential was also observed. This notion is

supported by previous studies in our laboratory where 2-ethyl-3-*O*-sulphamoyl-estra-1,3,5(10)16-tetraene, 2-ethyl-3-*O*-sulphamoyl-estra-1,3,5(10)15-tetraene-3-ol-17one reduced the mitochondrial membrane potential in the HeLa cell line (178). The depolarization of the mitochondrial membrane potential suggests apoptosis induction via the intrinsic pathway. EMBS induced the mitochondrial pathway as treatment resulted in depolarization of the mitochondrial membrane potential and cytochrome *c* release in MDA-MB-231 cell line and human umbilical vein endothelial cell (HUVEC) (161).

Apoptosis induction by 2MEBM have been reported in cell lines including the drug resistant human breast adenocarcinoma cell line (MCF-7 $_{DOX}$40), mitoxantrone resistant breast adenocarcinoma cell line (MCF-7 MR) and MDA-MB-231 cell line (248. 149, 179). Data also indicated the upregulation of initiator caspase 8, executioner caspase 6 and caspase 7 in all three cell lines. This supports the notion that EMBS induces apoptosis by means of both the intrinsic and extrinsic pathways. This is supported by increased number of cells exerting activated caspase 6 and caspase 8 activity accompanied with a reduced mitochondrial membrane potential in human epithelial cervical cell line (HeLa) exposed to 2-ethyl-3-*O*-sulphamoyl-estra-1,3,5(10)16-tetraene and 2-ethyl-3-*O*-sulphamoyl-estra-1,3,5(10)15-tetraene-3-ol-17one (214).

Increased lysosomal staining after exposure to EMBS indicates cell death via autophagy induction. However, accumulation of acridine orange in acidic organelles and lysosomes suggests autophagy induction but (194). Since LC3-II is tightly associated with the autophagosome membrane and is thus considered a marker for autophagy induction (251, 252). This study also employed LC3B conjugated to DyLight 488 and flow cytometry to provide quantitative autophagy data. LC3-I in its cytosolic form is activated by ATG7, transferred to ATG3 and is then converted to its membrane-bound form, LC3-II. LC-II (251). Flow cytometry results confirmed autophagy induction by exposure to EMBS in all three cell lines. The latter is supported by upregulation of RAB7, member RAS oncogene family and downregulation of Rapamycin-insensitive companion of mTOR (RICTOR) in global arrays performed after exposure to EMBS in the MDA-MB-231 cell line (236). Rab7

is a small GTPase vital to the fusion of late endosome and lysosomes in the endocytic pathway (253). Furthermore, Rab7 is essential for vacuole formation and maturation of late autophagic vesicles (254). RICTOR regulates autophagy and inhibition of the mTORC resulting in autophagy induction in the non-small H383 cell lung cancer cell line (225). 2-Ethyl-3-*O*-sulphamoyl-estra-1,3,5(10)16-tetraene induced autophagy in human cervical adenocarcinoma cell line (HeLa) (256). Another bis-sulphamoylated analogue, 2MEBM, induces autophagy in the MCF-7 cell line and the SNO cell line (179, 257).

The source and processing of ROS and the role they play in EMBS-induced growth inhibition and cell death remain to be elucidated. Flow cytometry studies demonstrated that EMBS exposure resulted in statistically significant increased hydrogen peroxide-and superoxide production in all three cell lines. However, The novel discovery regarding the *in vitro* effects of EMBS on ROS production in tumorigenic and non-tumorigenic lines has not been reported previously. Exposure to 2-ethyl-3-*O*-sulphamoyl-estra-1,3,5(10)16-tetraene increased hydrogen peroxide and superoxide production in MCF-7, MDA-MB-231 and MCF-12A cells (238).

Reactive oxygen species (ROS) also participate in the intrinsic pathway since they serve as a second messenger converging at the mitochondria resulting in cytochrome *c* release. High ROS levels leads to cellular stress and subsequent release of pro-apoptotic factors and proteins including cytochrome *c*, AIF, EndoG and HtA1/Omi resulting in the formation of the apoptosome (258). Although ROS are not responsible for the direct activation of the extrinsic pathway, ROS can alter the intracellular environment optimizing the engagement between receptors and ligands by upregulating of CD95 and TRAIL death receptors (259). Furthermore, ROS are necessary for Fas phosphorylation at the tyrosine residue, signaling for consequent employment of Fas-associated protein with death domain and caspase 8 for apoptosis induction. ROS are also required for the ubiquitination and subsequent degradation of the FLICE inhibitory protein to further enhance Fas activation (260).

Escalated ROS production is related to Akt that is an essential inhibitor of mitochondrial ROS scavenging. Akt phosphorylates forkhead box O (FOXO) transcription factors with subsequent cytosolic sequestration through interaction with

14-3-3 adaptor proteins. FOXOs encompasses a family of transcription factors that encourage expression of genes associated with cell cycle arrest, apoptosis and tumor suppression (261). Mediators such as TNFs that activate ASK1 also encourage ROS production (262). ASK1 regulates activation of NK and p38 MAPK pathways required for cell death. The link between ROS production and the subsequent activation of ASK1-dependent signaling appears to involve a redox-dependent interaction between ASK1 and thioredoxin (262).

Elevated ROS levels also result in oxidative stress culminating in autophagy. Thus, antioxidizing agents that decrease ROS would result in decreased autophagy levels (263). The notion that exposure to EMBS results in elevated ROS production leading to autophagy induction accompanied with decreased antioxidizing levels is supported by a gene expression study that demonstrated decreased superoxide dismutase 1, soluble (SOD1) expression after treatment with EMBS (235). The mouse cell model (L929) with catalase degradation resulted in ROS accumulation, loss of plasma membrane integrity and autophagy induction (264). MCF-7 exposure to hydrogen peroxide inhibited phosphorylation of mTORC1 at p70/s6 and 4EBP1 occurred in a dose- and time-dependent manner (<60 min; <0.1 mM hydrogen peroxide) (264). The mTORC1 repression results in autophagy induction in MCF-7 cells (265). Hydrogen peroxide induces autophagy by targeting HsATG4 protease by means of oxidation modification at a cysteine residue situated in the proximity of the catalytic site). Cysteine protease HsAtg4 activity is stringently regulated in conjugating Atg8 to the autophagosomal membranes via cleaving the C-terminal of recently synthesized proteins and in recycling it from the membrane by the delipidation of ATG8-PE, which is a characteristic of autophagy (266). Although ROS are well-known important signaling molecules in the crosstalk between apoptosis and autophagy pathways, the molecular mechanisms linking these processes are complex and several questions remains to be unravelled.

This *in vitro* study also demonstrated that EMBS exposure (0.4 µM; 24 h) resulted in a statistically significant increase in p53 expression in all three cell lines when compared to cells propagated in growth medium and vehicle-treated cells. The latter is supported by reports that another sulphamoylated analogue, 2-ethylestrone-3-sulfamate upregulated p53 expression in CAL-51 cell lines, HUVEC cell line and

MCF-7 cells line (267, 268). The p53 tumor suppressor is the primary mediator of proliferation arrest, senescence and apoptosis induction. In unstressed cells, MDM2, the main antagonist of p53, continuously mono-ubiquitinates p53 and thus is the essential step in regulating its degradation by nuclear and cytoplasmic proteosomes (269). Due to the inhibitory activity of MDM2 on p53, MDM-2 overexpression is associated with unrestrained cell proliferation and tumorigenesis (270). Furthermore, Akt phosphorylates MDM2 at serine 166 and serine 186 resulting in MDM2 translocating from the cytoplasm into the nucleus. Akt activation of is adequate to promote nuclear entry of Mdm2, where it inhibits the p53 tumor suppressor protein and its transcriptional activity and target it for degradation by the proteasome (271).

Increased p53 expression after exposure to EMBS suggests decreased MDM2 and Akt expression. P53 targets several pro-apoptotic genes including BAX, Fas/Apo1, Killer/DR5, PUMA, Noxa, AFAF1 and Bcl-2 (272). Gene array studies conducted in our laboratory revealed that BAX expression was increased in the MDA-MB-231 cell line after exposure to EMBS (235). Transcriptional upregulation by p53 of BAX results in a conformational change and triggers the intrinsic apoptotic pathway (273). Nutrient deprivation and stress results in p53 activation which can then interact with various pro-autophagic modulators including AMP-activated protein kinase (AMPK) activation death-associated protein kinase 1 (DAPK-1), damage-regulated autophagy modulator (DRAM), proapoptotic Bcl-2 proteins, sestrin 2, and tuberous sclerosis protein 2 (TSC2) (274).

The results indicate that EMBS exposure can lead to decreased Bcl-2 expression and a decrease in pBcl-2(s70) phosphorylation when compared to cells propagated in growth medium and vehicle-treated cells. Bcl-2 is an anti-apoptotic protein that occurs on the cytoplasmic face of the mitochondrial outer membrane, ER and nuclear envelope and possibly registers injury and potentially changes it's the cellular organelle's behaviour by modifying the flux of small molecules or proteins (211). Bcl-2 protects against apoptosis by stabilization the mitochondrial membrane potential and preventing subsequent release of cytochrome *c* and activation of caspase 2 and caspase 9 (275). Downregulation of Bcl-2 expression results in Bax upregulation, caspase 3 activation and apoptosis induction in a liver adenocarcinoma

cell line (SK-Hep-1) (276). Bcl-2 phosphorylation at serine 70 located in the flexible loop domain (FLD), is essential for full anti-apoptotic activity exerted by Bcl-2 (277). However, Bcl-2 phosphorylation at multiple sites (serine 70, threonine 69 and serine 87) resulted in a pro-apoptotic effect with subsequent cytochrome c release (278).

Bcl-2 also plays a role in suppressing autophagy induction by binding to the protein Beclin 1, which is necessary for autophagosome formation in autophagy (279). Overexpression of Bcl-2 has been show to inhibit autophagy. In addition, small interfering ribonucleic acid (siRNA)-mediated Bcl-2 downregulation in MCF-7 cells resulted in significantly increased levels of autophagy induction (280). An antagonist of Bcl-2, ethyl 2-amino-6-bromo-4(1-cyano-2-ethoxy-2-oxoethyl)-4H-chromene-3 carboxylate, binds to the surface pocket of Bcl-2 inducing apoptosis and autophagy in murine leukaemia cells (L1210) (280). Similarly, ABT-737, a BH3-mimetic compound, binds to the BH3-binding groove of Bcl-2, releasing beclin1 and inducing autophagy in HeLa cells (281). Starvation of Hela cells and MCF-7 cells resulted in Bcl-2 phosphorylation via JNK1 at threonine 69, serine 70 and serine 87, and subsequent dissociation from beclin-1 and autophagosomes formation (282).

This *in vitro* study demonstrated that EMBS exposure resulted in antiproliferative- and antimitotic activity and induced cell death via apoptosis and autophagy without compromising the cell membrane in a sufficient manner to allow for severe LDH leakage in MCF-7, MDA-MB-231 and MCF-12A cells in an estrogen-independent manner. The morphological findings include hallmarks of apoptosis including cell density, apoptotic bodies, shrunken cells, hypercondensed chromatin and several cells trapped in metaphase culminating in apoptosis. Autophagy characteristics were also found including vacuoles and autophagosomes. Apoptosis induction was verified by activation of initiator caspase 8, executioner caspase 6 and caspase 7 accompanied with a reduction in the mitochondrial membrane potential. Antimitotic activity culminating in apoptosis was established by means of cell cycle progression and mitotic indices. Autophagy induction was confirmed by means of increased lysosomal staining and elevated LC3-II levels. The crosstalk between apoptosis and autophagy induced by EMBS in an estrogen-independent manner was substantiated

by increased ROS production and p53 expression accompanied by reduced Bcl-2 expression and phosphorylation of Bcl-2 at serine 70.

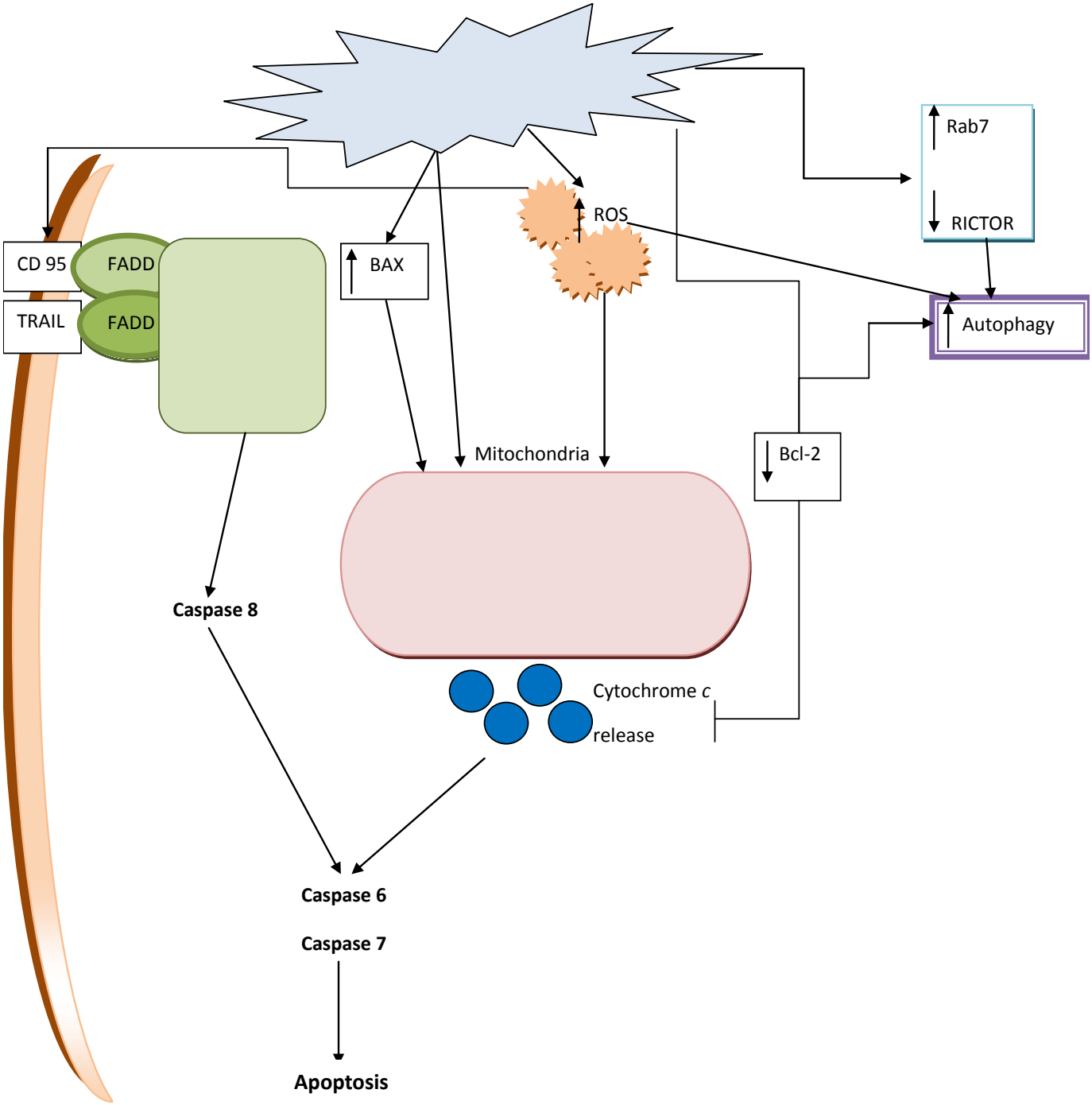

Figure 4.1: A schematic diagram showing the proposed signaling utilized by EMBS. EMBS results in increased ROS production resulting in activation of autophagy, increased CD 95 and Trail receptors and depolarisation of the mitochondrial membrane potential thus inducing the intrinsic and extrinsic apoptotic pathway. Caspases 8 is also activated in the intrinsic pathway. Bcl-2 downregulation also promotes induction of autophagy and apoptosis. Subsequent activation of executioner caspases 6 and 7 resulting in the demise of the cell.

Chapter 5

5. Conclusion

In conclusion, the aims of this study namely, to investigate the effects of EMBS in estrogen receptor positive- and estrogen receptor negative breast adenocarcinoma cell lines (MCF-7 and MDA-MB-231) and the non-tumorigenic epithelial breast cell line (MCF-12A) respectively by analyzing its influence on cell growth, cytotoxicity, metabolism, morphology, cell cycle progression, mitochondrial membrane potential, caspase activation, reactive oxygen species generation and induction of cell death via apoptosis and autophagy and the crosstalk between them were achieved. EMBS exposure resulted in antiproliferative-and antimitotic activity and induced apoptosis and autophagy in an estrogen receptor independent manner. The induction of both the intrinsic- and extrinsic apoptotic pathway by EMBS exposure is implicated. Molecular crosstalk between apoptosis and autophagy induced by EMBS was demonstrated by increased ROS production and p53 expression accompanied by reduced Bcl-2 expression and phosphorylation of Bcl-2 at serine 70. The novel discovery regarding the *in vitro* effect of EMBS on autophagy induction, increased ROS production, p53 expression, Bcl-2 expression and phosphorylation of Bcl-2 at serine 70 in tumorigenic and non-tumorigenic lines has not been reported previously. This study is the first to report on the *in vitro* effect of EMBS on non-tumorigenic MCF-12A cell line and the main conclusions are summarized in figure 4.1.

Data generated from this project elucidated cell signaling events exerted by EMBS in tumorigenic and non-tumorigenic cell lines and contributes to novel *in vitro* targets for cancer therapies including the mitochondria, reactive oxygen species and bcl-2 protein. Future studies of EMBS will involve *ex vivo*- and *in vivo* studies that will contribute to the development and/or improvement of novel chemotherapeutic agents paving the way for efficient *in vivo* studies.

References

1. Jemal A, Bray F, Center MM, Ferlay J, Ward E, Forman D. Global Cancer Statistics. Ca Cancer J Clin 2011; 61: 69-90.
2. Bhikoo R, Srinivasa S, Tzu-Chieh Y, Moss D, Hill AG. Systematic review of breast cancer biology in developing countries (Part 1): Africa, the Middle East, Eastern Europe, Mexico, the Caribbean and South America. Cancers 2011; 3: 2358-2381.
3. Siegel R, Naishadham D, Jemal A. Cancer statistics 2012. CA Cancer J Clin 2012; 62(1): 10-29.
4. Gerber B, Freund M, Reimer T. Recurrent breast cancer: treatment strategies for maintaining and prolonging good quality of life. Dtsch Arztebl Int 2010; 107(6): 85-91.
5. Kwan ML, Kushi LH, Weltzien E, Maring B, Kutner SE, Fulton RS, et al. Epidemiology of breast cancer subtypes in two prospective cohort studies of breast cancer survivors. Breast Cancer Res 2002; 11(3): R31.
6. Kelsey JL, Berstein L. Epidemiology and prevention of breast cancer. Annu. Rev. Public Health. 1996; 17: 47-67.
7. Mayi-Tsong S, Kamga H, Meye JF, Belembaogo E. Risk factors of bilaterazation of breast cancer: description of five cases in Libreville (Gabon) and review of the literature. Med Trop (Mars) 2009: 69(9): 583-586.
8. Runnebaum IB, Nagarajan M, Bowman M, Soto D, Sukumar S. Mutations in p53 as a potential molecule marker for human breast cancer. Proc Natl Acad Sci U S A 1991; 88(23): 10657-10661.
9. Potter P. "Westernizing" Women's Risks? Breast Cancer in Lower-Income Countries. N Engl J Med 2008; 358 (3): 213-216.
10. Tariq R, Huma S, Butt MZ, Amin F. Risk factors and prevalence of breast cancer: a review. J Pak Med Assoc 2013; 63(8): 1075-1078.
11. Shapiro CL, Recht A. Side effects of adjuvant treatment of breast cancer. N Engl J Med 2001; 344(26): 1997-2008.
12. Al-Baitaineh O, Jenne J, Huber P. Clinical and future applications of high intensity focused inltrasound in cancer. Cancer Treat Rev 2012; 38(5): 346-353.
13. Popat S, Smith IE. Breast cancer. Update Cancer Ther 2009; 1: 187-210.

14. Chen S, Masri S, Wang X, Phung S, Yuan YC, Wu X. What do we know about the mechanism of aromatse inhibitor resistance. J Steroid Mol Biol 2006; 102(1-5): 232-240.
15. Raobaikady B, Purohit A, Chander SK, Woo LWL, Leese MP, Potter BVL, et al. inhibition of MCF-7 breast cancer cell proliferation and in vivo steroid sulphatase activity by 2-methoxyestradiol-bis-sulphamate. J Steroid Biochem Mol Biol 2003; 84: 351-358.
16. Jonat W, Howell A, Blomqvist C, Eiermann W, Winbad G, Tyrrell C, et al. A romdomised trail comparing two doses of the new selective aromatase inhibitor anastrozole (arimidex) with megastrol acetate in postmenopausal patients with advanced breast cancer. Eur J Cancer 1996; 32A(3): 404-412.
17. Thiery JP, Sastre-Garau X, Vincent-Salomon B, Sigal-Zafrani X, Pierga JY, Decraene C, et al. Challenges in the stratification of breast tumors for tailored therapies. Bull Cancer 2006; 93(8): E81-89.
18. Partridge AH, Burstein HJ, Winer EP. Side effects of chemotherapy and combined chemohormonal therapy in women with early stage breast cancer. J Natl Cancer Inst Monogr 2001; 30: 135-142.
19. Moy B, Goss PE. Lapatininb: Current status and future directions on breast cancer. Oncologist 2006; 11: 1047-1057.
20. Muti P, Bradlow LH, Micheli A, Krogh V, Fredenheim JL, Schünemann HJI, et al. Estrogen metabolism and risk of breast cancer: a prospective study of the 2:16α-hydroxyestrone ratio in premenopausal and postmenopausal women. Epidiomology 2000; 11(6): 635-640.
21. Hollie TV, Reeves GK, Key TJA. Endogenous estrogen and postmenopausal breast cancer: a quantitative review. Cancer Causes Control 1997; 8(6): 911-928.
22. Yager JD, Davisdon NE. Estrogen carcinogenesis in breast cancer. N Engl J Med 2006; 354: 270-282.
23. Yue W, Yager JD, Wang J, Jupe ER, Santen RJ. Estrogen receptor-dependent and independent mechanisms of breast cancer carcinogenesis. Steroids 2013; 78(2): 161-170
24. Fillmore CM, Gupta PB, Rudnick JA, Caballero S, Keller PJ, Laner ES, et al. Estrogen expands breast cancer stem-like cells through paracrine FGF/Tbx3 signaling. Proc Natl Acad Sci USA 2010; 107(50): 2137-21742.

25. Arpino, G, Green SJ, Allred DC, Lew D, Martino S, Osborne CK, et al. HER-2 amplification, HER-1 expression, and tamoxifen response in estrogen receptor-positive metastatic breast cancer: a southwest oncology group study. Clin Cancer Res 2004;10:5670-5676

26. De Laurentiis M, Arpino G, Massarell E, Ruggiero A, Carlomagno C, Ciardiello F, et al. A meta-analysis on the interaction between HER-2 expression and response to endocrine treatment in advanced breast cancer. Clin Cancer Res 2005;11:4741-4748

27. Fu X, Osborn CK, Schiff R. Biology and therapeutical potential of PI3K signaling in ER+/Her2-negative breast cancer. Breast 2013; 22(1): 12-18.

28. Budirahardja Y, Gönczy P. Coupling the cell cycle to development. Development 2009; 136(17): 2861-2872.

29. Harper JW, Adams JW. Cyclin-dependent kinases. Chem Rev 2001; 101: 2511-2526.

30. Inzé D. Green light for the cell cycle. The EMBO J 2005; 24: 657-662.

31. Nigg EA. Cyclin-dependent protein kinases: key regulators of the eukaryotic cell cycle. Bioassays 1995; 17(6): 471-480.

32. Miller ME, Cross FR. Cyclin specificity: How many wheels do you need on a unicycle? J Cell Sci 2001; 114: 1811-1820.

33. Chivukula RR, Mendell JT. Circular reasoning: microRNAs and cell cycle control. Trends Biochem Sci 2008; 33(10): 474-481.

34. Díaz-Martínez LA, Giménez-Abián JF, Clarke DJ. Chromosome cohesion-rings, knots, orcs and fellowship. J Cell Sci 2008; 121(13): 2107-2114.

35. Dutta A, Bell SP. Initiation of DNA replication in eukaryotic cells. Ann Rev Cell Dev Biol 1997; 13: 293-332.

36. Duncker BP, Chesnokov IN, McConkey BJ. The origin recognition complex protein family. Genome Biol 2009; 10(3): 214.1-214.8.

37. Sivaprasad U, Machida YJ, Dutta A. APC/C- master controller of origin licensing? Cell Division 2007;2(8).

38. Balk SP, Knudsen KE. AR, the cell cycle and prostate cancer. Nuclear receptor signaling 2008; 6: 1-12.

39. Kitagawa R., Law E, Tang L, Rose AM. The Cdc20 homolog, FZY-1, and its interacting protein, IFY-1, are required for proper chromosome segregation in Caenorhabditis elegans. Curr Biol 2002; 12, 2118–2123.

40. Queralt E, Uhlmann F. Cdk-counteracting phosphatases unlock mitotic exit. Curr Opin Cell Biol 2008; 20(6): 661-668.

41. Furuta T, Tuck S, Kirchner J, Koch B, Auty R, Kitagawa R, et al (2000). EMB-30: an APC4 homologue required for metaphase-to-anaphase transitions during meiosis and mitosis in Caenorhabditis elegans. Mol. Biol. Cell 11, 1401–1419.

42. Li M, Zhang P. The function of APC/C^{CDH1} in cell cycle and beyond. Cell Div 2009;4(2).

43. Teixeira LK, Reed SI. Ubiquitin ligases and cell cycle control. Annu Rev Biochem 2013; 82: 387-414.

44. Belizario JE, Alves J, Garay-Malpartida M, Occhiucci JM. Curr Protein Pept Sci 2008; 9: 210-220.

45. Fung TK, Siu WY, Yam CH, Lau A, Poon RYC. Cyclin F is degraded during G_2-M by mechanisms fundamentally different from other cyclins. J Biol Chem 2002; 277(38): 35140-35149.

46. Thornton TM, Rincon M. Non-classical P38 Map Kinase functions: cell cycle checkpoints and survival. Int J Bio Sci 2009; 5: 44-51.

47. Willis N, Rhind N. Regulation of DNA replication by the S-phase DNA damage checkpoint. Cell Div 2009; 4(13): 1-10.

48. Peeper DS, Bernards R. Communication between the extracellular environment, cytoplasmic signaling cascades and the nuclear cell-cycle machinery. FEBS Lett 1997; 410(1):11-16.

49. Malumbres M, Sotillo R, Santamaría D, Galán J, Cerezo A, Ortega S, et al. Mammalian cells cycle without the D-type cyclin-dependent kinases Cdk4 and Cdk6. Cell 2004; 118(2): 493-504.

50. Todd R, Hinds PW, Munger K, Rustgi AK, Opitz OG, Suliman Y, Wong DT. Cell cycle dysregulation in oral cancer. Crit Rev Oral Biol 2002; 13(1): 51-61.

51. Tyner AL. A new year, a new role for p21. Cell Cycle 2009; 8(2): 183-184.

52. Gillis LD, Leidal AM, Hill R, Lee PWK. $P21^{Cip1/WAF1}$ mediates cyclin B1 degradation in response to DAN damage. Cell Cycle 2009; 8(2): 253-256.

53. May KM, Hardwick KG. The spindle checkpoint. J Cell Sci 2006; 119(20): 4139-4142.
54. Ciliberto A, Shah JV. A quantitative systems view of the spindle assembly checkpoint. EMBO J 2009; 28: 2162-2173.
55. Fang G, Yu H, Kirschner MW. Control of mitotic transitions by the anaphase-promoting complex. Philos Trans R Soc Lond Biol Sci 1999; 354(1389): 1583-1590.
56. Elmore S. Apoptosis: a Review of programmed cell death. Toxicol Pathol 2007; 35: 495-516.
57. Yu L, Wan F, Dutta S, Welsh S, Liu Z, Freundt E, et al. Autophagic programmed cell death by selective catalase degradation. Proc Natl Acad Sci 2006; 103(13): 4952-4957.
58. Kroemer G, Galluzzi L, Van de Nabeele P, Abrams J, Alnemri ES, Baehrecke EH, et al. Classification of cell death: recommendations of the nomenclare committee on cell death 2009. Cell Death Differ 2009; 16: 3-11.
59. Taatjes DJ, sobel BE, Budd RC. Morphological and cytochemical determination of cell death by apoptosis. Histochem Cell Boil 2008; 129: 33-43.
60. Hergartner MO. The biochemistry of apoptosis. Nature 2000; 407: 770-776.
61. Igney, FH, Krammer P H. Death and anti-death: tumor resistance apoptosis. Nat Rev Cancer (2002); 2: 277–288.
62. Balasubramanian K, Mirnikjoo B, Schroit AJ. Regulated externalization of Phosphatidylserine at the Cell Surface: Implications for apoptosis. Biol Chem 2007; 22; 282(25): 18357-18364.
63. Kumar S. Caspase function in programmed cell death. Cell Death Differ 2007; 14: 32-43.
64. Wolf BB, Green DR. Suicidal tendencies: apoptotic cell death by caspase family proteinases. J Biol Chem 1999; 274(29): 20049-20052.
65. Bao Q, Shi Y. Apoptosome: a platform for the activation of initiator caspases. Cell Death Differ 2007; 14: 56-65.
66. Boatright KM, Salveson GS. Mechanisms of caspase activation. Curr Opin Cell Biol 2003; 15(6): 725-731.
67. Allan LA, Clarke PR. Apoptosis and autophagy: regulation of caspase-9 by phosphorylation. FEBS 2009; 276: 6063-6073.

68. Khosravi-Far R, Esposti MD. Death receptor signals to mitochondria. Cancer Biol Ther 2004; 3(11): 1051-1057.
69. Peter ME, Krammer PH. The CD95(APO-1/Fas) DISC and beyond. Cell Death Differ 2003; 10: 26–35.
70. Jin Z, EL-Deiry WS. Overview of cell death signaling pathways. Cancer Biol Ther 2005; 4(2): 139-163.
71. Kim R. Recent advances in understanding the cell death pathways activated by anticancer therapy. Cancer 2005; 103(8): 1661-1680.
72. Yang JK. Flip as an anti-cancer therapapeutic target. Yonsei Med J 2008; 49(1): 19-27.
73. Fischer U, Jänicke RU, Schulze-Osthoff K. Many cuts to ruin: a comprehensive update of caspase substrates. Cell Death Differ. 2003; 10: 76–100.
74. Qiang FX, Guo YJ. Apoptosis in oncology. Cell Res 2001; 11(1): 1-7.
75. Pitti RM, Masters SA, Ruppert S, Donahuel CJ, et al. Induction of Apoptosis by Apo-2 Ligand, a New Member of the Tumor Necrosis Factor Cytokine Family. J Biol Chem 1996; 271(22): 12687-12690.
76. Russo A, Terrasi M, Agnese V, Santini D, Bazan V. Apoptosis : a relevant tool for anticancer therapy. Ann Oncol 2006; 17(7): vii115-vii123.
77. Gliniak B, Le T. Tumor necrosis factor-related apoptosis-inducing ligand's antitumor activity in vivo is enhanced by the chemotherapeutic agent CPT-11. Cancer Res 1999; 59: 6153–6158.
78. Wu XX, Ogawa O, Kakehi Y. TRAIL and chemotherapeutic drugs in cancer therapy. Vitam Horm 2004; 67: 365–383.
79. Chipuk JE, Bouchier-Hayes L, Green DR. Mitochondrial outer membrane permeabilization during apoptosis: the innocent bystander. Cell Death Differ 2006; 13: 1396-1402.
80. Narita M, Shimizu S, Ito T, Chittenden, T, Lutz RJ, Matsuda H, et al. Bax interacts with the permeability transition pore to induce permeability transition and cytochrome c release in isolated mitochondria. Proc Natl Acad Sci USA 1998; 95: 14681-14686.
81. Basanez G, Nechushtan A, Drozhinin O, Chanturiya A, Choe E, Tutt S, et al. Bax, but not Bcl-XL decreases the lifetime of planar phospholipid bilayer membranes at subnanomolar concentrations. Proc Natl Acad Sci USA 1999; 96: 5492-5497.

82. Luo X, Budihardio I, Zou H, Slaughter C, Wang X. Bid, a Bcl-2 interacting protein, mediates cytochrome c release from mitochondria in response to activation of cell surface death receptors. Cell 1998; 94: 481-490.

83. Green DR, Kroemer G. The pathophysiology of mitochondrial cell death. Science 2004; 305: 626-629.

84. Danial NN. BCL-2 family proteins: critical checkpoints of apoptotic cell death. Clin Cancer Res 2007; 13(24): 7254-7263.

85. Wang K,Yin XM, Chao DT, Milliman CL, Korsmeyer SJ. BID: a novel BH3 domain-only death agonist. Genes Dev 1996; 10: 2859-2869.

86. Solá S, Aranha MM, Steer CJ, Rodrigues CM. Game and Players: Mitochondrial Apoptosis and the Therapeutic Potential of Ursodeoxycholic Acid. Curr Issues Mol Boil 2007; 9(2): 123-138.

87. Bayir H, Kagan VE. Bench-to-bedside review: mitochondrial injury, oxidative stress and apoptosis-there is nothing more practical than a good theory. Crit Care 2008; 12(1): 1-11.

88. Li P, Nijhawan D, Budihardjo I, Srinivasula SM, Ahmad M, Alnemri ES et al. Cytochrome c and dATP-Dependent Formation of Apaf-1/Caspase-9 Complex Initiates an Apoptotic Protease Cascade. Cell 1997; 91: 479-489.

89. Qin H, Srinivasula SM, Wu G, Fernandes-Alnemri T, Alnemri ES, Shi Y. Structural basis of procaspase-9 recruitment by the apoptotic protease-activating factor 1. Nature 1999; 399: 547–555.

90. Bao Q, Shi Y. apoptosome: a platform for the activation of initiator caspases. Cell Death Differ 2007; 14: 56-65.

91. Brentnall M, Rodriguez-Menocal L, De Guerva RL, Cepero E, Boise L. Caspase-9, caspase-3 and caspase-7 have distinct roles during intrinsic apoptosis. BMC Cell Biol 2013; 14: 32.

92. White MJ, Schoenwaelder SM, Josefsson RC, Jarman KE, Henley KJ, James C. Caspase-9 mediates the apoptotoc death of megakaryocytes and platelets, but it is dispensable for their generation and function. Blood 2012; 119 (18): 4283-4290.

93. Chiang N, Lin C, Liou C, Kuo C, Chang C, Chen, et al. A novel synthetic microtubule inhibitor, MPT08214 exhibits antitumor in human tumor cells through mitochondria-dependent intrinsic pathway. PlosOne 8(3): e58953.

94. Yang X, Chen L, Liu Y, Yang Y, Chen T, Zheng W, et al. Ruthenium methylimidazole complexes induced apoptosis in lung A549 cells through intrinsic mitochondrial pathway. Biochemie 2012; 94(2): 345-353.

95. Tsai S, Huang W, Huang W, Lu C, Chiang J, Peng S, et al. Erk-modulated intrinsic signaling and G2/M phase arrest contribute to the induction of apoptotic death y allyl isothiocyanate in MDA-MB-468 human breast adenocarcinoma cells. Int J Oncol 2012; 41(6): 2065-2072.

96. Strappazzon F, Campello S, Cecconi F. Non-apoptotic roles for death-related molecules: when mitochondria chose cell fate. Exp Cell Res 2012; 318(11): 1309-1315.

97. Rao RV, Ellerby HM, Bredensen DE. Coupling endoplasmic reticulum stress to the cell death program. Cell Death Differ 2004; 11: 372-380.

98. Groenedyk J, Mickalak M. endoplasmic reticulum quality control and apoptosis. Acta Biochimica Polonica 2005; 52(2): 381-395.

99. Wang W, Groenedryk J, Michalak. Endoplasmic reticulum stress associated response in cancer. Biochim Biophys Acta 2014: **In Press**

100. Hitomi J, Katayama T, Eguchi Y, Kudo T, Taniguchi M, Koyama Y, et al. Involvement of caspase-4 in endoplasmic reticulum. J Cell Biol 2004; 165: 347-356.

101. Ng FW, Nguyen M, Kwan T, Branton PE, Nicholson DW, Cromlish JA, Shore GC. p28 Bap31, a Bcl-2/Bcl-XL- and procaspase-8-associated protein in the endoplasmic reticulum. J Cell Biol 1997, 139: 327–338.

102. Jin Z, El-Deiry WS. Overview of cell death signaling pathways. Cancer Biol Ther 2005; 4(2): 139-163.

103. Johnson DE. Noncaspase proteases in apoptosis. Leukemia 2000; 14: 1695-1703.

104. Low RL. Mitochondrial Endonuclease G function in apoptosis and mtDNA metabolism: a historical perspective. Mitochondrion; 2(4): 225-236.

105. Widlak P, Garrard WT. Discovery, regulation, and action of the major apoptotic nucleases DFF40/CAD and endonuclease G. J Cell Biochem 2005; 94(6): 1078-1087.

106. Moffitt KL, Martin SL, Walker B. the emerging role of serine proteases in apoptosis. Biochem Soc Trans 2007; 35(3): 559-560.

107. Heibein JA, Goping IS, Barry M, Pinkoski MJ, Shore GC, Green DR, et al. Granzyme B-mediated cytochrome C release is regulated by the Bcl-2 family members bid and Bax. J Exp Med 2000; 192(10): 1391-1402.
108. Plantini F, Perez-Thomas R, Santiago A, Tessitore L. Understanding autophagy in cell death control. Curr Pharm Des 2010; 16(1): 101-113.
109. Jaeger PA, Wyss-Coray. All-you-can-eat: autophagy in neurodegeneration and neuroprotection. Mol Neurodegener 2009; 4: 16-38.
110. Xie Z, Klionssky DJ. Autophagosome formation: core machinery and adaptions. Nature Cell Biol 2007; 9 (10): 1102-1109.
111. Dice JF. Chaperone-mediated autophagy. Autophagy 2007; 3(4): 295-299.
112. Zhang C, Cuervo AM. Restoration of chaperone-mediated autophagy in aging liver improves cellular maintenance and hepatic function. Nat Med 2008; 14(9): 959-965.
113. Mizushima N, Levine B, Cuervo AM, Klionksy DJ. Autophagy fights disease through cellular self-digestion. Nature 2008; 451(7182): 1069-1075.
114. Cuervo AM, Mann L, Bonten EJ, d'Azzo A, Dice JF. Cathepsin A regulates chaperone-mediated autophagy through cleavage of the lysosomal receptor. EMBO J 2003; 22(1): 47-59.
115. Jones RG, Thompson CB. Tumor suppressors and cell metabolism: a recipe for cancer growth. Genes Dev 2009; 23: 537-548.
116. Russel RC, Yuan H, Guan K. Autophagy regulation by nutrient signaling. Cell Res 2014; 24: 42-57.
117. Kabeya Y, Mizushima N, Ueno T, Yamamoto A, Kirisako T, Noda T, et al. LC3, a mammalian homologue of yeast Apg8p, is localized in autophagosome membranes after processing, Embo J 2000; 19: 5720–5728.
118. Mizushima N, Yamamoto A, Hatano M, Kobayashi Y, Kabeya Y, Suzuki K, et al. Dissection of autophagosome formation using Apg5-deficient mouse embryonic stem cells. J Cell Biol 2001; 152: 657–667.
119. Yoshimori T. Autophagy: a regulated bulk degradation process inside cells. Biochem Biophys Res Commun 2004; 313: 453-458.
120. Sinha S, Levine B. The autophagy effector Beclin 1: a novel BH3-only protein. Oncogene 2008; 27(1): 137-148.

121. Salvador N, Aguado C, Horst M, Knecht E. Import of a cytosolic protein into lysosomes by chaperone-mediated autophagy depends on its folding state. Journal Biol Chem 2000; 275(35): 27447-27456.

122. Mijaljica D, Prescott M, Devenish RJ. Microautophagy in mammalian cells: revisiting a 40 year old conundrum. Autophagy 2011; 7(7): 673-682.

123. Dubouloz F, Deloche O, Wanke V, Cameroni E, De Virgilio C. The TOR and EGO protein complexes orchestrate microautophagy in yeast. Mol Cell 2005; 19: 15-26.

124. Schadeck RJG, Randi MAFR, Buchi DF, Leite B. Vacuolar system of ungerminated collectotrichum graminicola condidia: convergence of autophagy and endocytic pathways. FEMS Microbiol Lett 2003; 218(2): 277-283.

125. Okada H, Mak TW. Pathways of apoptotic and non-apoptotic death in tumor cells. *Nature Rev Cancer* 2004; 4: 592-603.

126. Letai AG. Diagnosing and exploiting cancer's addiction to blocks in apoptosis. Nat Rev Cancer 2008; 8: 121-132..

127. Castedo M, Perfettini JL, Roumier T, Kroemer G. Cyclin dependent kinase-1: linking apoptosis to cell cycle and mitotic catastrophe. Cell Death Differ 2002; 9: 1287-1293.

128. Vakifahmetoglu H, Olson M, Zhivotovsky B. Death through a tragedy: mitotic catastrophe. Cell Death Differ 2008; 15: 1153-1162.

129. Musacchio A, Ciliberto A. The spindle-assembly checkpoint and the beauty of self-destruction. Nat Struct Biol 2012; 19: 1059-1061.

130. Bensinger SJ, Christofk HR. New aspects of the Warburg effect in cancer biology. Semin Cell Dev Biol 2012; 23(4): 352-361.

131. Arsham AM, Plas DR, Thompson CB, Simon MC. Akt and hypoxia-1-inducible factor-1 independently enhance tumor growth and angiogenesis. Cancer Res 2004; 640: 3500-3507.

132. Rankin EB, Giaccia AJ. The role of hypoxia-inducible factors in tumorigenesis. Cell Death Differ 2008; 15: 678-685.

133. Wenger RH. Cellular adaptation to hypoxia: O2-sensing protein hydroxylases, hypoxia-inducible transcription factors, and O2-regulated gene expression. FASEB J 2002; 16: 1151-1162.

134. Grabacka M, Reiss K. anticancer properties of PPARα-effects on cellular metabolism and inflammation. PPAR Res 2008: 1-9.
135. Jin S, Dipaola RS, Mathew R, White E. metabolic catastrophe as a means to cancer cell death. J Cell Sci 2007; 120(3): 379-383.
136. Majno G and Joris I. Apoptosis, oncosis and necrosis. An overview of cell death. Am J Pathol 1995. 146: 3-15.
137. Van Cruchten S, Van den Broeck W. morphological and biochemical aspects of apoptosis, oncosis and necrosis. Anat Histo Embryol 2002; 31: 214-223.
138. Mills EM, Xu D, Fergusson MM, Combs CA, Xu Y, Finkel T. regulation of cellular oncosis by uncoupling protein 2. J Biol Chem 2002; 277(30): 27385-27392.
139. Shirai T. commentary: oncosis and apoptosis: two faces of necrosis in a new proposal to clear up the confusion regarding cell death. Toxicol Pathol 1999; 27: 495-496.
140. Matsouka S. A cell surface receptor defined by a mAB mediates a unique type of cell death similar to apoptosis. Proc Natl Acad Sci 1998; 95: 6290-6295.
141. Weerasinghe P, Buja LM. Oncosis: an important non-apoptotic mode of cell death.Exp Mol Path 2012; 93(3): 302-308.
142. Koyama AH, Irie H, Ueno F, Ogawa M, Nomoto A, Adachi A. Suppression of apoptotic and necrotic cell death by poliovirus. Journal Of General Virology 2001; 85: 2965-2972.
143. Jain M, Kasetty S, Khan S, Desai A. An insight to apoptosis. J Res Pract Dent 2014: 2014: 1-12.
144. Zheng Y, Humphry M, Maguire JJ, Bennet MR, Clarke MCH. Intracellular interleukin-1 receptor 2 binding prevents cleavage and activity of interleukin-1α, controlling necrosis-induced sterile inflammation. Immunity 2013; 38(2): 285-295.
145. Chai H. Hydrogen peroxide regulation of endothelial function: origins, mechanisms, and consequences. Cardiovasc Res 2005; 68: 26-36.
146. Bensaad K, Cheung EC, Voudsen KH. Modulation of intracellular ROS levels by TIGAR controls autophagy. EMBO J 2009; 28: 3015-3026.
147. Lu W, Ogasawara MA, Huang P. Models of reactive oxygen species in cancer. Drug Disc Today Dis Models 2007; 4(2): 67-73.
148. Pan JS, Hong MZ, Ren JL. Reactive oxygen species: a double-edged sword in oncogenesis. World J Gastroenterol 2009; 15(14): 1702-1707.

149. Pelicano H, Feng L, Zhou Y, Carew JS, Hileman EO, Plunkett W, et al. Inhibition of mitochondrial respiration. J Biol Chem 2003; 278(39): 37832-37839.
150. Huang J, Brumell JH. NADPH oxidases contribute to autophagy regulation. Autophagy 2009; 5(6): 887-889.
151. Sena LA, Chandel NS. Physiological roles of mitochondrial reactive oxygen species. Mol Cell 2012; 48(2): 158-167.
152. Mitchison TJ. The proliferation rate paradox in antimitotic chemotherapy. Mol Biol Cell 2012; 23 (1): 1-6.
153. Rovini A, Savry A, Braguer D, Carré M. Microtubule-targeted agents: when mitochondria become essential to chemotherapy. Biochim Biophys Acta 2011; 1807 (6): 379-688.
154. Pribluda VS, Gubish ER, La Vallee TM, Treston A, Swartz GM, Green SJ. 2-Methoxyestradiol: An endogenous antiangiogenic and antiproliferative drug candidate. Cancer Metastasis Rev 2000; 19: 173-179.
155. Azab SS, Salama SA, Hassan MH, Khalifa AE, El-Demerdash E, Fouad H, et al. 2-Methoxyestradiol reverses doxorubicin resistance in human breast tumor xenograft. Cancer Chemother Pharmacol 2008; 62(5): 893-902.
156. Field JJ, Kanakkanthara A, Miller JH. Microtubule-targeting agents are clinically successful due to both mitotic and interphase impairment of microtubule function. Bioorg Med Chem 2014: **In Press.**
157. Lavallee TM, Zhan XH, Herbstritt CJ, Kough EC, Green SJ, Pribluda VS. 2-Methoxyestradiol inhibits proliferation and induces apoptosis independently of estrogen receptors alpha and beta. Cancer Res 2002; 62: 3691–3697.
158. Banerjeei SK, Zoubine, MN, Sarkar, DK, Weston AP, Shah JH Campbell DR. 2-Methoxyestradiol blocks estrogen-induced rat pituitary tumor growth and tumor angiogenesis: possible role of vascular endothelial growth factor. Anticancer Res 2000; 20: 2641–2645.
159. Lippert TH, Adlercreutz H, Berger MR, Seeger H; Elger W, Mueck AO. Effect of 2-methoxyestradiol on the growth of methyl-nitroso-urea (MNU)-induced rat mammary carcinoma. J Steroid Biochem Mol Biol 2003; 84: 51–56.
160. Lakhani NJ, Lepper ER, Sparreboom A, Dahut WL, Venitz J, Figg WD. Determination of 2-methoxyestradiol in human plasma, using liquid

chromatography/tandem mass spectrometry. Rapid Commun Mass Spectrom 2005; 19: 1176-1182.

161. Foster PA, Ho YT, Newman SP, Kasprzyk MP, Leese MP, Potter BVL, et al. 2-MeOE2bisMATE and 2-EtE2bisMATE induce cell cycle arrest and apoptosis in breast cancer xenografts as shown by a novel ex vivo technique. Breast Cancer Res Treat 2008; 111: 251-260.

162. Stanway SJ, Delavault P, Purohit A, Woo LWL, Thurieau C, Potter BVL, et al. Steroid sulfatase: a new target for the endocrine therapy of breast cancer. Oncologist 2007; 12(4): 370-374.

163. Duncan L, Purohit A, Howarth M, Potter BVL, Reed MJ. Inhibition of estrogen sulfatase activity by estrone-3-methylthiophosphonate: potential therapeutic agent in breast cancer. Cancer Res 1993; 53: 298-303.

164. Evans TR, Rowlands MG, Silva MC, Law M, Coombes RC. Prognostic significance of aromatase and estrone sulfatase enzymes in human breast cancer. J Steroid Biochem Mol Biol 1993; 44: 583-587.

165. Billich A, Nussbaumer P, Lehr P. Stimulation of MCF-7 breast cancer cell proliferation by estrone sulphate and dehydroepiandrosterone sulphate: inhibition by novel non-steroidal steroid sulfatase inhibitors. J Steroid Biochem Mol Biol 2000; 72: 225-235.

166. Honma N, Saji S, Hirose M, Horiguchi S, Kuroi K, Utsumi T, et al. Sex steroid hormones in pairs of tumor and serum from breast cancer patients and pathobiological role of androstene-3β, 17β-diol. Cancer Sci 2011; 102(10): 1848-1854.

167. Raobaikaby B, Purohit A, Chander SK, Woo L, Leese MP, Potter VL, et al. Inhibition of MCF-7 breast cancer cell proliferation and *in vivo* steroid sulphatase activity by 2-methoxyoestradiol-bis-sulphamate. J Steroid Biochem Mol Biol 2003; 84: 351-358.

168. Reed MJ, Purohit A, Woo LWL, Newman SP, Potter BVL. Steroid sulfatase: molecular biology, regulation and inhibition. Endocr Rev 2005; 26(2): 171-202.

169. Tu C, Alvarado A, McKenna R, Silverman DN, Frost SC. Role of zinc in catalytic activity of carbonic anhydrase IX. Arch Biochem Biophys 2012; 521 (1-2): 90-94.

170. Dhup S, Dadhich RK, Porporato PE, Sonveaux P. Multiple biological activities of lactic acid in cancer: influences on tumor growth, angiogenesis and metastasis. Curr Pharm Des 2012; 18(10): 1319-1330.
171. Fang JS, Gillies RD, Gatenby RA. Adaptation to hypoxia and acidosis in carcinogenesis and tumor progression. Semin Cancer Biol 2008; 18: 330-337.
172. Wood L, Leese MP, Mouzakiti A, Purohit A, Potter BV, Reed MJ, et al. 2-MeOE2bisMATE induces caspase-dependent apoptosis in CAL51 breast cancer cells and overcomes resistance to TRAIL via cooperative activation of caspases. Apoptosis 2004; 9: 323-332.
173. Leese LP, Jourdan FL, Gaokroger K, Mahon MF, Newman SP, Foster PA, et al. Structure-activity relationship of C-17 cyano-substituted estratriene as anticancer agents. J Med Chem 2008; 51: 1295-1308.
174. Jourdan F, Leese MP, Dohle W, Hamel E, Ferrandism E, Newman SP, et al. Synthesis, antitubulin, and antiproliferative SAR of analogues of 2-methoxyestradiol-3- 17-*O*, *O*-bis-sulfamate. J Med Chem 2010; 53: 2942-2951.
175. Stander A, Joubert F, Joubert A. Docking, synthesis, and *in vitro* evaluation of antimitotic estrone analogues. Chem Biol Drug Des 2011; 77: 173-181.
176. Stander XX, Stander BA, Joubert AM. *In vitro* effects of an *in silico*-modelled 17β-estradiol derivative in combination with dichloroacetic acid on MCF-7 and MCF-12A cells. Cell Prolif 2011; 44: 567-581.
177. Liu B, Fan Z, Edgerton SM, Deng XS, Alimova IN, Lind SE, et al. Metformin induces unique biological and molecular responses in triple negative breast cancer cells. Cell Cycle 2009; 8 (13): 2031-2040.
178. Visagie MH, Joubert AM. *In vitro* effects of 2-methoxyestradiol-bis-sulphamate on cell numbers, membrane integrity, morphology and possible induction of apoptosis and autophagy in a non-tumorigenic breast epithelial cell line. Cell Mol Biol Lett 2010; 15: 564-581.
179. Visagie MH, Joubert AM. 2-Methoxyestradiol-bis-sulfamate induces apoptosis and autophagy in a tumorigenic breast epithelial cell line. Mol Cell Biochem 2011; 357: 343-352.
180. Gillies RJ, Robey I, Gatenby RA. Causes and consequences of increased glucose metabolism of cancers. J Nucl Med 2008; 49 Suppl 2: 24S-42S.

181. Castro-Garza J, Barrios-Garcia HB, Cruz-Vega DE, Said-Fernandez S, Carranza-Rosales P, Molina-Torres CA, et al. Use of a colorimetric assay to measure differences in cytotoxicity of *Myobacterium Tuberculosis* strains. J Med Microbiol 2007; 56: 733-737.

182. Kueng W, Silber E, Eppenberger U. Quantification of cells cultured on 96-well plates. Anal Biochem 1989; 182(1): 16-19.

183. Irelan JT, Wu M, Morgan J, Ke N, Xi B, Wang X, et al. Rapid and quantitative assessment of cell quality, identity, and functionality for cell-based assays using real-time cellular analysis. J Biomol Screen 2011;16(3): 313-322.

184. Urcan E, Haertel U, Styllou M, Hickel R, Scherthan H, Reichl FX. Real time xCELLigence impedance analysis of the cytotoxicity of dental composite components on human gingival fibroblasts. Dent Mater 2010; 26(1): 51-58.

185. DeBarardinis RJ, Sayed N, Ditsworth D, Thompson CB. Brick by brick: metabolism and tumor cell growth. Curr Opin Genet Dev 2008; 18(1): 54-61.

186. Ying W. NAD+/NADH and NADP+/NADPH in cellular functions and cell death: regulation and biological consequences. Antioxid Redox Signal 2008; 10(2): 179-206.

187. Avwioro G. Histochemical uses of haematoxylin- a review. JPCS 2011; 1: 24-34.

188. Taatjes DJ, Sobel BE, Budd RC. Morphological and cytochemical determination of cell death by apoptosis. Histochem Cell Biol 2008; 129: 33-43.

189. Kroemer G, El-Deiry WS, Golstein P, Peter ME, Vaux D, Vandenabeele P, et al. Classification of cell death: recommendations of the nomenclature committee on cell death. Cell Death Differ 2005; 12: 1463-1467.

190. Hayes TL, Pease RF. The scanning electron microscope: principles and applications in biology and medicine. Adv Biol Med Phys 1968;12: 85-137.

191. Danilatos GD, Robison VNE. Principles of scanning electron microscopy at a high specimen chamber pressures. Scanning 1979; 2: 72-82.

192. Peracchio C, Alabiso O, Valente G, Isidoro C. Involvement of autophagy in ovarian cancer: a working hypothesis. J Ovarian Res 2012; 5(1): **In Press**

193. Jin Z, El-Deiry WS. Overview of cell death signalling pathways. Cancer Biol Ther 2005; 4(2): 139-163.

194. Kusuzaki K, Murata H, Takeshita H, Hashiguchi S, Nozaki T, Emoto K, et al. Intracellular binding sites of acridine orange in living osteosarcoma cells. Anticancer Res 2000; 20(2A): 971-975.

195. Brana C, Benham C, Sundstrom L. A method for characterising cell death in vitro by combining propidium iodide staining with immunohistochemistry. Brain Res Protoc 2002; 10(2): 109-114.

196. Elstein KH, Zucker RM. Comparison of cellular and nuclear flow cytometric technisques for discriminating apoptotic subpopulations. Exp Cell Res 1994; 211(2): 322-331.

197. Mao X, Nawaz AA, Lin SS, Lapsley MI, Zhao Y, McCoy JP, El-Deiry WS, Huang TJ. An integrated, multiparametric flow cytometry chip using "microfluidic drifting" based three-dimensional hydrodynamically focusing. Biomicrofluidics 2012; 6: 024113.

198. Givan AL. Chapter 2 Principles of flow cytometry. Methods Cell Biol 2001; 63: 19-60.

199. Eray M, Mätto M, Kaartinen M, Anderson LC, Pelkonen J. Flow cytometric analysis of apoptotic subpopulations with a combination of annexin V-FITC, propidium iodide, and SYTO 17. Cytometry 2001; 43: 134-142.

200. Von Engeland M, Nieland LJW, Ramaekers FCS, Schutte B, Reutelingsperger CPM. Annexin v-affinity assay: a review on an apoptosis detection system based on phosphatidylserine exposure. Cytometry 1998; 31: 1-9.

201. Boon JM, Lambert TN, Sisson AL, Davis AP, Smith BD. Facilitated phosphatidylserine (PS) flip-flop and thrombin activation using a synthetic PS scramblase. J AM Chem 2003; 125: 8195-8201.

202. Li PF, Dietz R, Von Harsdorf R. p53 regulates mitochondrial membrane potential through reactive oxygen species and induces cytochrome c-independent apoptosis blocked by Bcl-2. EMBO J 1999; 18(21): 6027-6036.

203. Bras M, Queenan B, Sushin SA. Programmed cell death via mitochondria: different modes of dying. Biochemistry (Mosc) 2005; 70(2): 231-239.

204. Breckenridge DG, Germain M, Mathai JP, Nguyen M, Shore GC. Regulation of apoptosis by endoplasmic reticulum pathways. Oncogene 2003; 22: 8608-8618.

205. Ischiropoulos H, Gow A, Thom SR, Kooy NW, Royall JA, Crow JP. Detection of reactive nitrogen species using 2,7-dichlorodihydrofluorescein and dihydrorhodamine 123. Methods Enzymol 1999; 301: 367–373.

206. Rothe G, Valet G. Flow cytometric analysis of respiratory burst activity in phagocytes with hydroethidine and 29,79 dichlorofluorescin. J Leukoc Bio l990; 47, 440-448.

207. Liu B, Chen Y, St Clair DK. ROS and p53: versatile partnership. Free Radic Biol Med 2008; 44(8): 1529-1535.

208. Iwakuma T, Lozano G. Mdm2, an introduction. Mol Cancer Res 2003; 1: 993-1000.

209. Oren M. Decision making by p53: life, death and cancer. Cell death Differ 2003; 10: 431-442.

210. Moretti L, Attia A, Kim KW, Lu B. Crosstalk between Bak/Bax and mTOR signaling regulates radiation-induced autophagy. Autophagy 2007; 3(2): 142-144.

211. Cory S, Adams JM. The Bcl-2 family: regulators of the cellular life-or-death switch. Nat Rev Can 2002; 2: 647–656.

212. Adams JM, Cory S. The Bcl-2 protein family: arbiters of cell survival. Science 1998; 281(5381): 1322–1326.

213. Gross A, Jockel J, Wei MC, Korsmeyer SJ. Enforced dimerization of BAX results in its translocation, mitochondrial dysfunction and apoptosis. The EMBO journal 1998; 17(14): 3878–3885.

214. Visagie M, Theron A, Mqoco T, Vieira W, Prudent R, Martinez A, Lafanechère L, Joubert A. Sulphamoylated 2-methoxyestradiol analogues induce apoptosis in adenocarcinoma cells. Plos One 2013: 5(9): e71935.

215. Junka AE, Janczura A, Smutnicka D, Macazynska B, Secewicz, Nowicka J, et al. Use of the real time xCelligence system for purposes of medical microbiology. Pol J Microbiol 2012; 61 (3): 191-197.

216. Limonciel A, Ashuaer L, Wilmes A, Prajczer S, Leonard MO, Pfaller W, et al. Lactate is an ideal non-invasive marker for evaluating temporal in cell stress and toxicity in repeat dose testing regimes. Toxocol In Vitro 2011; 25(8): 1855-1862.

217. Ussher JR, Jaswal JS, Lopaschuk GD. Pyridine nucleotide regulation of cardiac intermediately metabolism. Circ Res 2012; 111: 628-641.

218. Van Zijl C, Lottering ML, Steffens F, Joubert A. *In vitro* effects of 2-methoxyestradiol on MCF-12A and MCF-7 cell growth, morphology and mitotic spindle formation. Cell Biochem Func 2008; 26: 632-642.
219. Ha HC, Snyder SH. Poly(ADP-ribose)polymerase is a mediator of necrotic cell death by ATP depletion. Proc Natl Acad Sci 1999; 96 (24): 13978-13982.
220. Zdolsek JM, Olsson GM, Brunk UT. Photooxidative damage to lysosomes of cultured macrophages by acridine orange. Photochem Photobiol 1990; 51 (1): 67-76.
221. Du W, Wang Y, Hong J, Su W, Lin Y, Lu R, Xiong H, Fang J. Stat5 isoforms regulate colorectal cancer cell apoptosis via reduction of mitochondrial membrane potential and generation of reactive oxygen species. J Cell Physiol 2012; 227: 2421-2429.
222. Qi F, Li A, Inagaki Y, Xu H, Wang D, Cui X, Zhang L, et al 2012 Induction of apoptosis by cinobufacini preparation through mitochondria- and Fas-mediated caspase-dependent pathways in human hepatocellular carcinoma cells. Food Chem Toxicol 2012; 50(2): 295-302.
223. Liu C, Xu P, Chen D, Fan X, Xu Y, Li M, et al. Roles of autophagy-related genes beclin-1 and LC3 in the development and progression of prostate cancer and benign prostatic hyperplasia. Biomed Rep 2013: 855-860.
224. Rhee SG, Chang TS, Jeong W, Kang D. Methods for detection and measurement of hydrogen peroxide inside and outside of cells. Mol Cell 2010; 29: 539-549.
225. Bindokas VP, Jordán J, Lee CC, Miller RJ. Superoxide production in rat hippocampal neurons: selective imaging with hydroethidine. J Neurosci 1996; 16(4): 1324-1336.
226. Haupt S, Berger M, Goldberg Z, Haupt Y. Apoptosis- the p53 network. J Cell Sci 2003; 166: 4077-4085.
227. Toledo F, Wahl GM. MDM2 and MDM4: p53 regulators as targets in anticancer therapy. Int J Biochem Cell Biol 2007; 39 (7-8): 1476-1482.
228. Balaburski GM, Hontz RD, Murphy ME. p53 and ARF: unexpected players in autophagy. Trends Cell Biol 2010; 20(6): 363-369.
229. Stander BA, Joubert F, Tu C, Sippel KH, McKenna R, Joubert AM. 2012. *In vitro* evaluation of ESE-15-ol, an estradiol analogue with nanomolar antimitotic and carbonic anhydrase inhibitory activity. PlosOne 7(12): e52205.

230. Tsujimoto Y. Role of Bcl-2 family proteins in apoptosis: apoptosomes or mitochondria. Genes Cells 1998; 3(11): 697-707.

231. Vantieghem A, Xu Y, Assefa Z, Piette J, Vandenheede JR, Merlevede W, et al. Phosphorylation of Bcl-2 in G_2/M phase-arrested cells following photodynamic therapy with hypericin involves a CDK1-mediated signal and delays the onset of apoptosis. J Biol Chem 2002; 277: 37718-37731.

232. Pattingre S, Tassa A, Qu X, Garuti R, Liang XH, Mizushima N, et al. Bcl-2 antiapoptotic proteins inhibit beclin 1-dependent autophagy. Cell 2005; 122(6): 927-939.

233. Peyrat J, Brion J, Alami M. Synthetic 2-methoxyestradiol derivatives : structure activity relationships. Curr Med Chem 2012; 19 (24): 4142-4156.

234. Frank E, Schneider G. Synthesis of sex hormone-derived modified steroids processing antiproliferative activity. J Steroid Biochem Mol Biol 2013; 137: 301-315.

235. Visagie MH, Stander BA, Birkholtz L-M, Joubert AM. Effects of a 17-beta estradiol analogue on gene expression and morphology in a breast epithelial adeno-carcinoma cell line: A potential antiproliferative agent. Biomed Res 2013: 24 (4): 525-530.

236. Leese MP, Leblond B, Smith A, Newman SP, Fiore AD, Simone GD. 2-Substituted estradiol bis-sulfamates, multitargeted antitumor agents: synthesis, in vitro SAR, protein crystallography, and in vitro activity; J Med Chem 2006; 49: 7683-7696.

237. Panchapakesan G, Dhayalan V, Moorthy ND, Saranya N, Mohanakrishnan AK. Synthesis of 2-substitued 17β-hydroxy/17-methylene estratrienes and their in vitro cytotoxicity in human cancer cell cultures. Steroids 2011; 76: 1491-1504.

238. Stander BA, Joubert F, Tu C, Sippel KH, McKenna R, Joubert AM. 2013. Signaling pathways of ESE-16, an antimitotic and anticarbonic anhydrase estradiol analog, in breast cancer cells. PlosOne 2013; 8 (10): e5853.

239. Visagie MH, Mqoco TV, Joubert AM. Sulphamoylated estradiol analogue induces antiproliferative activity and apoptosis in breast cell lines. Cell Mol Biol Lett 2012; 17(4): 549-585.

240. Ireson CR, Chander SK, Purohit A, Perera S, Newman SP, Parish D, et al. Pharmacokinetics and efficacy of 2-methoxyoestradiol and 2-methoxyoestradiol-bis-sulphamate in vivo in rodents. Br J Cancer 2004; 90: 932-937.

241. Foster PA, Ho Y, Newman SP, Leese MP, Potter BV, Reed MJ, et al. STX 140 and STX 641 cause apoptosis via the intrinsic mitochondrial pathway and downregulate survivan and XIAP expression in ovarian and prostate cancer cells. Anticancer Res 2009; 29(10): 3751-3757.

242. Foster PA, Stengel C, Ali T, Leese MP, Potter BV, Reed MJ, et al. A comparison of two orally bioavailable anti-cancer angents, IRC-110160 and STX140. Anticancer Res 2008; 28(3A): 1483-1491.

243. Raobaikady B, Reed MJ, Leese MP, Potter BVL, Purohit A. Inhibition of MDA-MB-231 cell cycle progression and cell proliferation by C-2-substituted oestradiol *mono*- and *bis*-3-O-sulphamates. Int J Cancer 2005 ;117: 150-159.

244. Kappert K, Caglayan E, Huntgeburth M, Bäumer AT, Sparwel J, Rosenkranz S. 17β-Estradiol attenuates PDGF signaling in vascular in vascular smooth muscle cells at the postreceptor level. Am J Physiol Heart Circ Physiol 2006; 290: H538-H546.

245. Visagie MH, Joubert AM. The in vitro effects of 2-methoxyestradiol-bis-sulphamate on cell numbers, membrane integrity and cell morphology, and the possible induction of apoptosis and autophagy in a non-tumorigenic breast epithelial cell line. Cell Mol Biol 2010; 15(4): 564-581.

246. Vorster CJ, Joubert AM. In vitro effects of 2-methoxyestradiol-bis-sulphamate on cell numbers, morphology and cell cycle dynamics in the MCF-7 breast adenocarcinoma cell line. Biocell 2010; 34(2): 71-79.

247. Mqoco T, Marais S, Joubert AM. Influence of estradiol analogue on cell growth, morphology and cell death in easophageal carcinoma cells. Biocell 2010; 34: 113-120.

248. Suzuki RN, Newman SP, Purohit A, Leese MP, Potter BV, Reed MJ. Growth inhibition of multi-drug-resistant breast cancer cells by 2-methoxyoestradiol-bis-sulphamate and 2-ethyloestradiol-bis-sulphamate. J Steroid Biochem Mol Biol 2003; 84: 269-278.

249. Day JM, Foster PA, Tutill HJ, Newman SP, Ho YT, Leese MP, et al. BCRP expression does not result in resistance to STX140 in vivo, despite the increased expression of BCRP in A2780 cells in vitro after long-term STX140 exposure. Br J Cancer 2009; 100: 476-486.

250. Nkandeu DS, Mqoco TV, Visagie MH, Stander BA, Wolmerans E, Cronje MJ, et al. In vitro changes in mitochondrial potential, aggresome formation and caspase activity by a novel 17-β-estradiol analogue in breast adenocarcinoma cells. Cell Biochemistry and Function: 2013: 31(7): 566-574

251. Tanida I, Ueno T, Kominami E. LC3 conjugation system in mammalian autophagy. Int J Biochem Cell Biol 2004 ; 36(12): 2503-2518.

252. Kouroka Y, Fujita E, Tanida I, Ueno T, Isoai A, Kumagai H, et al. ER stress (PERK/eIF2$_{\alpha}$ phosphorylation) mediates the polyglutamine-induced LC3 conversion, an essential step for autophagy formation. Cell Death Differ 2007; 14: 230-239.

253. Bains M, Zaegel V, Mize-Berge J, Heidenreich KA. IGF-I stimulates Rab7-RILP interaction during neuronal autophagy. Neuroscience 2011; 488(2): 112-117.

254. Jia F, Li Y, Huang Y, Chen T, Li S, Xu Y, et al. Molecular characterization and expression of Rab7 from Clonorchis sinensis and its potential role in autophagy. Parasitol Res 2013; 112(7): 2461-2467.

255. Sini P, James D, Chresta C, Guichard S. Simultaneous inhibition of mTORC1 and mTORC2 by mTOR kinase inhibitor AZD8055 induces autophagy and cell death in cancer cells. Autophagy 2010; 6: 553-554.

256. Theron AE, Nolte EM, Lafanechère L, Joubert AM. Molecular crosstalk between apoptosis and autophagy induced by a novel 2-methoxyestradiol analogue in cervical adenocarcinoma cells. Cancer Cell Int 2013; 16: 97.

257. Mqoco TV, Joubert AM. 2-Methoxyestradiol-bis-sulphamate induces apoptosis and autophagy in an oesophageal carcinoma (SNO) cell line.Biomed Res 2012; 23(4): 469-474.

258. Portt L, Norman G, Clapp C, Greenwood M, Greenwood M. Anti-apoptosis and cell survival: a review. Biochim Biophys Acta 2011; 1813: 238-259.

259. Indran I, Tufo G, Perfaiz S, Brenner C. Recent advances in apoptosis, mitochondria and drug resistance in cancer cells. Biochim Biophys Acta 2011; 1807(6): 735-745.

260. Gupta SC, Hevia D, Patchva S, Park B, Koh W, Aggarwal BB. Upsides and downsides of reactive oxygen species for cancer: the roles of reactive oxygen species in tumorigenesis, prevention, and therapy. Antioxidant Redox Signal 2012; 16(11): 1295-1322.

261. Hamanaka RB, Chandel NS. Mitochondrial reactive oxygen species regulate cellular signaling and dictate biological outcomes. Trends Biochem Sci 2010; 35 (9): 505-213.

262. Finkel T. Signal transduction by reactive oxygen species. J Cell Biol 2011; 194: 7-15.

263. Scherz-Shouval R, Elazar Z. Regulation of autophagy by ROS: physiology and pathophysiology. Trends Cell Biol 2011; 36(1): 30-38.

264. Singletary K, Milner J. Diet, autophagy and cancer: a review. Cancer Epidiomol Niomarkers Prev 2008; 17(7): 1596-1610.

265. Alexander A, Chia S, Kim J, Nanez A, Sahin M, MacLean KH, et al. ATM signals to TSC2 in the cytoplasm to regulate mTORC1 in response to ROS. Proc Natl Acad Sci 2010; 107(9): 4153-4158.

266. Bellot GL, Liu D, Perviaz S. ROS, autophagy and cancer: RAS, the hidden master. Mitochondria 2013; 13(3): 155-162.

267. MacCarthy-Morrogh L, Townsend PA, Purohit A, Hejaz HAM, Potter BVL, Reed MJ, et al. Differential effects of estrone and estrone-3-O-sulfamate deratives on mitotic arrest, apoptosts, and microtubule assembly in human breast cancer cells. Cancer Res 2000; 60: 5441-5450.

268. Newman SP, Leese MP, Purohit A, James DRC, Rennie CE, Potter BVL. Inhibition of in vitro angiogenesis by 2-Methoxy- and 2-ethyl-estrogen sulfamates. *Int* J Cancer 2004; 109: 533-540.

269. Moll UM, Petrenko O. The MDM2-p53 interaction. Mol Cancer Res 2003; 1: 1001-1008.

270. Resetkova E, Gonzalez-Angulo A, Sneige N, McDonnell TJ, Buzar A, Kua AW, et al. Prognostic value of p53, MDM2, and MUC-1 for patients with inflammatory breast carcinoma. Cancer 2004; 110(5): 913-917.

271. Mayo LD, Donner DB. The PTEN, mdm2, p53 tumor expression-oncoprotein network. Trends Cell Biol 2002; 27(9): 462-467.

272. Hickman ES, Moroni MC, Helin K. The role of p53 and rRB in apoptosis and cancer. Curr Opin Genet Dev 2002; 12(1): 60-66.

273. Gottlieb TM, Oren M. p53 and apoptosis. Semin Cancer Biol 1998; 8: 359-368.

274. Maiuri MC, Galluzzi L, Morselli E, Kepp O, Malik SA, Kroemer G. Autophagy regulation by p53. Curr Opin Cell Biol 2010; 22(2): 181-185.
275. Susin SA, Lorenzo HK, Zamzami N, Marzo I, Brenner C, Larochette N, et al. Mitochondrial release of caspase-2 and -9 during the apoptotic process. J Exp Med 1999; 189(2): 381-394.
276. Jung M, Kang H, Moon A. Capsaicin-induced apoptosis in SK-Hep-1 hepatocarcinoma cells involves downregulation and caspase-3 activation. Cancer Lett 2001; 165(2): 139-146.
277. Ruvolo PP, Deng X, May WS. Phosphorylation of Bcl-2 and regulators of apoptosis. Leukemia 2001; 15(4): 515-522.
278. Niemi NM, MacKeigan JP. Mitochondrial phosphorylation in apoptosis: flipping the switch. Antioxidant Redox Signal 2013; 19(6): 572-582.
279. Zhou F, Yang Y, Xing D. Bcl-2 and Bcl-$_X$L play important roles in the crosstalk between autophagy and apoptosis. FEBS 2010; 278(3): 403-413.
280. Kessel D, Reners JJ. Initiation of apoptosis and autophagy by Bcl-2 antagonist HA14-1. Cancer Lett 2007; 249(2): 294-299.
281. Maiuri MC, Criolla A, Tasdemir E, Vicencio JM, Tajeddine N, Hickman JA. BH3-Only proteins and BH3 mimetics induce autophagy by competitively disrupting the interaction between Beclin-1 and Bcl-2/Bcl-X_L. Autophagy 2007; 3(4): 374-376.
282. Wei Y, Pattingre S, Sinha S, Bassik M, Levine B. JNK1-mediated phosphorylation of Bcl-2 regulates starvation-induced autophagy. Mol Cells 2008; 30(6): 678-688.